

The RXFP3 receptor is functionally associated with cellular responses to oxidative stress and DNA damage

Jaana van Gastel^{1,2}, Hanne Leysen^{1,2}, Paula Santos-Otte³, Jhana O. Hendrickx^{1,2}, Abdelkrim Azmi², Bronwen Martin⁴, Stuart Maudsley^{1,2}

¹Receptor Biology Lab, Department of Biomedical Sciences, University of Antwerp, Antwerp, Belgium

²Translational Neurobiology Group, Centre for Molecular Neuroscience, VIB, Antwerp, Belgium

³Center for Molecular and Cellular Bioengineering (CMCB), Technische Universität Dresden, Dresden, Germany

⁴Faculty of Pharmaceutical, Veterinary and Biomedical Science, University of Antwerp, Antwerp, Belgium

Correspondence to: Stuart Maudsley; **email:** Stuart.Maudsley@uantwerpen.be

Keywords: relaxin family peptide 3 receptor, relaxin 3, GPCR, DNA damage, aging

Received: September 4, 2019

Accepted: November 18, 2019

Published: December 3, 2019

Copyright: van Gastel et al. This is an open-access article distributed under the terms of the Creative Commons Attribution License (CC BY 3.0), which permits unrestricted use, distribution, and reproduction in any medium, provided the original author and source are credited.

ABSTRACT

DNA damage response (DDR) processes, often caused by oxidative stress, are important in aging and -related disorders. We recently showed that G protein-coupled receptor (GPCR) kinase interacting protein 2 (GIT2) plays a key role in both DNA damage and oxidative stress. Multiple tissue analyses in GIT2KO mice demonstrated that GIT2 expression affects the GPCR relaxin family peptide 3 receptor (RXFP3), and is thus a therapeutically-targetable system. RXFP3 and GIT2 play similar roles in metabolic aging processes. Gaining a detailed understanding of the RXFP3-GIT2 functional relationship could aid the development of novel anti-aging therapies. We determined the connection between RXFP3 and GIT2 by investigating the role of RXFP3 in oxidative stress and DDR. Analyzing the effects of oxidizing (H₂O₂) and DNA-damaging (camptothecin) stressors on the interacting partners of RXFP3 using Affinity Purification-Mass Spectrometry, we found multiple proteins linked to DDR and cell cycle control. RXFP3 expression increased in response to DNA damage, overexpression, and Relaxin 3-mediated stimulation of RXFP3 reduced phosphorylation of DNA damage marker H2AX, and repair protein BRCA1, moderating DNA damage. Our data suggests an RXFP3-GIT2 system that could regulate cellular degradation after DNA damage, and could be a novel mechanism for mitigating the rate of age-related damage accumulation.

INTRODUCTION

Disruption of the glucose metabolic system is nearly universal in aging and as this primary metabolic process falters, a negative energy balance occurs, as ATP levels reduce while reactive oxygen species (ROS) levels increase. This simultaneous loss of the capacity to maintain energetic processes in the face of increasing oxidative stress will eventually overwhelm cellular antioxidant capabilities, resulting in oxidative damage of DNA, one of the most well-known and recognized hallmarks of aging [1]. Many age-related disorders that affect our population, such as neurodegeneration, type 2

diabetes mellitus (T2DM) and cardiovascular disorders, are caused by these hallmarks [2].

Stress-induced DNA damage is arguably the most prominent underlying cause of aging and in turn may be one of the primary players in almost all age-related disorders [3]. This hypothesis has been supported by the investigation of accelerated aging disorders, *i.e.* Hutchinson–Gilford progeria syndrome, Ataxia Telangiectasia and Werner syndrome, which have one commonality, they are a direct effect of DNA damage response (DDR) and repair disruption [4–8]. As such, therapeutic amelioration of this stress-induced DNA

damage could be very effective for treating age-related disorders. We recently identified the G protein-coupled receptor (GPCR) associated protein, GIT2, as a potential keystone in aging [9]. Further work demonstrated that this receptor scaffolding protein also plays a role in oxidative stress responses [10], and is crucial for integrating several components of the DDR [11]. GIT2 knockout (GIT2KO) mice showed an increased vulnerability to DNA damage [12], displayed symptoms of T2DM [13], showed signs of ‘inflammaging’ [14, 15], and most importantly, showed accelerated aging compared to their wild-type littermates [12]. While this makes GIT2 an interesting target for treating multiple age-related disorders, GIT2 is a scaffolding protein and is therefore difficult to target directly. Typically, drugs are designed to be directed at enzymes, ion channels or receptors. However, as GIT2 is a GPCR interacting protein, it is highly likely that we can identify a receptor that is strongly associated with the GIT2 system. Our recent work has shown that GPCRs possess a potent capacity to control transcriptional and translational efficacies, often via non-G protein signaling activities [16, 17]. This likely contributes to their ability to generate and control the integrity and coherency of cellular signaling pathways, via the coordinated regulation of cascade proteins [18–20]. As there are likely to be strong transcriptional co-relationships between proteins linked via a common signaling function, it is possible that there are dedicated GPCRs that possess a profound link to specific signaling proteins via correlated expression. This ability to link an important target signaling protein to a tractable drug target, such as a GPCR, holds tremendous promise for the generation of intelligently-targeted therapeutics for age-related disorders. In this study, we investigated a receptor that shows an expressional and functional relationship with GIT2, the Relaxin Family Peptide 3 Receptor (RXFP3).

RXFP3 has been implicated in stress response [21], anxiety [22], depression [22, 23], feeding [24–27], arousal [24] and alcohol addiction [28] using RXFP3/RLN3 deficient mouse models. The first indications linking the RXFP3/RLN3 system to stress and metabolic control, was through its presence in the hypothalamic regions involved in the hypothalamic-pituitary-adrenal axis [27, 29–31] and the paraventricular nucleus [26, 27]. The relationship to stress has further been supported by the activation of RLN3 containing neurons in the nucleus incertus after administration of corticotropin releasing factor. The association to anxiety and depression was discovered as RLN3 expressing neurons also express inhibitory serotonin type 1A (5-HT_{1A}) receptors, suggesting functional interactions between these two systems [32]. There is currently emerging evidence linking anxiety to accelerated aging,

as several accelerated aging mouse models display anxiety [12, 13]. In addition, we have previously shown that RXFP3 expression is significantly affected when an aging-associated alteration occurs in the affect-modulating dopaminergic functionality in mice [33]. Thus, RXFP3 may be associated with controlling aging-related functions in addition to its anxiolytic and anti-depressant effects. Furthermore, RXFP3 may represent an important neurochemical markers of depression in Alzheimer's disease (AD), where Lee et al. demonstrated an increase in immunoreactivity in depressed AD patients [22]. Given our previous work concerning the role of GIT2 in the regulation of the aging process, the determination of a therapeutically targetable GIT2-RXFP3 synergistic signaling system may provide a basis for the design of novel GIT2-RXFP3 based therapeutics for the treatment of aging-related disorders.

RESULTS

Coordinated mRNA and protein expression profiles between GIT2 and RXFP3

In this study, multiple tissues, from the central nervous system (cortex, hippocampus and hypothalamus) and the periphery (pancreas and liver) were collected from male GIT2KO mice for mRNA expression profiling (Figure 1A), where we found a strong connection between GIT2 and RXFP3 expression, replicating what we have previously seen for murine GIT2 heterozygous KO hypothalamic extracts [34]. To validate these mRNA expression findings, we performed western blots to assess RXFP3 protein expression patterns in multiple GIT2KO mice (Figure 1B). Again, we found that in response to a diminution of GIT2 expression, there was a significant decrease in the levels of RXFP3 in all the assessed tissues. Additionally, upon introduction of a cDNA clone for human RXFP3 to either human neuronal SH-SY5Y or classical HEK293 cells, we found a significant increase in the expression of human GIT2 (Figure 1C).

Previously, we showed that hypothalamic functionality was altered in GIT2KO mice [13]. Thus, we investigated whether functional stimulation of endogenous RXFP3 at endogenous expression levels in murine hypothalamic neuronal GT1-7 cells with its cognate ligand relaxin 3 (RLN3, 1-100 nM, 6hrs of stimulation) would affect GIT2 expression. We found a significant dose-dependent elevation of GIT2 expression (Figure 1D). Hence, both in response to enhanced constitutive receptor activity (induced by augmented ectopic expression – Figure 1C) and ligand stimulation (Figure 1D), the active RXFP3 state seems to be functionally associated with GIT2 expression levels. In a previous study, we showed that GIT2 expression levels are associated with oxidative

stress, diabetic pathologies, advancing age and DNA damage [9–11, 13]. These data suggest that the GIT2-RXFP3 relationship may represent a molecular axis important for regulation of age-related damage. Thus, we next investigated further functional links between these two proteins with relation to oxidative stress and DNA damage.

RXFP3 constitutive activity regulates the expression of DNA damage response proteins

Recent research has demonstrated that in addition to short-term intermediary cell metabolism events mediated by G protein activation, GPCRs such as RXFP3 can regulate the expression profiles of multiple downstream signaling proteins. This occurs via the creation of more stable signaling entities, such as intricate G protein-

independent multi-protein ‘receptorsome’ complexes [17, 35]. The human (and murine) RXFP3 is a relatively unique receptor with respect to its basal activity status. It bears a pro-activating natural mutation in its ultra-conserved Asp-Arg-Tyr (DRY) amino acid triple motif, an Asp to Thr alteration, found at the juxtamembrane region of the second intracellular loop (Supplementary Figure 1A, 1B). This natural mutation increases its ligand independent activity [36]. Therefore, RXFP3 likely possesses a range of diverse signaling functions in the absence of its cognate ligand.

To assess these functions, likely generated by an ensemble of stably reinforced receptorsome structures, we used a stepwise ectopic expression process for generating the broadest possible range of ‘active’ receptorsome complexes, which we termed a

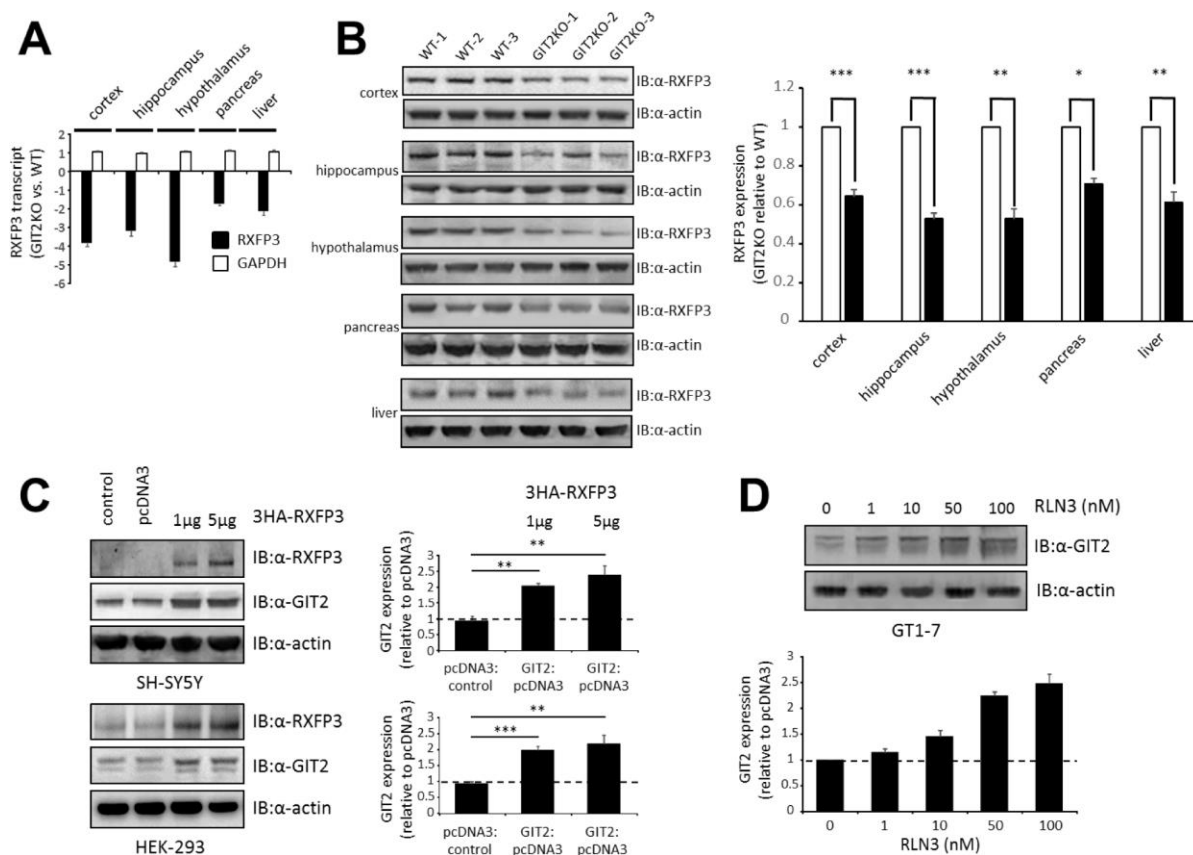


Figure 1. Discovery of RXFP3 as a possible controller for GIT2, identified through an expressional relationship. (A) Using transcriptome profiling, we investigated the expression levels of RXFP3 in GIT2-knock out (GIT2KO) mice (n=4). Both in the central nervous system (CNS) (cortex, hippocampus, and hypothalamus) and in peripheral tissues (pancreas, and liver) RXFP3 expression level was decreased compared to Wild-type (WT) littermates (n=4), GAPDH expression was shown to be stable as a control. (B) These results were replicated using western blotting, actin loading control was used. (C) Through transient transfection, RXFP3 was over expressed in SH-SY5Y and HEK293 cells at 1 and 2µg, as control cells were also overexpressed with an empty vector (pcDNA3). Actin was used as a loading control (n=3). A specific expression increase for GIT2 was seen after overexpression of RXFP3 in both cell types. (D) Stimulation of GT1-7 cells using the endogenous ligand Relaxin 3 (RLN3), showed a dose dependent increase in GIT2 expression, with increasing levels of RLN3 (n=3). Data represent the means ± SEM (standard error of the mean). Statistical analyses (Student’s t-test) were performed using GraphPad Prism version 7.0 (GraphPad Software, San Diego, CA, USA). Significance level is indicated in each figure as *p ≤ 0.05; **p ≤ 0.01; ***p ≤ 0.001.

'constellation curve' [37–39]. Without an unprecedented knowledge of receptorsome composition, or range of sub-state-selective or biased ligands, the ability to selectively induce distinct-signaling receptorsomes can only be achieved using such an expression-level variation protocol. By increasing expression levels, the range of receptorsomes will likely increase the diversity of distinct RXFP3 receptorsomes incrementally, revealing expression-specific function actions, until a saturation level is reached. As a gestalt readout of these distinct receptor forms, we employed a proteomic screening assessment of cellular alterations in response to the different RXFP3 receptorsomes, analogous (although less detailed) to a perturbagen 'constellation' process with the GIT2 scaffolding protein to assess which signaling pathways it was associated with [11]. In this current study, we performed a 'constellation' experiment in HEK293 cells, where we ectopically expressed an ascending level of an N-terminally 3xHA-tagged human RXFP3. Selective western-blot analyses specific for HA epitope tag (RXFP3) confirmed the effective constellation expression variance of the human RXFP3 receptor clone (Figure 2A). Using both anti-native RXFP3 antibody measurements and our quantitative mass spectrometric data we found that even a higher expression level of RXFP3 (5 µg) only engendered a relatively modest increase in total cellular RXFP3 content (1.5-2-fold increase). It is likely that such modest alterations are a) relatively within normal physiological expression ranges and b) more akin to the potentially elevated levels of RXFP3 that may be engineered by the cells after protracted periods of stressor exposure as is likely in the aging process.

We next assessed, in an unbiased manner, the proteomic 'constellation' perturbagen response to these ascending expression levels of RXFP3. Protein extracts were investigated as a multiplex using quantitative proteomics through iTRAQ labelling, with each RXFP3 expression level compared ratiometrically to the proteomic response effects to empty vector (E.V.) ectopic expression (Supplementary Table 1). We found that the introduction of various expression levels of RXFP3 (Figure 2A) caused significant and selective alterations in protein expression across the whole RXFP3 level range. The number of significantly altered proteins (compared to empty vector (E.V) transfected controls) responding to the specific RXFP3 expression levels were the following: 0.5 µg RXFP3 – 183; 1 µg RXFP3 – 293; 2 µg RXFP3 297; 5 µg RXFP3 – 278; 10 µg RXFP3 – 269. We next separated the common and distinctive RXFP3 perturbagen responsive proteins using InteractiVenn (Figure 2B). For each expression level, the percentage of uniquely-regulated proteins was relatively similar, *i.e.* 0.5 µg RXFP3 21.8% unique; 1 µg RXFP3 – 37.2% unique; 2 µg RXFP3 26.6% unique; 5 µg RXFP3 25.2% unique;

10 µg RXFP3 40.8% unique (Figure 2B). In contrast to these unique expression events, 12 proteins were significantly altered across all five RXFP3 expression levels (Supplementary Figure 3: PRR14L, SCYL1, CCDC9, NEK7, HIST1H3A, ATP1F1, CDCA2, PAGR1, POTEKP, MTMR1, ZCCHC3, MEPCE). Many of these commonly regulated proteins are known to be associated with energy balance regulation (PRR14L [40]), inflammaging (NEK7 [41]; ATP1F1 [42]), aging associated DNA damage (SCYL1 [43]; CCDC9 [44]; HIST1H3A [45]; ATP1F1 [46]; PAGR1 [47]; ZCCHC3 [48]) or cell senescence (CDCA2 [49]). As such it appears that in addition to expression level effects, a core functionality of the RXFP3 was also evident, which was tightly linked to age-related pathologies.

Given the impact on protein complex formation and the regulation of cellular signaling paradigms, we next analyzed, using protein-protein interaction (PPI) pattern analysis, each distinct RXFP3 expression level dataset using Enrichr (Supplementary Figure 2A) [50], to discover the most DDR-related RXFP3 overexpression level. We observed a strong representation of multiple DNA damage repair and energy metabolism-related proteins across the RXFP3 expression ranges used (Figure 2C; Supplementary Tables 2–6). The strongest PPI dataset enrichment for DDR proteins such as PRKDC, p53, PARP1 and TOP1 was observed for proteins influenced by the 5 µg RXFP3 expression level (Figure 2C). This was also indicated by calculating a hybrid score, *i.e.* the number of input dataset proteins associating with the target PPI database protein multiplied by the negative log₁₀ of the enrichment probability, evidenced by the greater numbers of DDR-associated PPI proteins found (Figure 2D) as well as the total sum of the hybrid scores for DDR-associated PPI proteins associated with the different RXFP3 protein datasets (Figure 2E).

In a previous study, we demonstrated that when investigating novel GPCR-based signaling paradigms it is possible to assess selective signaling specificity using comparisons of empirical data with mass analysis-based 'theoretical' signaling datasets [17]. To this end, we created a GIT2-specific signaling set in an analogous manner to our previously created arrestin-signaling datasets [17], by isolating the intersection dataset between 'Cellular Signaling' and 'GIT2' associated text matrices (Figure 3A: Supplementary Table 7–9). This concatenated Latent Semantic Analysis (LSA)-based dataset comprised 760 GIT2-Signaling proteins. Initially we found that with canonical signaling pathway analysis (Supplementary Table 10) of this 'theoretical' dataset, a strong signaling pathway phenotype reminiscent of known GIT2 signaling capacities was apparent, *i.e.* cytoskeletal control, GPCR signaling, immune function,

stress responses as well as cell cycle and metabolism regulation [13, 51, 52] (Figure 3B). This GIT2-reminiscent mechanistic interpretation of our ‘theoretical’ GIT2 signaling dataset, strongly reinforces our unbiased informatics approach to aid novel signaling paradigm investigation. Furthermore, upon inspection of some exemplars of the significantly enriched pathways (Ingenuity Pathway Analysis-based) within this theoretical dataset, we not only demonstrate specific GIT2-associated activities, e.g. ‘Actin Cytoskeleton Signaling’ [53], ‘Breast Cancer Regulation by Stathmin

I’ [11] and ‘Mitochondrial dysfunction’ [13], but also novel functions, e.g. ‘Sirtuin Signaling’ and ‘Relaxin Signaling’ (Figure 3B). We then compared the overlap between this theoretical GIT2 dataset and the diverse RXFP3 expression levels, to help identify any potential biases towards GIT2-associated signaling functionality (Supplementary Figure 2B). Calculating both the numerical and percentage overlap of distinct RXFP3 expression range, we found that the strongest intersection with the theoretical GIT2-signaling set occurred with the 5 μ g RXFP3 expression level (Figure 3C).

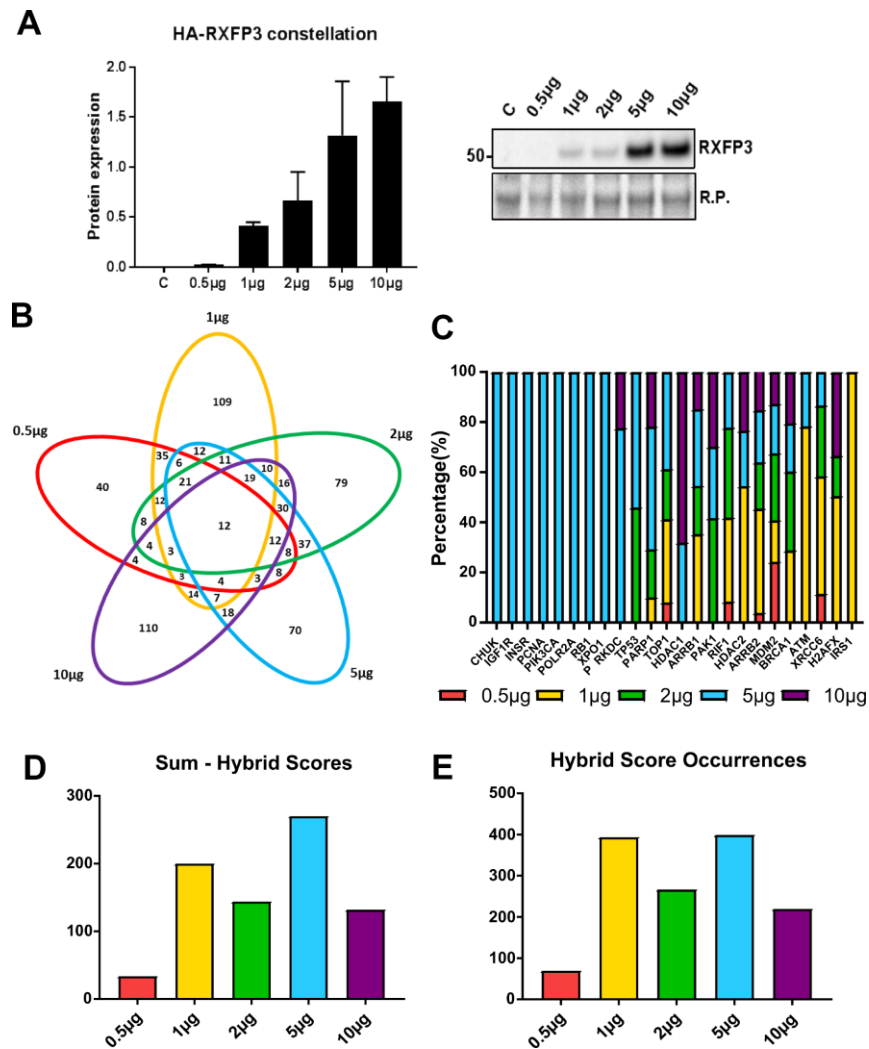


Figure 2. 5 μ g of RXFP3 overexpression indicates a role in the DNA damage response. (A) Western blot validation of the differential overexpression curve for RXFP3-HA (n=3). We see a clear increase of RXFP3-HA signal with an increased level of transfections. (B) We then selected the proteins unique to each overexpression level using a InteractiVenn for further investigation, obtaining the following percentages of uniquely-regulated proteins: 0.5 μ g RXFP3 21.8% unique; 1 μ g RXFP3 – 37.2% unique; 2 μ g RXFP3 26.6% unique; 5 μ g RXFP3 25.2% unique; 10 μ g RXFP3 40.8% unique. (C) Applying protein-protein interaction (PPI) pattern analysis through Enrichr, we were able to show a strong representation for DNA damage repair and energy metabolism-related proteins across the different RXFP3 expression ranges. We also observed a strongest PPI dataset enrichment for DNA damage response proteins for the 5 μ g RXFP3 expression level. (D–E) We next calculated the number of input dataset proteins associated with the target PPI database protein multiplied by the negative log₁₀ of the enrichment probability, or hybrid score. We see that for the (D) sum and the (E) total sum of hybrid score occurrences, the enrichment for DDR-associated factors was shown to be most profound for the 5 μ g RXFP3 level.

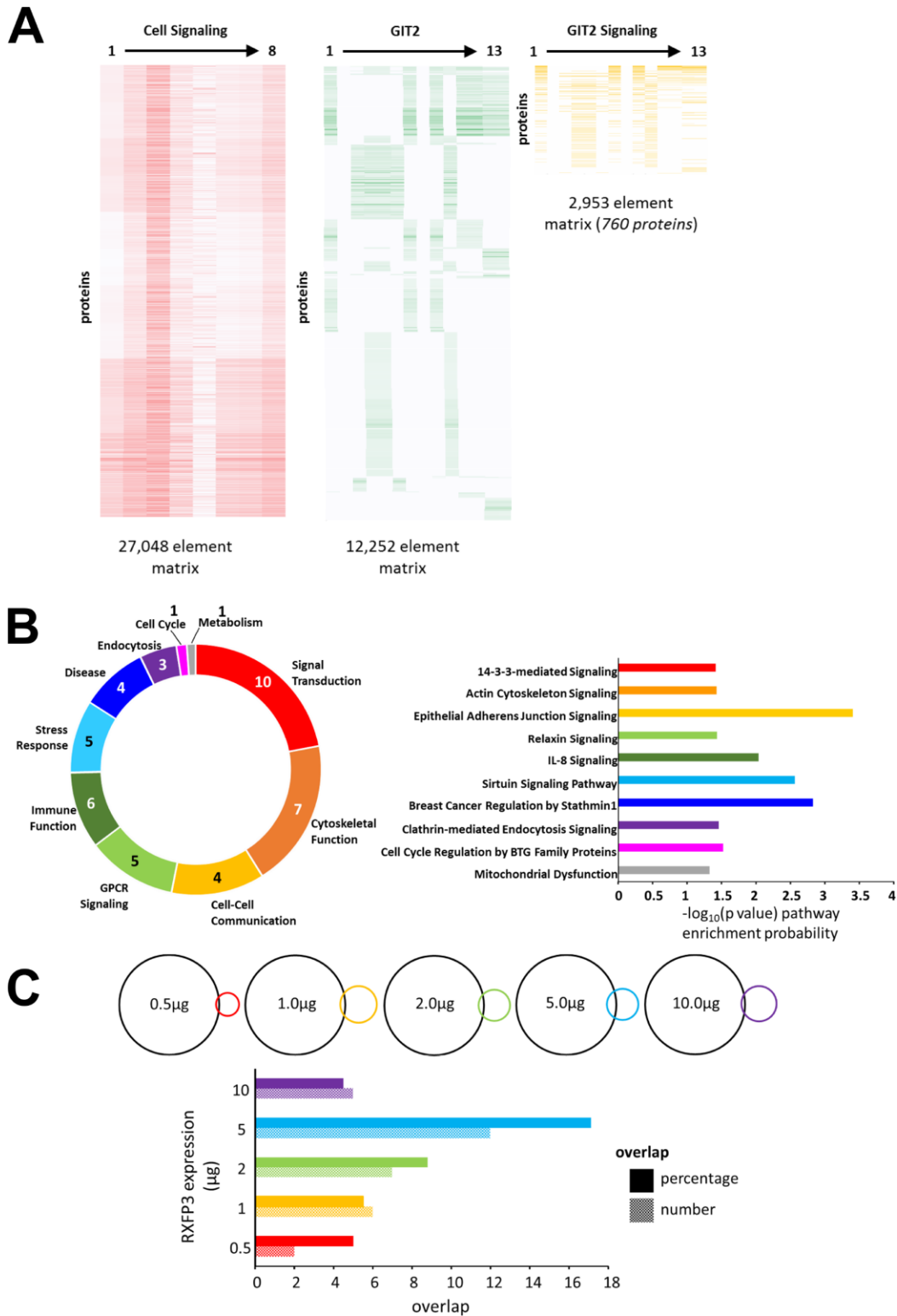


Figure 3. RXFP3 constellation comparison to a theoretical GIT2-Cell signaling dataset. (A) To further investigate the role for RXFP3 as a controller for GIT2, we created a GIT2-specific signaling set, comprised out of 760 proteins, by investigating the intersection dataset between ‘Cellular Signaling’ and ‘GIT2’ associated text matrices. **(B)** Analysis of this theoretical GIT2-signaling set using canonical signaling pathway analysis shows a strong recollection of the known GIT2 signaling capacities. But interestingly some other novel functionalities were also apparent such as Sirtuin Signaling and Relaxin Signaling. **(C)** Lastly, we investigated which overexpression level of the RXFP3 constellation showed a potential GIT2-associated bias. Calculating both the numerical and percentage overlap, we found that the strongest intersection with the theoretical GIT2-signaling set was clear with the 5 µg RXFP3 level.

From our unbiased multidimensional ‘constellation’ analysis it was clear that a strong phenotype related to the protection of nucleic acids was observed. To further investigate this, we then focused on two levels of RXFP3 expression – one relatively innocuous 0.5 μg (allowing ectopic expression to occur without the introduction of a profound cellular phenotype), and the second being the 5 μg level that was strongly associated with DNA protection activity. Protein expression patterns significantly regulated in response to 0.5 μg and 5 μg of RXFP3 overexpression were co-analyzed using Gene Ontology (GO) term enrichment analysis (Supplementary Figure 2C), demonstrating the presence of common (RNA binding, cadherin binding) as well as distinct (transmembrane transport activity – 0.5 μg ; Double stranded DNA binding – 5 μg) significantly enriched GO term groups (Figure 4A). The strongest clustering proteins at the 0.5 μg RXFP3 level were associated with mitochondrial activity (ATP5C1) and RNA methylation (YTHDF3, YTHDF2) – while in response to the 5 μg RXFP3 expression level, strongly clustering proteins were associated with DNA damage/repair (TOP1), stress responsiveness (HMGB1) and cell senescence (HMGB2). Using the natural language processing informatic platform Textrous! [54] (Supplementary Figure 2D), we also found a strong functional divergence between these two datasets, *i.e.* the lower level of expression was associated with histone and microtubular function while the 5 μg RXFP3 expression level again was strongly associated with DNA repair activities. The WriteWords phrase frequency counter was used (Supplementary Figure 2D) to extract the top 4 highest frequency phrases from Textrous! visualized in Figure 4B, 4C. Given these results and our PPI enrichment analysis results (Figure 2) we next decided to further investigate the physical interactome of the human RXFP3 receptor in control and aging stress-associated conditions.

Aging-related cellular stress alters the physical RXFP3 interactome

As complex signal transduction occurs through the dynamic modulation of PPIs [55], especially with respect to receptors [37, 56, 57], we next analyzed the nature of the proteins which physically associate with RXFP3, and how these interactions are modulated in response to oxidative stress (peroxide-induced) and DNA damage (CPT-induced). Using western blotting and confocal microscopy we observed the presence of DNA damage foci in the nucleus, specifically demonstrated by γ -H2AX as well as the increase of phospho-ATM – both these factors indicate DNA damage and DDR (Supplementary Figure 4A) [58, 59].

Employing a cellular SILAC (Stable Isotope Labeling with Amino Acids in Cell Culture)-based affinity

purification-mass spectrometry (AP-MS) approach, we were able to identify and quantify the potential interacting proteins that may represent components of the RXFP3 interactome. Three AP-MS RXFP3 interactomes were extracted, *i)* control interactome ‘Control’: E.V. *vs.* RXFP3 no stress ($n=3$); *ii)* oxidative stress interactome ‘Ox Stress’: E.V. *vs.* RXFP3 stressed with 100 nM H_2O_2 for 90 minutes ($n=3$); and *iii)* DNA damage interactome ‘DNA damage’: E.V. *vs.* RXFP3 stressed with 1 μM of CPT for 3 hours ($n=3$). We then compared the different protein compositions of these interactomes and investigated the proteins unique to each condition (Figure 5A, proteins are listed in Supplementary Table 2). In control conditions we reliably observed 47 distinct RXFP3 interacting partner proteins (Figure 5A – Supplementary Table 11). Among these control condition interacting proteins, we found several that were strongly associated with DNA stability management, *e.g.* EIF4A1 [60], RPS27A [61], MAP4 [62] and PHB [63]. Upon the introduction of the two age-related perturbagens, H_2O_2 and CPT, we found a profound increase – potentially due to a functional stabilization of the interactome complexes [64] – in the size of the stress-associated RXFP3 interactomes (Figure 5A). In response to peroxide exposure, multiple factors linking oxidative stress to DNA damage management and senescence were found to physically associate with RXFP3 receptorsomes including PRDX6 [65, 66], PCNA [67, 68], FUS [69], RBMX [70], PARP1 [71], PRDX1 [72–74], SOD1 [75, 76], LDHB [77] and YBX1 [78]. In response to a DNA damaging perturbagen, multiple factors linking cellular stress to DNA damage management, senescence and organismal longevity were also found to be physically associated with RXFP3 receptorsomes, including PHB2 [79–82], TRAP1 [83, 84], AIMP1 [85, 86], KPNA2 [87, 88], TUFM [89], EMD [90, 91], MAT2A [92, 93], NONO [94–100], IGFBP2 [101–103], SNRPA1 [104], HNRNPF [105], FAM98A [106] and ELAVL1 [107–110]. It is likely that during pathological aging, the generation of oxygen radicals, *e.g.* ROS, precedes the eventual DNA damage that is induced by this ongoing oxidative stress [111], which is what our results demonstrate. These data indicate that, with respect to PPI-associated signaling events, RXFP3 can be ‘activated’ or stabilized into distinct states by aging-associated stress and thus dynamically modifies its stable interactome profile.

To further investigate this dynamic receptorsome aspect of RXFP3 biology (Supplementary Figure 5), we performed unbiased natural language processing analytics to generate a gestalt appreciation of the distinctive phenotypes of the stress-associated RXFP3 interactomes (Supplementary Figure 5A). Applying the collective processing mode of Textrous! to the specific

RXFP3 interactomes we found that the extracted words with the strongest association frequency to the entire peroxide-induced interactome dataset (measured using WriteWords) were all linked to DNA damage repair

processes (Figure 5B), while the CPT-induced RXFP3 interactome, was linked to cell cycle regulation – indicative of potential senescent related behavior (Figure 5B). Using noun-phrase chunking platform of Textrouis!

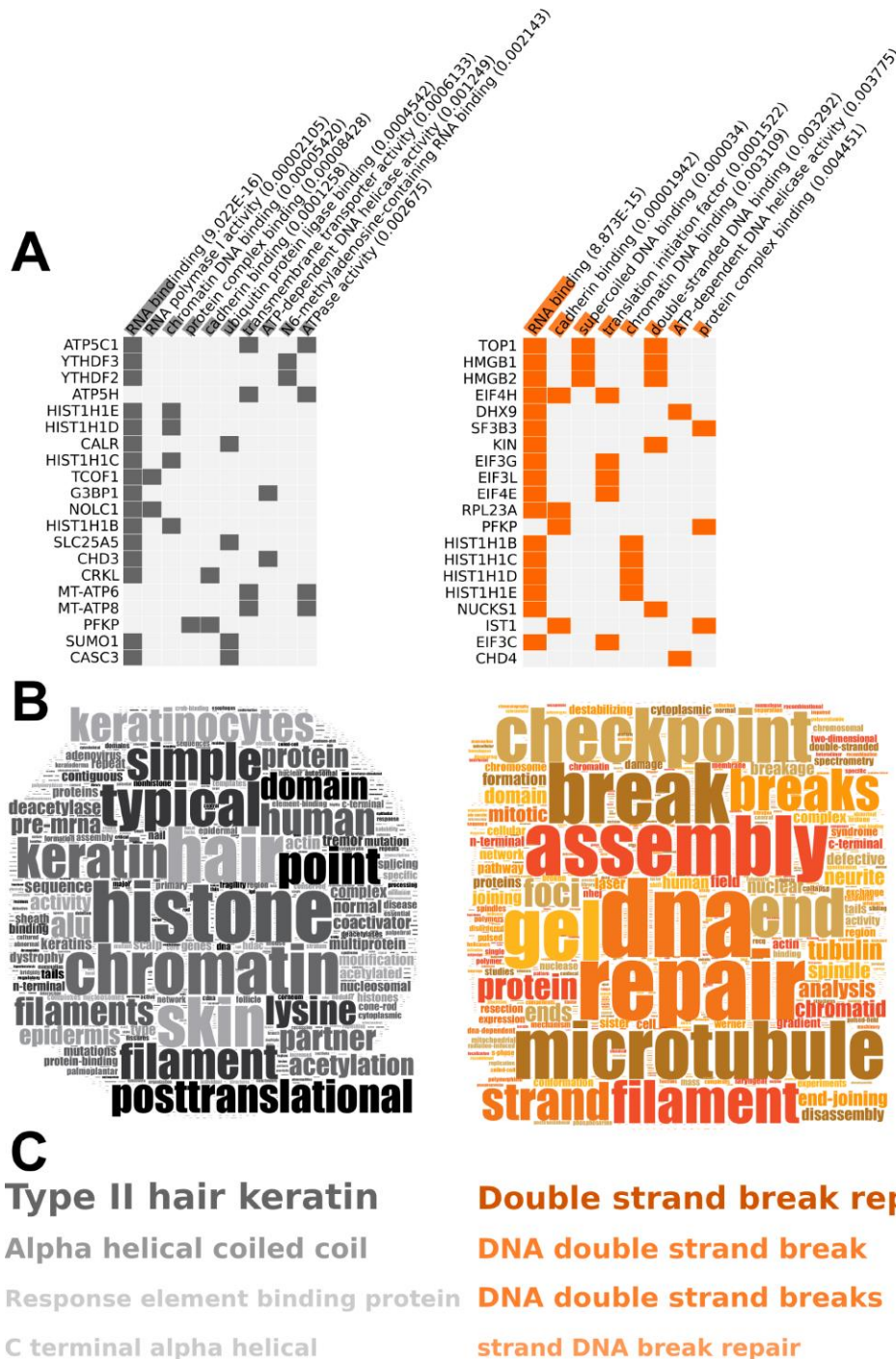


Figure 4. RXFP3 constellation, differential overexpression of RXFP3 indicates a role in DNA damage response. (A–C) The results from the bioinformatic analysis of 0.5 µg RXFP3-HA (Left, grey), and 5 µg RXFP3-HA overexpression (Right, orange) using (B) Gene Ontology through Enrichr [50]; (C) Wordcloud generation and (D) phrase frequency counting (WriteWords) of the words and noun-phrases extracted from Textrouis! [54]. Here we see that a different overexpression level of RXFP3, indicates a different role of RXFP3, where with 0.5 µg RXFP3 we see a role in translation, and chromatin structure, while for 5 µg RXFP3 overexpression a role for DNA damage response and repair.

[54], allowing more natural syntactic interpretations of the interactome datasets, we again demonstrated a DNA damage versus cell cycle regulation distinction between peroxide- or CPT-induced interactomes (Figure 5C). Inspecting the specific agglomerative wordcloud structures for the control (Figure 5D) RXFP3 interactome bore a strong association with

neurodegenerative conditions such as dementia, and more specifically frontotemporal dementia, that are strongly associated with age-related damage accumulation [112] suggesting a basic and fundamental role of RXFP3 systems in age-related disease. The RXFP3 interactomes stabilized by peroxide (Figure 5E) or CPT (Figure 5F) treatment again revealed a strong bias towards DNA

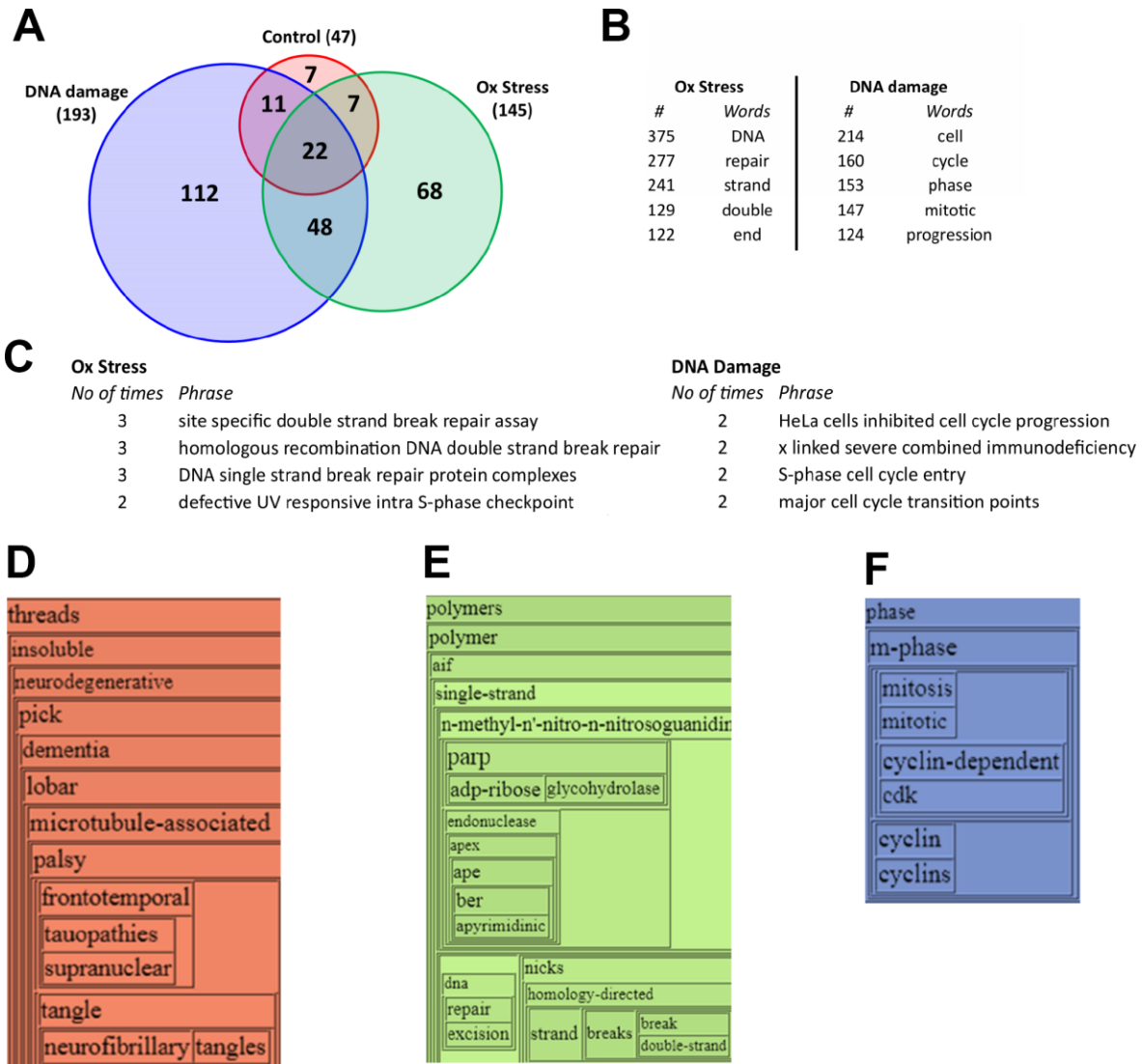


Figure 5. Initial analysis of the unique RXFP3 interactomes under stress conditions indicates a role in DNA damage response and cell cycle control. (A) VennPlex analysis of the different RXFP3 interactomes, RXFP3 without stress (control; orange) (n=3), RXFP3 in response to Oxidative stress using 100 nM hydrogen peroxide for 90 minutes (Ox Stress; Green) (n=3), and DNA damage using 1 μM of camptothecin for 3 hours (DNA damage; blue) (n=3). For further analysis, the proteins unique to Oxidative stress and DNA damage were used for further analysis using *Textrousl!* (textrousl.irlp.nia.nih.gov), which employs latent semantic indexing to achieve an easy and unbiased appreciation of our data, supplying a list of words and noun-phrases related to our dataset. Further analysis of these wordlists using WriteWords (<http://www.writewords.org.uk>), enabled us to count the most prominently present (B) words, and (C) noun-phrases associated to the specific datasets, from this it becomes clear that RXFP3 interacts with proteins involved in DNA damage response (Oxidative Stress) and Cell cycle control (DNA damage) in response to stress. Next, we extracted the hierarchical wordcloud from Textrousl!, where we see the specific words for (D) Control, indicating a role in control of neurodegenerative disorders such as Alzheimer’s disease and frontotemporal dementia (FTD), (E) Oxidative Stress, again indicating an association with DNA damage repair; and (F) DNA damage, indicating a connection to cell cycle control.

damage repair and cell cycle regulatory behavior respectively. Further adding to the connection between RXFP3 biology and its ability to interact with cell cycle machinery, we indeed found that the RXFP3 can physically interact with mitotic spindle structures (Supplementary Figure 4B), thus potentially revealing an additional role of the RXFP3 in anti-aging and Senescence Associated Secretory Phenotype (SASP)-associated mechanisms [113, 114] that have also been linked previously to GIT2 functionality [13, 15].

Stress sensitive RXFP3 network analysis

Using the specific and consistent peroxide- (Figure 6A, 6B) or CPT-induced (Figure 6C, 6D) RXFP3 interactome protein datasets, we investigated the potential dynamic physical networks of these proteins using the Network Analyst platform (Supplementary Figure 5C) [115]. We employed both generic (non-tissue specific) and hypothalamic-specific datasets (given the initial identification of GIT2 as an aging keystone in this tissue) as background databases to generate statistically-significant interaction networks for KEGG pathway enrichment (Figure 6A, 6C) and Gene Ontology (GO; biological process; Figure 6B, 6D). At the level of both GO and KEGG pathway enrichment, the use of either background databases resulted in highly similar enriched GO terms and KEGG pathways. For GO analysis the percentage overlap of hypothalamic (Supplementary Table 12 (Peroxide) – Supplementary Table 13 (CPT)) vs. generic tissue (Supplementary Table 14 (Peroxide) – Supplementary Table 15 (CPT)) was 72.1 and 87.1% for peroxide- and CPT-induced interactomes respectively. At the KEGG pathway level, these same analytical values were 56.5 and 45.5% respectively for KEGG analysis of peroxide or CPT effects.

Using the peroxide-induced RXFP3 interactome we found that at the KEGG pathway level (Supplementary Table 16 (Generic) – 17 (Hypothalamic)) the interacting protein network was strongly associated (indicated by significant pathway enrichment values) with DNA protection management (Base Excision Repair $p=0.0403$; Mismatch Repair $p=0.0206$), cell cycle control (Cell Cycle $p=0.0319$), energy management diversity (Glycolysis/Gluconeogenesis $p=0.028$) and lifespan (Longevity Regulating Pathway $p=0.022$; Figure 6A). Using GO biological annotation of the peroxide-induced RXFP3 interactome network we found that this protein cluster was strongly linked to DNA integrity management (Response to DNA Damage Stimulus $p=0.00702$; Base Excision Repair $p=0.0319$) and age-associated oxidative damage (Response to Oxidative Stress $p=0.0079$; Aging $p=0.0346$) (Figure 6B). Performing similar KEGG pathway analysis of the CPT-induced RXFP3 interactome (Supplementary

Table 18 (generic) – 19 (hypothalamic)) we again found a strong aging-associated network phenotype of proteins, *i.e.* a strong representation (indicated by significant pathway enrichment values) of KEGG pathways associated with cell cycle control (Cell Cycle $p=0.0455$) and age-associated tissue pathology (Cellular Senescence $p=0.0297$; Necroptosis $p=0.0311$) (Figure 6C). GO biological process analysis of the CPT-induced RXFP3 interactome supported these results, *i.e.* energy diversification (Mitochondrion organization $p=0.00854$) and stress resilience (Response to DNA Damage Stimulus $p=0.00000159$; Cellular Response to Stress $p=0.000377$) (Figure 6D). Upon meta-analysis of these GO/KEGG annotations we found that for the oxidative stress RXFP3 interactome, the most dominant interacting protein factor was proliferating cell nuclear antigen (PCNA), through multiple (6 independent associations) links to different annotations (both GO and KEGG). In a similar manner, in response to CPT the most multidimensional factor (5 independent associations) linked to multiple significant annotations was cyclin-dependent kinase Inhibitor 2A (CDKN2A). Recent evidence has shown that one of the most specific functions of PCNA is to control the oxidative stress sensitivity of cells in concert with DNA damage repair mechanisms [116]. CDKN2A is an active connector between oxidative and DNA damage [117] with cellular senescence/pathological aging programs [118, 119]. The dynamic physical interaction of RXFP3 with these key factors in stress-related aging mechanisms underpins the potential importance of RXFP3 system in pathological aging.

Comparative interactome analysis

To simplify the following analysis, we combined the peroxide- and CPT-induced RXFP3 interactomes to make one generic ‘stress’ interactome (Supplementary Figure 5B). We then compared the RXFP3 ‘control’ and combined ‘stress’ datasets to each BioGRID-derived protein interactomes. We extracted specific curated physical interactome database entries from BioGRID version 3.5, for well-known oxidative stress (G3BP1 – 299 proteins, SIRT1 – 251 proteins, SOD1 – 294 proteins) and DDR (PRKDC – 283 proteins, H2AFX – 300 proteins, MDM2 – 299 proteins, MDC1 – 198 proteins, TP53 – 300 proteins, BRCA1 – 301 proteins) proteins (Supplementary Table 20), to assess the potential PPI-based functionality of RXFP3 receptorsomes (Supplementary Figure 5D). To control for the differences in numerical size between the ‘control’ (47 proteins) and ‘stress’ RXFP3 interactome (268 proteins) we also employed multiple ($n=3$) randomly generated (www.molbiotools.com/randomgenesetgenerator.html) protein datasets (47 for ‘control’ RXFP3 and 268 for the ‘stress’ RXFP3 interactome) for comparative interactome

analyses. We found that with both the ‘control’ and ‘stress’ interactomes, versus the random datasets, there were considerable functional overlaps with many of the aging/metabolism BioGRID interactome datasets (Figure 7A, 7B). The largest overlap was seen for G3BP1 (G3BP Stress Granule Assembly Factor 1), H2AFX (H2A Histone Family Member X), and BRCA1 (BRCA1, DNA repair associated) (Figure 7A). As an additional workflow control for this comparative interactome experiment we created an extra list of proteins relatively unrelated to aging and DNA damage (CNTRL, CRP, LONP2: ‘Non-stress’), where we clearly see a minimal overlap compared to the oxidative stress and DNA damage proteins (Figure 7B). The large overlap seen for

all these proteins indicates an important regulatory role for RXFP3 in stress response. How this correlates to aging and age-related disorders was analyzed next.

We extracted available meta-data for several age-related disorders and non-age-related disorders from GEN3VA [120] and compared these to our interactome datasets (Figure 7C, 7D; Supplementary Figure 5E). We extracted datasets for classical Aging, Schizophrenia, in fact a potential aging-associated disorder [121] and non-specifically age-associated condition, *i.e.* aortic aneurysm as a control to assess whether the protein overlap is specific (Supplementary Table 21). As can be seen in Figure 7C and 7D, the numerical protein overlap with

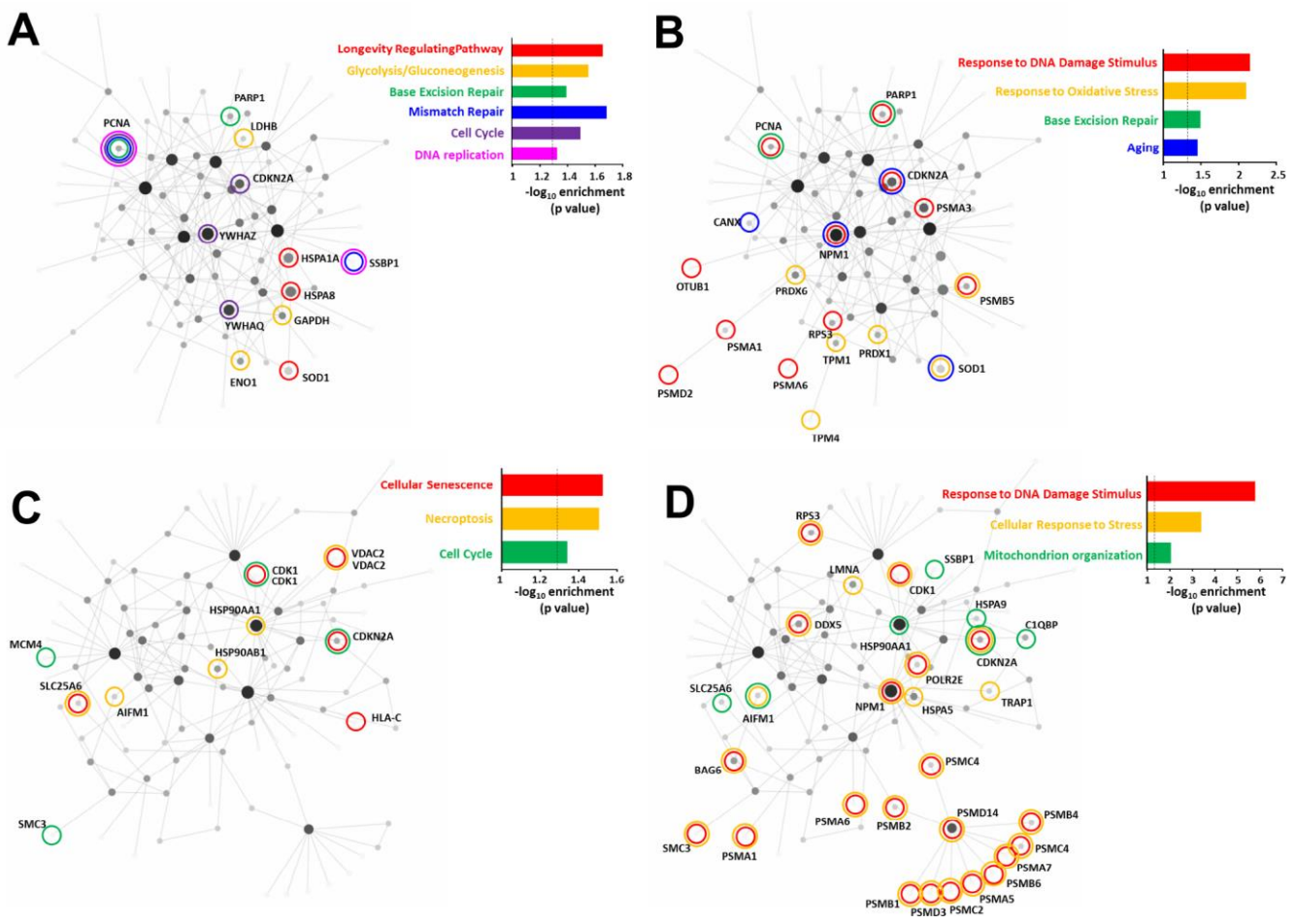


Figure 6. Comparison of the oxidative stress and DNA damage RXFP3 interactome indicates roles in age-related processes. Using the specific and consistent peroxide (A, B) and CPT-induced (C, D) RXFP3 interactome datasets we investigated the potential of these proteins to form a network using NetworkAnalyst. To generate statistically-significant interaction network KEGG enrichment (A and C) and Gene Ontology – Biological process (B and D) analysis were performed. Using both generic and hypothalamus-specific backgrounds resulted in highly similar enriched GO terms and KEGG pathways. Using the peroxide-induced RXFP3 interactome we found that the interacting protein network was (A) strongly associated with DNA protection management, cell cycle control, energy metabolism, and lifespan at the KEGG pathways level, (B) while at the GO biological annotation, we also see a strong connection to DNA integrity management, and additional age-associated oxidative damage. (C) Using the same KEGG pathways analysis on the CPT-induced interactome we again found a strong network phenotype associated with aging, *i.e.* cell cycle control, and age-related tissue pathology. (D) GO biological process analysis showed a strong association with pathological aging responses, such as energy diversification and stress resilience.

‘Aging’ is larger than the other two datasets, where 64 of the combined RXFP3 ‘stress’ dataset show overlap, which is 23.88% of the total RXFP3 ‘stress’ set. Perhaps not completely unsurprising [121], we also see a strong overlap with ‘schizophrenia’, *i.e.* 54 proteins, or 20.90%. We see only one protein overlapping with ‘aortic aneurysm’ for the RXFP3 ‘stress’ dataset, namely PHGDH (Phosphoglycerate Dehydrogenase) and none for the RXFP3 ‘control’ set. These results gained from human curated dataset collections further support our hypothesis that RXFP3 may play a role in aging and the related disorders.

Lastly, we used the Latent Semantic Indexing (LSI)-based informatic platform GeneIndexer [122], to interrogate our RXFP3 ‘control’ and ‘stress’ datasets with the following age-related syntactic concepts (Aging): *Neurodegeneration, Cognitive impairment, Senescence, Parkinson's Disease, Amyotrophic lateral sclerosis, Alzheimer's Disease*; and non-age-related terms (non-Aging): *Tuberculosis, Spina Bifida, Asthma, Tourette syndrome, ADHD, Achondroplasia* (Figure 8A, 8B; Supplementary Figure 5F). Using this, we were able to assess the (RXFP3 ‘control’ (Supplementary Table 22) or ‘stress’ (Supplementary Table 23)) strength of

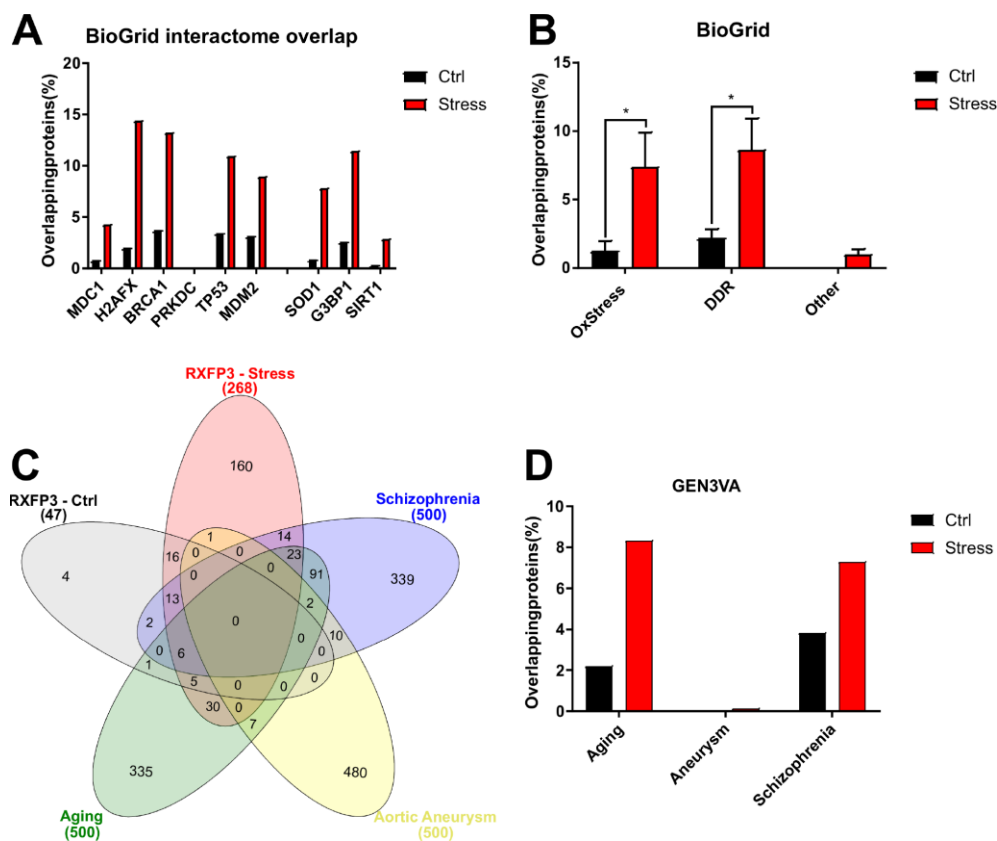


Figure 7. RXFP3 interactome analysis using BioGRID extracted interactomes and GEN3VA extracted signatures, a first indication of a role in Aging. Using the BioGRID database (<https://www.thebiogrid.org>) the interacting proteins of several known oxidative stress and DNA damage proteins were extracted, and assembled into specific interactomes. (A) Here we show the number of overlapping proteins between the unstressed RXFP3 interactome (Ctrl; black) versus the stressed interactomes (combined both the response to oxidative stress and DNA damage, Stress; Red) and the interacting proteins of DNA damage response/repair proteins (MDC1, H2AFX, BRCA1, PRKDC, TP53, MDM2) and oxidative stress proteins (SOD1, G3BP1, SIRT1). We see that while the RXFP3 interactome in control conditions already shows overlap, this overlap is considerably increased under stress. (B) When we assemble the interactomes of the oxidative stress and DNA damage proteins separately, Ox Stress and DDR, respectively, we again see this greater overlap for the RXFP3 “stress” interactome. When this was repeated for three proteins unrelated to oxidative stress, DNA damage or aging (other), we did not see this overlap. (C) Next, GEN3VA (<http://amp.pharm.mssm.edu/gen3va/>) was used to extract protein signatures pertaining to aging, which is of most interest to us, schizophrenia, of which we hypothesize RXFP3 might be a controlling factor, and as a negative control we extracted protein signatures for aortic aneurysm, where we suspect RXFP3 is not associated with at all. The overlap was visualized using InteractiVenn (<http://www.interactivenn.net>). (D) The overlapping proteins were then visualized in a bar chart, showing the large differences between “ctrl” and the “stress” interactomes of RXFP3. In addition, we see nearly no overlap with the signature for aneurysm, a decent overlap for schizophrenia, and a large overlap with aging. This data not only indicates the large differences between RXFP3 in control versus RXFP3 in stress conditions, but that RXFP3 possible plays an important role in oxidative stress, DNA damage response and aging.

correlation with specific aging- and non-aging related interrogator concepts and the RXFP3 interactome datasets (Figure 8C, 8D), by averaging the different extracted individual protein cosine similarity scores. In this instance we see a larger average cosine similarity score for both RXFP3 datasets with the age-related terms compared to the non-aging interrogation paradigm.

RXFP3 is a possible protective factor against DNA damage

If RXFP3 acts as a regulatory factor for aging-related stress management we hypothesized that, like GIT2 [10, 11], its expression may be directly altered by aging-associated stress perturbations. We compared 24 hours of vehicle to 24 hours of CPT stimulation and saw a significant increase in RXFP3 expression with CPT-induced DNA damage, which was indicated by an increase in γ -H2AX and phospho-ATM (Figure 9A). To assess the potential mechanistic role of RXFP3 in DNA damage repair, we overexpressed RXFP3 in cells prior to stressing the cells using CPT (Figure 9B). We investigated how this RXFP3 overexpression affected the phosphorylation status of DNA damage repair proteins, such as BRCA1, H2AX, ATM and PRKDC. The phosphorylation of BRCA1 is indicative of the cells' attempt to repair and recover from the damage caused [123–125]. The phosphorylation of H2AX, generating the γ -H2AX form, is the first sign of DNA damage, which is dephosphorylated immediately after DNA damage has been repaired. ATM activation mediates DDR through homologous recombination (HR), while PRKDC (also known as DNA-PKc) activates non-homologous end-joining (NHEJ). With the introduction of ectopic RXFP3 expression we observed a decrease in ATM and H2AX phosphorylation, while we observed a concomitant increase in BRCA1, PRKDC phosphorylation (Figure 9B), suggesting that the cellular DNA-reparative process is likely induced with increased RXFP3 expression. When stress is applied to the cells, we observed a clear increase in ATM and PRKDC phosphorylation, while BRCA1 activation was diminished compared to control levels. This data suggests that RXFP3 overexpression likely enhances the cellular stress responsivity to potential DNA damage – in a similar manner previously observed with GIT2 expression potentiation and protection against DNA-damaging insults [11].

In addition to this passive functionality of RXFP3, we tested the DNA-protective ability of RLN3-mediated stabilization of RXFP3. In this experimental paradigm, cell cultures were strongly stimulated with RLN3 (100 nM) for 1 and 2 hours before the introduction of CPT-induced DNA damage. We observed an effective

reduction in ATM, BRCA1, and H2AX phosphorylation, compared to our control conditions. These results indicate that the activation of RXFP3 with its endogenous ligand RLN3 attenuated the potential impact of DNA damage stress and thus may be associated with an augmented cellular protection from stress and thus aid in cellular recovery via a more effective stress resilience mechanism. This relationship between ligand-stimulated RXFP3 and DNA damage recovery proteins was next investigated using confocal microscopy (Figure 9C) and western blotting (Figure 9D). Here we observed a strong decrease in the number of nuclear foci identified using γ -H2AX and phospho-BRCA1 antibodies in conditions where the cells were pre-stimulated with RLN3 compared to the control cells (Figure 9C, D). In addition to this, we investigated the dynamic phosphorylation status of the DNA damage regulating kinase, PRKDC. Here we saw the opposite, PRKDC phosphorylation is higher in RLN3 compared to vehicle control conditions (Figure 9C, D). To assess the potential therapeutic (as opposed to prophylactic) DNA-protecting capacity of RXFP3 activity, we first stressed the cells with CPT and then stimulated them with two doses of RLN3. Similar to our findings in Figure 9D, we see that when administered after the DNA-stressing insult we again revealed the ability of RLN3 to reduce the extent of eventual DNA stress, suggesting that, in addition to a prophylactic DNA-protective capacity, RLN3 can also induce an efficient, post-stress, DNA-damage attenuation therapeutic action (Figure 9E).

DISCUSSION

We investigated the potential connectivity of RXFP3 with the DDR signaling domain. Our previous studies demonstrated that the GPCR scaffolding protein GIT2 likely plays a potent and trophic level regulatory role in the aging process [52]. We have found that GIT2 expression is sensitive to oxidative perturbations [126], normal and pathological aging [9, 13, 127], alterations of dietary energy intake [13], age-related neurodegeneration [33], somatic glycemic and metabolic status [13] and DNA-damaging insults [11]. GIT2 genomic deletion has been shown to disrupt pancreatic beta cell development [13], adipose deposition [127], immune cell migration [53], control cellular senescence as well as attenuate overall lifespan [15]. These multidimensional findings suggest that GIT2 could indeed represent a novel therapeutic target for aging related disorders. One mechanism that is currently being investigated is the synthetic chemical mediated regulation of ADP ribosylation factor GTPase Activating Protein (ARF GAP) enzymatic activity, with the experimental agent QS11 [128]. While small molecules are a simple mechanism to regulate ARF GAP activity, the GIT molecules (both GIT1 and GIT2) are highly

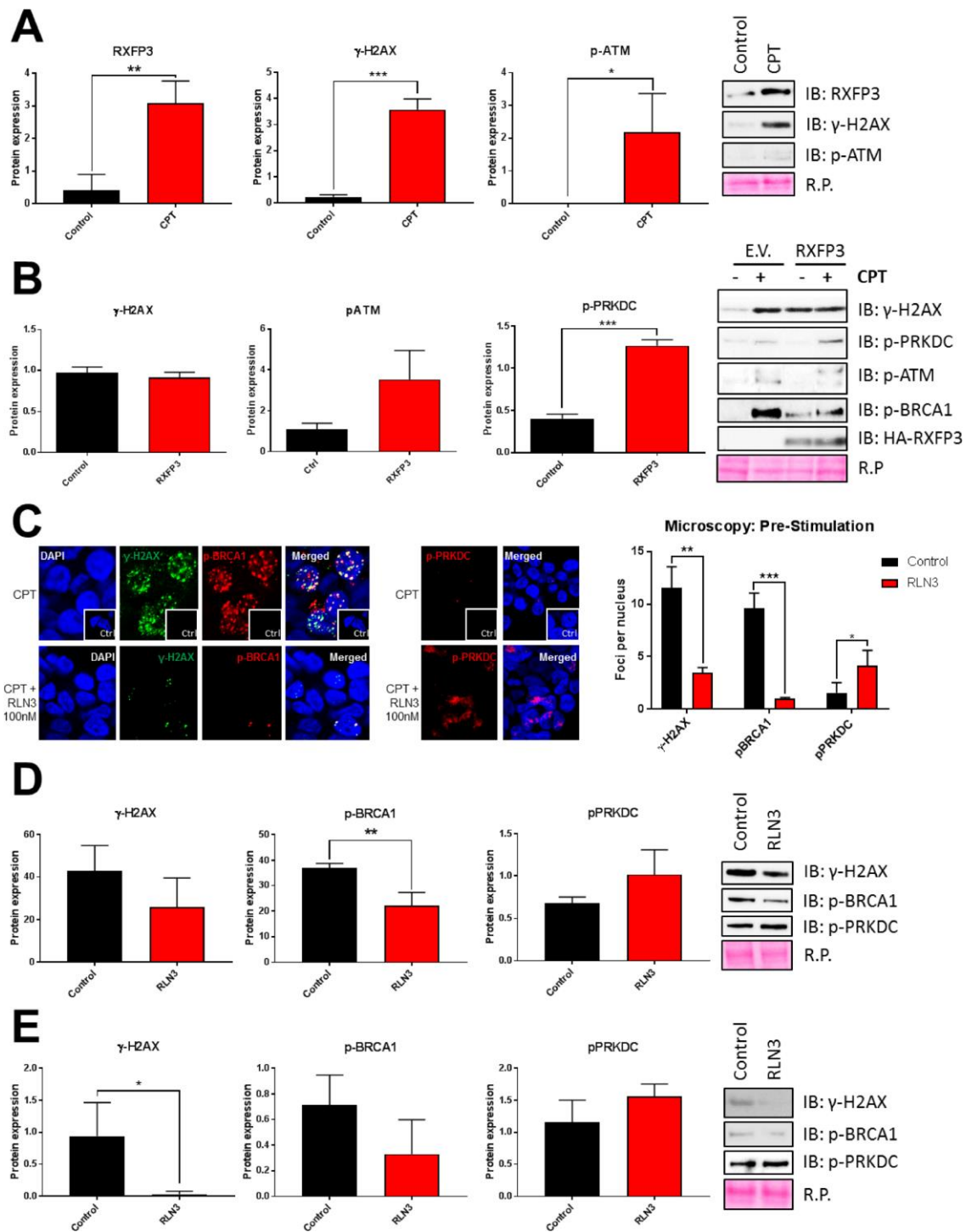


Figure 9. RXFP3 acts as a protective factor of DNA damage. (A) RXFP3 expression increases significantly with DNA damage caused by 10 μ M CPT for 24 hours (n=3). Induction of DNA damage was validated using γ -H2AX and p-ATM. (B) Overexpression of RXFP3 compared to control (E.V.) elicits a specific response of DNA damage-associated proteins in unstressed (CPT-treated) cells. Overexpression of the RXFP3, in the absence of CPT exposure, appears to prepare the cell for stress responsivity as this results in the activation of BRCA1 (p-BRCA1), PRKDC (p-PRKDC), ATM (p-ATM) and H2AX (γ -H2AX). However, we also see a decrease in activation compared to control (E.V.) transfected cells after stress of these proteins, indicating that the RXFP3 potentially facilitates DNA damage repair (n=3). (C) RXFP3 stimulation using RLN3 (100 nM, 1 and 2 hours prior to stress induction using 10 μ M CPT), directly affects the number of γ -H2AX, pBRCA1 and pPRKDC foci (n=30) using confocal microscopy, where we see a specific decrease in γ -H2AX, and p-BRCA1 foci, and an increase in PRKDC activation. (D) These results were also shown using immunoblotting (n=6). (E) Stimulating RXFP3 after stress induction (2 shots, 1 and 2 hours after 3h 10 μ M CPT), here called post-stimulation, induced similar effects (n=6).

interconnected proteomic factors and simple indiscriminate inhibition of enzymatic activity will not likely elicit specific signaling effects. In addition, as GIT2 is a scaffolding protein, as well as an ARF GAP, it is also possible that simple chemical inhibition/modulation of ARF GAP activity, will not control all the additional protein-protein binding functionalities of GIT2. Our work over recent years has demonstrated that in addition to the simple regulation of intermediary cell metabolism events such as calcium mobilization or activation of protein kinases, GPCRs possess a functional efficacy profile that exists at the transcriptional and protein translational level [16, 17, 129-131]. Thus, GPCRs likely possess a translational relationship with signaling factors that they then employ as components in their diverse signaling outputs – hence each signaling molecule possesses an intrinsic priority relationship to their associated GPCRs. In this study, we investigated this potential for linking a cell surface GPCR to intracellular signaling protein GIT2, and to modulate its age-controlling functionality. Thus, we present a novel paradigm for therapeutic drug development and prioritization. Using a genomic deletion model for GIT2 analysis we found that the RXFP3 was reflexively altered in its expression in a coordinated manner with GIT2 (Figure 1). In addition to this expression-based relationship, we also demonstrated that both ectopic expression and ligand stimulation (using RLN3) of the RXFP3 receptor was able to exert an expression level effect (in multiple cell types) upon GIT2, suggesting a close functional synergy between GIT2 and the RXFP3 receptor. The cognate ligand of RXFP3, RLN3, is also termed insulin-like peptide 7 and like insulin, is composed of an A- and B-chain connected by two disulfide bonds [132]. While RXFP3 responds to the binding of its ligand, its amino acid structure (Supplementary Figure 1A, 1B) reveals the presence of a natural modification of the canonical third transmembrane helix (TM3) activity-regulating ‘DRY’ motif - replaced by a ‘TRY’ motif, where the aspartic acid is replaced by a threonine in humans and an alanine in mice. DRY motif disruption typically results in enhanced constitutive active levels in the absence of the cognate orthosteric ligand [36]. In typical class A GPCRs, the DRY motif Asp is bound to a Gln/Glu in TM6 which allows the formation of a salt bridge, creating an ionic lock which is further stabilized by the interaction between the Asp and Arg in the DRY motif itself [133, 134]. This ionic lock, which typically constrains the receptor in an ‘inactive’ state until a ligand is bound, is absent in RXFP3 allowing it to exist in the active conformation [36, 133, 134]. While considerable research has been conducted into how structural alterations can affect constitutive activity levels, these studies were conducted initially in the context of a monodimensional mode of GPCR signaling, *i.e.* through heterotrimeric G

proteins. Subsequent discoveries concerning first β -arrestin [135] and then further multi- [16] and pluridimensional [136] GPCR signaling modes necessitates the application of a nuanced understanding of which multiple output efficacies are constitutively active, and which are not. Within the pluridimensional signaling context, it is likely that a broad receptorsome ensemble [137] is responsible for the multiple modes of receptor signaling. Therefore, the measurement of a single, often soluble second messenger index, is unlikely to reveal a diverse range of efficacy profiles.

Using our ‘constellation’ curve analysis, we correlated such a divergent signaling profile with a ‘theoretical’ GIT2 dataset approach we have pioneered recently to investigate uncharted signaling paradigms [17]. Employing this approach (Figure 3) we found that the RXFP3 expression level most associated with DDR functionalities was also most strongly intersecting (at the protein expression level) with the GIT2-signaling ‘theoretical’ dataset. It is interesting to note that the natural DRY motif mutation in the RXFP3 has been associated with preferences for enhanced receptor internalization. It may be possible therefore that this internalized RXFP3 receptor pool could initiate distinct signaling modalities independent from that emanating from the plasma membrane [138, 139]. In this context, it is unsurprising that such a functional idiosyncrasy may be associated with a protein strongly linked to internalization behavior and microvesicular movement, *i.e.* GIT2 [51]. This theory coincides with the possibility that RXFP3 might be a stress sensor within the cellular interior.

With our RXFP3 constellation expression data we saw a clear suggestion of a role in DNA damage response at 5 μg overexpression level compared to 0.5 μg (Figures 2 and 4; top 15 up and down-regulated proteins in Supplementary Table 24). In addition to these most strongly regulated proteins, we observed proteins that specifically relocate to another cellular fraction, *e.g.* Thioredoxin (TXN2) involved in oxidative stress response [140], translocated from the nucleus to the plasma membrane. Using LSI (Textrou!) we revealed a strong connection between DDR activity and increased RXFP3 expression (Figure 4B). While this may suggest that RXFP3 causes DNA damage, we hypothesize, that increased expression of RXFP3 prepares the cells for damage. Therefore, RXFP3 activity may enhance innate cellular resilience and thus engender an augmented, more sensitive response mechanism to DNA damage, which was supported by the elevation in RXFP3 expression after DNA damage (Figure 9A), which may be a response of the cell to prepare for the presence of incipient damage and thus responds by enhancing its coterie of interacting DDR proteins. In turn, our data

also demonstrates that RXFP3 interacts with many proteins involved in the DNA damage response and repair process (Figure 5).

As signaling proteins are unlikely to exist as discrete unitary entities, it is now widely accepted that the formation of coherent and co-functional protein complexes lies at the basis of nearly each physiological and pathophysiological process [141–143]. Our AP-MS investigation into the dynamic RXFP3 interactome was interrogated using multiple unbiased approaches (Figs. 5-8) to generate an accurate gestalt appreciation of this signaling entity. From a receptor-based point of view our current research was primarily focused on the augmentation of our understanding of molecular interactomes in a high-dimensionality manner, *i.e.* focusing on proteins as a collective functional group rather than focusing down specifically on one protein in a more reductionist manner [144–146]. Hence, while not focusing in-depth on specific protein-protein interactions, albeit an entirely valid scientific endeavor, here we chose to appreciate molecular signaling at a more collective, gestalt, level [147–149]. Our follow-up manuscript on this topic, addresses in a combinatorial manner both a low-dimensionality (*i.e.* specific protein-protein interaction analysis) and high-dimensionality data analysis of DNA-repair complexes linked with this receptor system. Hence, the most effective appreciation of GPCR associated signaling dynamics will likely emerge from such synergistic approaches.

We found a potent link between RXFP3 and a role in DNA damage response and repair, cell cycle control and potentially even cell senescence regulation. We identified multiple proteins related to senescence, *e.g.* CDKN2A [150, 151], LMNA [152], PARP1 [153], PSMA5 [154], and PHB [155]. Senescence occurs naturally during embryonic development and recently it has received considerable attention through its potential role in the development of age-related disorders. Senescent cells arise due to replicative telomeric attrition or stress-associated cellular damage and can have either an unfavorable or beneficial impact on tissues and organs depending on the cell type and metabolic state. As senescent cells amass in tissues with progressing age, they have been connected to many aging declines and diseases [150]. CDKN2A (p16)/RB (Retinoblastoma-associated protein) directs one of the two pathways which is responsible for the initiating and maintaining cellular senescence programs, where CDKN1A or p21 together with p53, a consistent GIT2-interacting protein [11] directs the other [150].

BioGRID was used to compare the interactome of RXFP3 to known oxidative stress and DDR proteins (Figure 7). A large interactome overlap was found for

several canonical DDR proteins, (MDC1 [156]; H2AFX - [157, 158]; BRCA1 [159, 160]; PRKDC [161], TP53 [162], MDM2 [160]) and anti-oxidative stress associated proteins (SOD1 [163]; SIRT1 [164, 165]; G3BP1 [166]). MDC1 is recruited to the double strand break (DSB) sites [156] after the initiation of the signaling cascade caused by these lesions, which starts with the phosphorylation of H2AX, generating the γ -H2AX species. The interaction between MDC1 and γ -H2AX allow for binding and retaining of additional DDR factors at DNA damage sites including GIT2 and BRCA1 [12, 167]. With DNA damage, p53 expression elevates significantly in cells and functions as a transcription factor to control the expression of proteins that coordinate the DDR related post-translational modification of the E3 ubiquitin ligase MDM2, which may act as the master regulator of p53 [160]. BRCA1 is a tumor suppressor gene, which contributes to DNA repair and transcriptional regulation in response to DNA damage, and protects the genome from damage. In addition, this repair protein regulates the transcription of proteins involved in the repair of DNA. Lastly, PRKDC is recruited to DSBs and aids in the repair of DNA via NHEJ, interacts with the GIT2-interactor p53 and appears to play a pivotal role in DNA repair in non-proliferating cells [168].

SOD1 scavenges ROS such as superoxide radicals produced in the body, thus playing a vital role in oxidative stress and lifespan management [169–171]. SIRT1, similar to SOD1, is an oxidative stress-sensitivity [172] and longevity regulator that has stress attenuation functions in vascular endothelial and neuronal cells, indicating a role in cardiovascular and neurodegenerative disorders. G3BP1, while not directly related to oxidative stress, is important in stress granule formation in response to this oxidative stress. Cells have two methods following exposure to environmental stress, *i)* induce apoptosis, *ii)* inhibit apoptosis and repair the damage induced by stress. These two options minimize cell loss, while preventing the damaged cells, with abnormal DNA and protein changes [173–175]. Stress granules control these two alternatives and this antioxidant activity is partially regulated by G3BP1 [176, 177].

The overlap over RXFP3 with these proteins related to oxidative stress and subsequent stress granule (SG) formation – which is also associated with senescence mechanisms [166] piqued our interest. SGs are formed by RNA binding proteins which consolidate important transcripts required to maintain cell viability during the presence and after the alleviation of stress [178]. In this context in our constellation data we found that SOD1, ATXN2 and G3BP1 were seen to be specifically translocated from the nucleus to the cytoplasm in response to RXFP3 overexpression. In addition, we

have shown that RXFP3 interacts with SOD1 and G3BP1 proteins in response to oxidative stress and DNA damage, respectively, using AP-MS. This in combination with the considerable overlap of the RXFP3 and the curated SOD1 and G3BP1 interactomes, supports our hypothesis that RXFP3 acts as a stress sensor and then controls translation of DDR proteins and interacts with these SGs in order to protect the cell from potential harm. However, further investigation into this role of RXFP3 as an oxidative stress sensor and responder will be the subject of further studies.

Using GEN3VA-based curated data we were able to establish independently that there may be a role for RXFP3 in aging, and a new potential role was found for RXFP3 in the development of schizophrenia (Figure 7), a mental disorder characterized by delusions and hallucinations [179] that is being increasingly associated with pro-aging mechanisms [121]. One of the plausible underlying mechanisms for schizophrenia is a disruption in dopaminergic neurotransmission, possibly due to oxidative stress [180]. While this connection between RXFP3 and schizophrenia has previously not yet been made, as RXFP3 plays a potential role in dopamine transmission [181] and protection against oxidative stress, shown in this paper, this association with schizophrenia is not entirely surprising. Reinforcing this point we have also recently shown that in pro-aging murine models areas of the central nervous system whose dopaminergic connectivity is affected also show deficits in both GIT2 and RXFP3 expression [33].

Following our molecular investigation of RXFP3 at the dynamic interactome level we have demonstrated that stimulation of the RLN3/RXFP3 system in cells, appears to be protective against DNA damage. Both prior to stress or following stressor exposure, RLN3 application decreased the phosphorylation of H2AX and BRCA1, while increasing PRKDC phosphorylation. This shows that RLN3 is a protective factor prior to damage, indicating it could possibly be used as a DNA-damage protecting agent.

Furthermore, BRCA1 is bound and phosphorylated by ATM kinase [125, 182], as well as G2/M control kinase, CHK2, and potentially many other kinases [183]. Further investigation has shown that BRCA1 is involved in complexes that promote and activate the repair of DSB and initiate HR. This is supported by the co-localization and interaction with important DDR proteins such as Rad51 [184], Rad50, MRE11 [185, 186], ATM [125, 182], H2AX [187, 188], and p53 [183]. Lastly, BRCA1 and PARP, whilst involved in completely different response and repair mechanisms, appear to cooperate to repair DNA damage [189]. In addition, and underlining the role of DDR processes in neurodegenerative aging, BRCA1 has

also been recently implicated in AD [190]. Many of these stress repair proteins, *i.e.* H2AX, GIT2, PARP, BRCA1, and ATM, have been shown to be of importance in both here with the RXFP3 paradigm and our previous GIT2 signaling findings, *i.e.* GIT2 is phosphorylated by ATM upon DNA damage and form complexes with DDR-associated factors such as p53, ATM, PARP1 and γ -H2AX [11].

Using our current findings we have attempted to situate RXFP3 and its signaling functionality within the known DDR domain (Figure 10A, 10B). We propose that RXFP3 participates in PRKDC activation following RLN3 stimulation. This RXFP3-entrained process allows the cell to employ PRKDC-dependent NHEJ, in addition to typically ATM-associated HR. RXFP3 can potentially enhance DNA repair, thus explaining our observed accelerated decrease in ATM, H2AX and BRCA1 phosphorylation, while PRKDC phosphorylation is increased. This proposal is supported by the research of Riabinska, et al. [191] which demonstrated that in ATM-defective cells, PRKDC offers a backup mechanism for failed DSB repair through HR, using NHEJ. Their research was further reinforced by the early embryonic lethality of ATM+PRKDC-KO mice [192], while animals only lacking one of the two proteins are viable [193, 194]. This direct effect of RXFP3 stimulation and expression on the activation of PRKDC and the NHEJ DNA repair is supported by minimal PRKDC phosphorylation alteration in response to DNA damage caused by CPT (Figure 9B, 9C). While the overall effect of RXFP3 system activation upon PRKDC expression and phosphorylation, also supports our acquired information displayed in Figure 9, using co-IP we further demonstrated that activated PRKDC (pPRKDC) interacts with RXFP3 (Supplementary Figure 4C). This interaction supports our theory depicted in Figure 10B, where we suggested that RXFP3 interacts with PRKDC and allows its activation, in addition to the activation of ATM thus facilitating DNA damage repair. As can also be seen, the RXFP3 sequence (Supplementary Figure 1) contains three potential phosphorylation sites, two for ATM and one for PRKDC. Interestingly, however, the phosphorylation sites mentioned in Supplementary Figure 1 are located at the extracellular region of the receptor. This indicates that this GPCR is potentially available in the cell in a usual 'outside-out' conformation, but also in a novel 'outside-in' conformation. It may thus be very important to explore further, through receptor mutation, as performed previously for GIT2 [11].

Given our demonstration of a potential role for RXFP3 in controlling aging-associated disease we further tested the potential validity of our contention at an unbiased, mass analytical level. To this end we employed a recently demonstrated technique of reverse-database analysis

using LSI [195]. As such, we first created a database of proteins, extracted from the entire human genome (via PubMed Central text mining using GeneIndexer), explicitly and implicitly associated with input interrogator terms covering the majority of age-associated disease conditions (Supplementary Table 25), termed the ‘Disease Continuum’ (Figure 11A). To identify potential therapeutic targets that could interact and potentially control this ‘Disease Continuum’ in a multidimensional manner we isolated the proteins within this continuum most strongly associated with a battery of terms linked to central nervous system function, energy

metabolism and GPCR-focused signaling (Supplementary Table 26). Ranking the Cosine Similarity scores of the resultant factors that were prominent in the disease continuum and the ‘Therapeutic Interrogators’ (Figure 11B) we found that, based on a correlation ranking probability score ($p < 0.001$, ***) there were 37 specific protein targets demonstrating a number of correlations within the therapeutic interrogators that was greater than the 99% (representing only 0.67% of the input ‘Disease Continuum’ dataset). The top three ranked multidimensional proteins that could represent effective age-related disease interdiction targets were, arginine

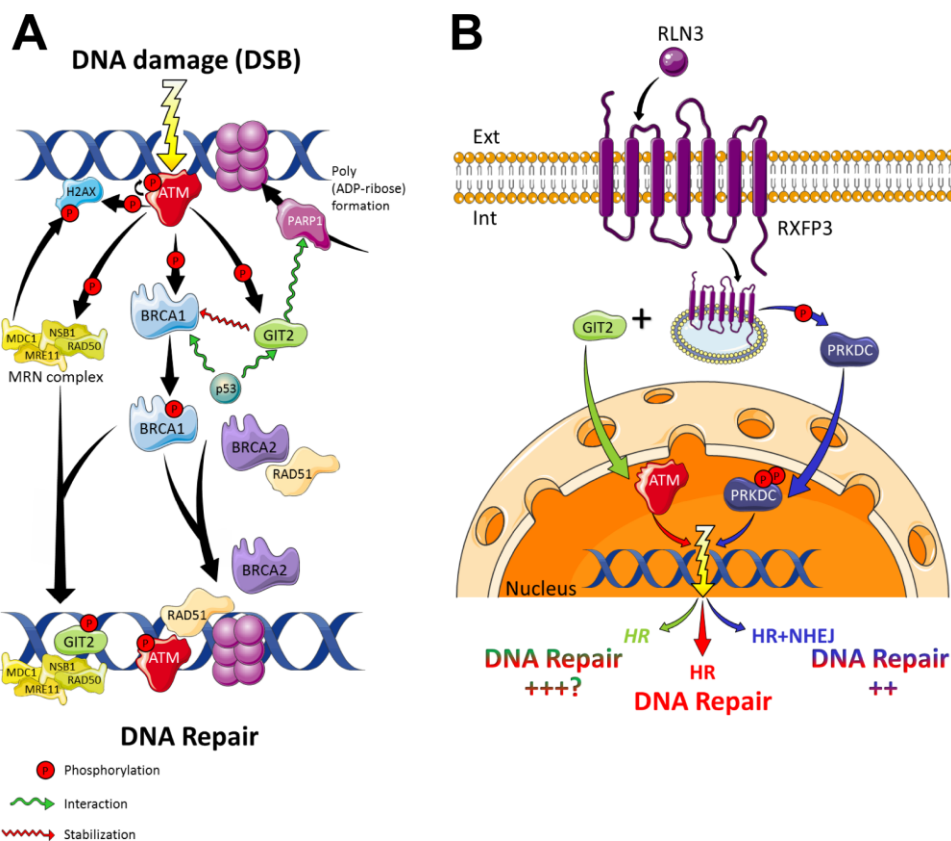


Figure 10. RXFP3 in DNA damage response and repair. (A) With DNA damage in the form of a double strand break (DSB), the cell has several mechanisms to respond and thus repair itself. The damage is recognized by the MRE11-RAD50-NBS1 complex (MRN complex), which recruits and activates ATM (Ataxia Telangiectasia Mutated), which is autophosphorylated. ATM, in turn phosphorylates multiple damage-associated proteins. H2AX (a variant of the histone H2A family) phosphorylation (generating γ -H2AX) allows for the recruitment of MDC1 (Mediator of Damage Checkpoint protein 1), also a phosphorylation substrate of ATM. Phosphorylated MDC1 serves as a scaffold for the recruitment of other proteins required for the activation of BRCA1 by ATM, thus promoting cell cycle arrest and DNA repair. BRCA1, in turn, then interacts with multiple proteins, *i.e.* p53, RAD50, RAD51, ATM, NSB1 and BRCA2, to modulate DNA repair, transcription, and the cell cycle. Phosphorylation of BRCA1 by ATM activates DNA repair through homologous recombination, in cooperation with BRCA2 and RAD51. Additionally, BRCA1 recruits the MRN-complex to the sites of DNA damage. ATM furthermore phosphorylates the aging keystone GIT2 promotes the repair of DNA damage via the stabilization of repair factor BRCA1, in the repair complex. GIT2 then allows the formation of a nuclear DSB focus dependent on H2AX, ATM, and MRE11. Also GIT2 is a strong interactor of the cell cycle checkpoint protein p53 and PARP1. PARPs play a pivotal role in DNA damage detection and repair, by the formation of ADP-ribose ribosylation complexes, allowing the recruitment of DDR proteins to the damaged DNA. After the DNA has been repaired, γ -H2AX is dephosphorylated by PP2A, a phosphatase. (B) Cells exploit two major DSB repair pathways, *i)* ATM-dependent homologous recombination (HR), and *ii)* PRKDC-mediated Non-homologous end joining (NHEJ). In the absence of a functional ATM, it seems cells are able to rely on functional PRKDC signaling for their survival, thus using the NHEJ pathway as a backup pathway for DSB repair [191].

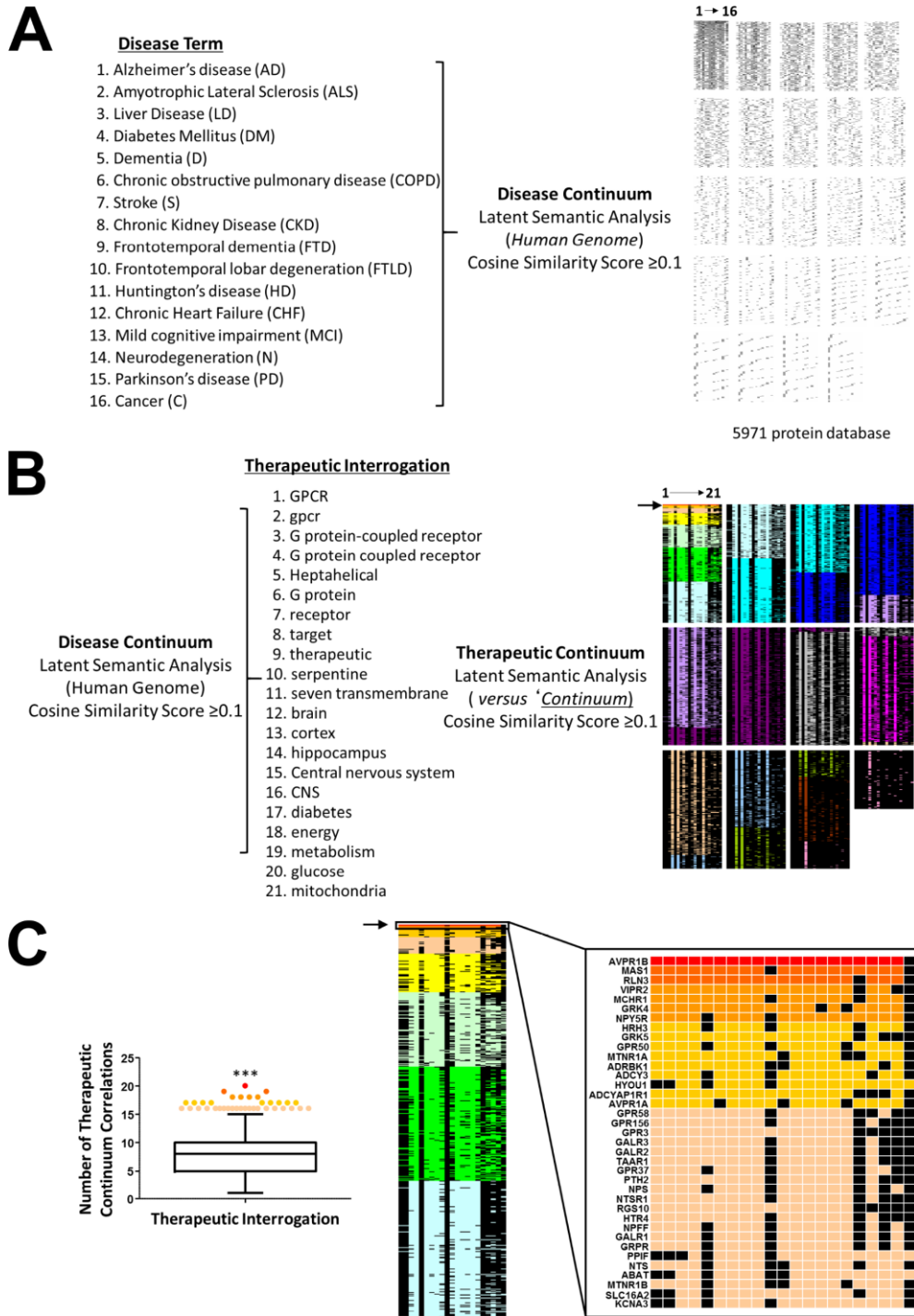


Figure 11. Unbiased analysis of the potential role for RXFP3 in controlling age-related disorders. To test the validity of our hypothesis in an unbiased manner, we used reverse-database analysis using latent semantic indexing platform GeneIndexer. **(A)** We started by creating a database of proteins, associated with input interrogator terms of the majority of age-related disorders, which we termed the 'Disease Continuum'. **(B)** We next tried to identify a potential therapeutic target for these diseases, a GPCR in particular. To do so we investigated the Disease continuum protein dataset with GPCR-related terms, to create the 'Therapeutic continuum'. **(C)** The proteins were ranked according to the cosine similarity scores, and based on a correlation ranking probability score ($p < 0.001$, ***) 37 specific proteins were identified demonstrating a large amount of correlation within the therapeutic interrogators greater than the 99th percentile. The top three ranked multidimensional proteins that could represent effective age-related disease targets were, AVPR1B, MAS1 and RLN3, the cognate ligand for the RXFP3.

vasopressin receptor 1B (AVPR1B), MAS1 proto-oncogene, GPCR (MAS1) and RLN3, the cognate ligand for the RXFP3 (Figure 11C). It is interesting to note that the MAS1 [196] and arginine vasopressin receptors [197] have recently been implicated in age-related disorder amelioration. In this context, using an unbiased multidimensional approach it is tantalizing to anticipate that therapeutic modulation of the RXFP3 may also hold significant promise for the attenuation of multiple age-related diseases.

Taken together, our findings suggest that RXFP3, may be involved in oxidative stress and DNA damage stress response, in addition to its role in corticotropin stress response [21, 198]. This involvement of GPCRs in DDR has only recently been observed [195], and it appears that the receptor systems have long been developed alongside DDR systems to act as stress sensors, as appears to be the case for RXFP3, *i.e.* oxidative stress, DNA damage and potentially age-related stress. When we combine this information with its expressional and functional relationship and association with GIT2 [9, 10, 12, 13], it appears that we may be able to target RXFP3, and as such control GIT2 and potentially treat or even prevent age-related disorders such as neurodegeneration. Future research should focus on further unraveling the relationship between GIT2 and RXFP3 so that RXFP3-targeted therapeutics can be designed.

MATERIALS AND METHODS

Cell culture, transfection and treatment

Human HEK293 (CRL 1573) were obtained from ECACC and propagated at 37°C with 5% CO₂ ambient tension, according to the approved culture protocols defined for these cell lines. Human neuronal SH-SY5Y (CRL-2266) were obtained from ATCC and again propagated according to the published protocols of the disseminating organization. Murine hypothalamic neuronal cells, GT1-7 cells were obtained from Pamela Mellon (San Diego, California, USA [199]). All cell lines were maintained in Dulbecco's Modified Eagle Medium (DMEM; Sigma-Aldrich) with 10% fetal bovine serum (FBS)-containing propagation media, supplemented with 1% Penicillin/Streptomycin antibiotics as previously described [200].

For the interactomic experiments, we used SILAC (Stable isotope labeling of amino acids in cell culture), in order to label our proteins/peptides prior to experimentation. As such this technique allows us to analyze a very small amount of peptides using mass spectrometry. Customized DMEM media, without arginine and lysine were purchased from AthenaES.

This medium was supplemented with 'medium' (L-lysine-U-¹³C₆ (K6), L-arginine-U-¹³C₆ (R6)) and 'heavy' (L-lysine-U-¹³C₆-¹⁵N₂ (K8), L-arginine-U-¹³C₆-¹⁵N₄ (R10)), respectively (Cambridge Isotope Laboratories [201], and with dialyzed FBS and 1% antibiotics. To engender at least 90% of protein labeling, cells were cultured in SILAC medium for at least five passages. The 'medium' and 'heavy' conditions were compared to avoid non-labeled peptide errors [201]. Dependent on prevailing growth rates, the cells were passaged on a regular basis.

One day prior to transfection, 3×10⁶ cells were seeded into 10cm plates to obtain a 50–80% cell confluence the day of the transfection. Cells were counted using a Luna II Automated Cell Counter (Invitrogen-Life Technologies). The cDNAs for a hemagglutinin (3xHA)-tagged human RXFP3 receptor (obtained from the Missouri S&T cDNA Resource Center: <https://www.cdna.org>) and an empty plasmid (pcDNA3.1+: Invitrogen-Life Technologies) were transfected into the cells with Lipofectamine® 3000, using the manufacturers' instructions. To investigate the effect of differential receptor overexpression on downstream proteins, we transfected the cells with a range of cDNA concentrations (0.5, 1, 2, 5, and 10 µg). To induce oxidative stress, cells were treated with 100 nM hydrogen peroxide (H₂O₂/peroxide) for 90 minutes. DNA damage was caused using 1 µM Camptothecin (CPT) for 3, and 24 hours, dependent on the experiment.

Investigation of the ability of RXFP3 to accelerate DDR, we initially overexpressed RXFP3 compared to E.V. (5µg) after which we stressed the cells with 10µM of CT, cells were extracted using RIPA 1% SDS (150mM NaCl, 50mM Tris, 0.5% Sodium deoxycholate, 1% NP-40) 1% SDS (sodium dodecyl sulphate). To assess whether stimulation of RXFP3 using its endogenous ligand RLN3 might have a possible protective ability, we pre-stimulated the cells with 100 nM of RLN3. We administered two stimulation points, 1 and 2 hours prior to stressing the cells with 10 µM CPT for 3 hours. As a control, an equal amount of TFA was used, which we used to dissolve RLN3. This experiment was repeated in reverse, where cells were stressed prior to RLN3 stimulation.

Cellular protein extraction

For generic low-definition cellular protein extraction, following a described cellular treatment, cells were washed three times with ice-cold PBS and scraped from dishes in the presence of either RIPA 0.1% or 1% SDS supplemented with phosphatase Inhibitor Cocktail

(PhosSTOP, Roche Diagnostics) and protease inhibitor cocktail (complete mini, Roche Diagnostics), dependent on the experiment. To generate differential cell fraction protein extracts, cells were first washed as monolayers with ice-cold PBS and then subjected to a detergent dependent fractionation process using a Q proteome extraction kit (Qiagen) according to the manufacturers' instructions. Before eventual analytical use, protein quantification of generated cellular lysates was performed using a standard colorimetric protein assay, *i.e.* the Bio-Rad RC DC™ assay (Bio-Rad).

iTRAQ sample preparation

The protein concentrations were assessed a second time after trichloroacetic acid (TCA) precipitation overnight at 4°C using 1/3 volume of TCA, to ensure correct protein levels. For each sample 100 µg of protein was reduced using 5mM Tris-2-(carboxyethyl)-phosphine hydrochloride solution (TCEP; Pierce Biotechnology) and cysteine blocking was performed with 2mM methyl methanethiosulphonate (MMTS) solution (Sigma-Aldrich). Each sample containing 100µg proteins, was digested using 10µg trypsin (Promega) at 37°C overnight. Samples were then labelled using iTRAQ reagents (ABSciex) before being pooled into one mixture. The following iTRAQ labels were used for the transfected cells: iTRAQ labels 113 was used for the transfected cells with the pcDNA3.1+ empty plasmid; iTRAQ labels from 114 to 118 were used to label the differentially transfected cells with RXFP3 (114-0.5µg_RXFP3-HA, 115-1µg_RXFP3-HA, 116-2µg_RXFP3-HA1, 117-5µg_RXFP3-HA, 118-10µg_RXFP3-HA). After labelling, the samples were pooled, dried down and dissolved with SCX buffer prior to SCX chromatography.

SILAC sample preparation

RXFP3 interactomes, extracted using RIPA 0.1% SDS, were isolated by immunoprecipitation using anti-HA bound beads (Sigma-Aldrich) overnight on an end-over-end shaker, after which the bound proteins were extracted using 100µl of 150mM Glycine-HCl buffer (pH 2.5). The samples were continuously vortexed for 5 minutes, then centrifuged. The supernatants, containing the proteins, were immediately transferred to a new tube containing 40µl neutralizing buffer (1M Tris, pH 8). Proteins were then precipitated overnight at 4°C using TCA, after which the pellet was washed with acetone and resuspended in 60µl resolubilization buffer (6M Urea, 2M ThioUrea, 10% SDS in 50mM TEAB). Equal amounts of proteins from 'medium' and 'heavy' conditions were mixed to prepare the SILAC mix. The sample was then reduced (TCEP), cysteine blocking was performed (MMTS), and the proteins were digested with trypsin (see section iTRAQ sample preparation).

Strong cation exchange chromatography separation (SCX)

The pooled samples were diluted 10-fold with HPRP buffer A (5mM KH₂PO₄ in 5% acetonitrile at pH 3.0), to reduce sample complexity during the LC-MS/MS analysis. These were then separated using a 1mm x 150mm polysulfoethyl aspartamide column (Dionex). The column was eluted with a gradient: 0 to 25 minutes 60% HPRP buffer B (5mM KH₂PO₄ at pH 3.0 in 5% acetonitrile containing 0.5M NaCl), 25 to 45 minutes 100% HPRP buffer B and 25 to 45 minutes 100% HPRP buffer A. For each sample, 40 fractions were eluted and then pooled into 10 fractions. These fractions were then diluted before being loaded into the C18 column.

Nano-LC-MS/MS analysis

The mass spectrometric analysis of the iTRAQ samples was performed using a nano-LC column (Dionex ULTIMATE 3000) coupled online to a Q Exactive™-Plus Orbitrap (ThermoScientific), the SILAC samples were analyzed using our Orbitrap Fusion™ Tribrid™ (ThermoScientific). Peptides were loaded onto a 75µm × 150mm, 2µm fused silica c18 capillary column, and mobile phase elution was performed using buffer A (0.05% formic acid, 99.5% Milli-Q water) and buffer B (0.05% formic acid in 80% acetonitrile/ Milli-Q water). The peptides were eluted using a gradient from 4% buffer B to 90% buffer B over 45 min at a flow rate of 0.3µl/min. The LC eluent was directed to an ESI source for Orbitrap analysis. The mass spectrometer was set to perform data dependent acquisition in the positive ion mode for a selected mass range of 350-1800 m/z for quantitative expression difference at the MS1 (70000 resolution) level followed by peptide backbone fragmentation with normalized collision energy (NCE) of 32, and identification at the MS2 level (17500 resolution). The raw data was analyzed using Thermo Fisher Proteome Discoverer 2.0, the software was connected to a Sequest HT search engine (Thermo Fisher Scientific) using UNIPROT/SWISSPROT annotated database. Each protein was assigned a confidence score (0% to 100%) based on the confidence scores of its constituent peptides based on unique spectral patterns. Proteins were only identified from the recovery and measurement of one peptide (from MS2) that is identified with a 99% confidence.

Bioinformatic analyses

We applied a multidimensional informatic approach to the analysis of our proteomic and interactomic data. To facilitate the specific separation of complex datasets, we employed the Venn diagram platforms, VennPlex, VENNTURE [202, 203] and interactivenn

(<http://www.interactivenet.net/>). To generate unbiased outputs, we employed the latent semantic indexing (LSI)-based informatic platform *Textroux!* [17] to create *de novo* signaling descriptions from selected datasets that facilitate a more nuanced appreciation of high-dimensionality receptor signaling paradigms [17]. From *Textroux!*-based natural language processing analyses wordclouds were generated with WordCloud (<https://www.wordclouds.com/>). To extract both word and phrase frequencies from our *Textroux!* output we employed the Frequency Counter application from WriteWords (<http://www.writewords.org.uk/wordcount.asp>). Furthermore, Enrichr (<http://amp.pharm.mssm.edu/Enrichr/#>) was employed to analyze the significantly relevant related pathways and diseases/ontologies, identified using Gene Ontology (GO).

In addition, we created interactomes of several important players in oxidative stress (G3BP1, SIRT1, and SOD1) and DNA damage (PRKDC, H2AFX, MDM2, MDC1, TP53, BRCA1) response *in silico*, using the freely available BioGRID (<https://thebiogrid.org/>). As a control for this experiment we made an additional list of proteins unrelated to these stress responses (Non-stress; *i.e.* CNTRL, CRP, LONP2).

Next, we used GEN3VA (GENE Expression and Enrichment Vector Analyzer; <http://amp.pharm.mssm.edu/gen3va/>), which is based on GEO (gene expression omnibus; <https://www.ncbi.nlm.nih.gov/geo/>), a web-based system enabling the integrative analysis of amassed collections of gene expression signatures identified and extracted from GEO. Allowing us to extract specific disease signatures, which we can compare to our own data. We have extracted the following signatures: *i*) Aging (found in GEN3VA under the name “Model of cerebral aging and Alzheimer's disease: temporal cortex”), *ii*) schizophrenia (in GEN3VA “Schizophrenia: postmortem superior temporal cortex”) and *iii*) aortic aneurysm (“Abdominal aortic aneurysm”). The latter was used as a control to assess whether the protein overlap is specific and this does not occur with non-aging-related datasets (Data sets found in Supplementary Table 4).

Lastly, LSI platform GeneIndexer (<https://geneindexer.com/>) was used to investigate the association of our protein set with our own input of interrogator terms. Here we used age-related and age-unrelated terms, *i.e.* Aging: *Neurodegeneration, Cognitive impairment, Senescence, Parkinson's Disease, Amyotrophic lateral sclerosis, Alzheimer's Disease* (Figure 8A); and non-Aging: *Tuberculosis, Spina Bifida, Asthma, Tourette*

syndrome, ADHD, Achondroplasia (Figure 8B). The use of this LSI allows us to use natural language processing for data extraction, identifying hidden connections between the proteins and the interrogation terms. The GeneIndexer database holds more than 1.5 million Medline abstracts, which correspond to over 21,000 mammalian genes. This program extracts all gene-to-word relationships from the literature using LSI. Here a cosine similarity score larger than 0.2 typically specifies an explicit association, while a score lower than 0.2 indicates an implied relationship, a cutoff score was set at 0.1.

For advanced network-based analysis we employed the NetworkAnalyst (<https://www.networkanalyst.ca/>) application that is designed to serve as a visual analytics platform for comprehensive gene expression profiling and meta-analysis. NetworkAnalyst allows for the creation, and eventual informatics interrogation, of multiple network types. Multiple types of protein interaction database are available for interactome enrichment analysis including the IMEx (International Molecular Exchange Consortium) consortium (<http://www.imexconsortium.org/>), STRING (<https://string-db.org>) and the CCSB-associated Rolland Interactome (http://interactome.dfci.harvard.edu/H_sapiens/: [204]).

Immunoblot, immunoprecipitation, and immunocytochemistry

To validate the proteomic data, the experiments were replicated and analyzed using immunoblotting with a standard protocol (Supplementary Figure 4C, 4D). In short, all samples separated on 4%–12% SDS-PAGE (Life Technologies), transferred to PVDF membrane (Amersham) and blocked using 5% BLOTTO milk. Primary antibodies for immunoblots: GIT2 (Bethyl), RXFP3 (LSBio), HA-tag, phospho-BRCA1 (ThermoScientific), G3BP1 (Santa Cruz Biotechnology), Actin (Sigma Aldrich), PARP1, EIF4a1, γ -H2AX, PHB (GeneTex), XPOI (Atlas Antibodies), phospho-ATM (Rockland), DDB1, phospho-PRKDC OSSA (Abcam), Src (Cell Signaling technology). The membrane was then incubated with species appropriate secondary antibodies conjugated to horseradish peroxidase (HRP), immune complexes were then identified using enhanced chemiluminescence (ECL, GE Healthcare) and an Amersham imager 680 system. WB quantification was performed with GE-ImageQuant TL and Image J software, using red ponceau staining as a loading control.

SILAC data was validated using a standard co-immunoprecipitation protocol coupled to immunoblotting, where the proteins were extracted from the anti-HA affinity beads through resuspension in

Laemmli buffer (DTT and LDS 2x), after which the samples were analyzed using immunoblotting (see above). Immunostaining was performed according to a standard protocol. Briefly, cells were fixed in 4% paraformaldehyde, for at least 20 min and no longer than 24h at room temperature. Non-specific labeling was blocked with 5% goat serum (1:500 dilution; Dako, Heverlee, Belgium) for 1 h, primary antibodies were incubated for 1 h (1:500 dilution) and secondary antibodies for 30 min at room temperature. Nucleus staining was performed with DAPI (Invitrogen), after which cells were mounted with Dako fluorescent mounting medium (Dako, Heverlee, Belgium) and examined with confocal microscopy LSM 700 (Zeiss).

Murine tissue RT-PCR

GIT2KO gene-trap animals [205] based on a standard C57BL/6 background, initially obtained from Duke University (Richard Premont, Durham, NC) were bred at the National Institute on Aging under NIH protocol numbers, 432-LCI-2015 and 433-LCI-2015, according to approval of the Institutional Review Board. All animal studies performed were approved according to the guidelines of the NIA Animal Care and Use Committee. Mice were maintained in a 12h light/dark cycle on an *ad libitum* regular diet. The RNeasy Mini kit (Qiagen) was used for cellular mRNA extraction from multiple tissues derived from wild type (C57Bl6) and GIT2KO mice. Reverse transcription was performed using proprietary kits (Life Technologies, Carlsbad CA). Genes were normalized to GAPDH. RT-PCR was performed using the ABI Prism 7300 Sequence Detector (Applied Biosystems, Carlsbad CA).

Statistical analyses

In each histogram or figure, data represent the means \pm SEM (standard error of the mean). Statistical analyses (Student's t-test) were performed using GraphPad Prism version 7.0 (GraphPad Software, San Diego, CA, USA). Significance level is indicated in each figure as * $p \leq 0.05$; ** $p \leq 0.01$; *** $p \leq 0.001$.

Abbreviations

AP-MS: Affinity Purification Mass Spectrometry; ATM: Ataxia Telangiectasia Mutated; CPT: Camptothecin; DDR: DNA damage response; DRY: aspartic acid (Asp) - arginine (Arg) - tyrosine (Tyr); GIT2: G protein-coupled receptor kinase interacting transcript 2; GPCR: G protein-coupled receptor; H₂O₂: Hydrogen peroxide; KO: Knockout; PRKDC: DNA-protein kinase C; RLN3: relaxin 3; RXFP3: relaxin family peptide 3 receptor.

AUTHOR CONTRIBUTIONS

Writing, J.v.G., S.M., Data acquisition, J.v.G., H.L. and S.M.; Reviewing and Editing, H.L., P.S.-O., J.O.H., B.M. and S.M.; Visualization, J.v.G.; Supervision, S.M.; Project Administration, S.M.; Funding Acquisition, J.v.G., J.O.H. and S.M.

CONFLICTS OF INTEREST

The authors declare that the research was conducted in the absence of any commercial or financial relationships that could be construed as a potential conflicts of interest.

FUNDING

This research was funded by the FWO-OP/Odysseus program #42/FA010100/32/6484, the University of Antwerp GOA (Geconcerteerde onderzoeksacties) Program #33931, the FWO Travelling Fellowship Program #V4.161.17N and the EU Erasmus+ training program.

REFERENCES

1. López-Otín C, Blasco MA, Partridge L, Serrano M, Kroemer G. The hallmarks of aging. *Cell*. 2013; 153:1194–217.
<https://doi.org/10.1016/j.cell.2013.05.039>
PMID:[23746838](https://pubmed.ncbi.nlm.nih.gov/23746838/)
2. Nkuiou-Kenfack E, Koeck T, Mischak H, Pich A, Schanstra JP, Zürgbig P, Schumacher B. Proteome analysis in the assessment of ageing. *Ageing Res Rev*. 2014; 18:74–85.
<https://doi.org/10.1016/j.arr.2014.09.002>
PMID:[25257180](https://pubmed.ncbi.nlm.nih.gov/25257180/)
3. Maynard S, Fang EF, Scheibye-Knudsen M, Croteau DL, Bohr VA. DNA Damage, DNA Repair, Aging, and Neurodegeneration. *Cold Spring Harb Perspect Med*. 2015; 5:5.
<https://doi.org/10.1101/cshperspect.a025130>
PMID:[26385091](https://pubmed.ncbi.nlm.nih.gov/26385091/)
4. Gonzalo S, Kreienkamp R. DNA repair defects and genome instability in Hutchinson-Gilford Progeria Syndrome. *Curr Opin Cell Biol*. 2015; 34:75–83.
<https://doi.org/10.1016/j.ceb.2015.05.007>
PMID:[26079711](https://pubmed.ncbi.nlm.nih.gov/26079711/)
5. Musich PR, Zou Y. Genomic instability and DNA damage responses in progeria arising from defective maturation of prelamin A. *Ageing (Albany NY)*. 2009; 1:28–37.
<https://doi.org/10.18632/aging.100012>
PMID:[19851476](https://pubmed.ncbi.nlm.nih.gov/19851476/)

6. Hyun M, Choi S, Stevnsner T, Ahn B. The Caenorhabditis elegans Werner syndrome protein participates in DNA damage checkpoint and DNA repair in response to CPT-induced double-strand breaks. *Cell Signal*. 2016; 28:214–23. <https://doi.org/10.1016/j.cellsig.2015.12.006> PMID:[26691982](#)
7. Rothblum-Oviatt C, Wright J, Lefton-Greif MA, McGrath-Morrow SA, Crawford TO, Lederman HM. Ataxia telangiectasia: a review. *Orphanet J Rare Dis*. 2016; 11:159. <https://doi.org/10.1186/s13023-016-0543-7> PMID:[27884168](#)
8. Shiloh Y, Lederman HM. Ataxia-telangiectasia (A-T): an emerging dimension of premature ageing. *Ageing Res Rev*. 2017; 33:76–88. <https://doi.org/10.1016/j.arr.2016.05.002> PMID:[27181190](#)
9. Chadwick W, Martin B, Chapter MC, Park SS, Wang L, Daimon CM, Brenneman R, Maudsley S. GIT2 acts as a potential keystone protein in functional hypothalamic networks associated with age-related phenotypic changes in rats. *PLoS One*. 2012; 7:e36975. <https://doi.org/10.1371/journal.pone.0036975> PMID:[22606319](#)
10. Chadwick W, Zhou Y, Park SS, Wang L, Mitchell N, Stone MD, Becker KG, Martin B, Maudsley S. Minimal peroxide exposure of neuronal cells induces multifaceted adaptive responses. *PLoS One*. 2010; 5:e14352. <https://doi.org/10.1371/journal.pone.0014352> PMID:[21179406](#)
11. Lu D, Cai H, Park SS, Siddiqui S, Premont RT, Schmalzigaug R, Paramasivam M, Seidman M, Bodogai I, Biragyn A, Daimon CM, Martin B, Maudsley S. Nuclear GIT2 is an ATM substrate and promotes DNA repair. *Mol Cell Biol*. 2015; 35:1081–96. <https://doi.org/10.1128/MCB.01432-14> PMID:[25605334](#)
12. Lu D, Cai H, Park SS, Siddiqui S, Premont RT, Schmalzigaug R, Paramasivam M, Seidman M, Bodogai I, Biragyn A, Daimon CM, Martin B, Maudsley S. Correction for Lu et al., “Nuclear GIT2 Is an ATM Substrate and Promotes DNA Repair”. *Mol Cell Biol*. 2017; 37:37. <https://doi.org/10.1128/MCB.00310-17> PMID:[28801458](#)
13. Martin B, Chadwick W, Janssens J, Premont RT, Schmalzigaug R, Becker KG, Lehrmann E, Wood WH, Zhang Y, Siddiqui S, Park SS, Cong WN, Daimon CM, Maudsley S. GIT2 Acts as a Systems-Level Coordinator of Neurometabolic Activity and Pathophysiological Aging. *Front Endocrinol (Lausanne)*. 2016; 6:191. <https://doi.org/10.3389/fendo.2015.00191> PMID:[26834700](#)
14. Li H, Guan SB, Lu Y, Wang F, Liu YH, Liu QY. Genetic deletion of GIT2 prolongs functional recovery and suppresses chondrocyte differentiation in rats with rheumatoid arthritis. *J Cell Biochem*. 2018; 119:1538–47. <https://doi.org/10.1002/jcb.26313> PMID:[28777475](#)
15. Siddiqui S, Lustig A, Carter A, Sankar M, Daimon CM, Premont RT, Etienne H, van Gastel J, Azmi A, Janssens J, Becker KG, Zhang Y, Wood W, et al. Genomic deletion of GIT2 induces a premature age-related thymic dysfunction and systemic immune system disruption. *Aging (Albany NY)*. 2017; 9:706–40. <https://doi.org/10.18632/aging.101185> PMID:[28260693](#)
16. Gesty-Palmer D, Yuan L, Martin B, Wood WH 3rd, Lee MH, Janech MG, Tsoi LC, Zheng WJ, Luttrell LM, Maudsley S. β -arrestin-selective G protein-coupled receptor agonists engender unique biological efficacy in vivo. *Mol Endocrinol*. 2013; 27:296–314. <https://doi.org/10.1210/me.2012-1091> PMID:[23315939](#)
17. Maudsley S, Martin B, Janssens J, Etienne H, Jushaj A, van Gastel J, Willemsen A, Chen H, Gesty-Palmer D, Luttrell LM. Informatic deconvolution of biased GPCR signaling mechanisms from in vivo pharmacological experimentation. *Methods*. 2016; 92:51–63. <https://doi.org/10.1016/j.ymeth.2015.05.013> PMID:[25986936](#)
18. López de Maturana R, Martin B, Millar RP, Brown P, Davidson L, Pawson AJ, Nicol MR, Mason JI, Barran P, Naor Z, Maudsley S. GnRH-mediated DAN production regulates the transcription of the GnRH receptor in gonadotrope cells. *Neuromolecular Med*. 2007; 9:230–48. <https://doi.org/10.1007/s12017-007-8004-z> PMID:[17914181](#)
19. Scheler G. Self-organization of signal transduction. *F1000Res*. 2013; 2:116. <https://doi.org/10.12688/f1000research.2-116.v1> PMID:[25506419](#)
20. Stolpe AV, Holtzer L, van Ooijen H, de Inda MA, Verhaegh W. Enabling precision medicine by unravelling disease pathophysiology: quantifying signal transduction pathway activity across cell and tissue types. *Sci Rep*. 2019; 9:1603. <https://doi.org/10.1038/s41598-018-38179-x> PMID:[30733525](#)
21. Tanaka M, Iijima N, Miyamoto Y, Fukusumi S, Itoh Y, Ozawa H, Iyata Y. Neurons expressing relaxin 3/INSL 7 in the nucleus incertus respond to stress. *Eur J Neurosci*. 2005; 21:1659–70. <https://doi.org/10.1111/j.1460-9568.2005.03980.x>

- PMID:[15845093](#)
22. Ryan PJ, Büchler E, Shabanpoor F, Hossain MA, Wade JD, Lawrence AJ, Gundlach AL. Central relaxin-3 receptor (RXFP3) activation decreases anxiety- and depressive-like behaviours in the rat. *Behav Brain Res*. 2013; 244:142–51.
<https://doi.org/10.1016/j.bbr.2013.01.034>
PMID:[23380674](#)
23. Lee JH, Koh SQ, Guadagna S, Francis PT, Esiri MM, Chen CP, Wong PT, Dawe GS, Lai MK. Altered relaxin family receptors RXFP1 and RXFP3 in the neocortex of depressed Alzheimer's disease patients. *Psychopharmacology (Berl)*. 2016; 233:591–98.
<https://doi.org/10.1007/s00213-015-4131-7>
PMID:[26542729](#)
24. McGowan BM, Stanley SA, Smith KL, White NE, Connolly MM, Thompson EL, Gardiner JV, Murphy KG, Ghatei MA, Bloom SR. Central relaxin-3 administration causes hyperphagia in male Wistar rats. *Endocrinology*. 2005; 146:3295–300.
<https://doi.org/10.1210/en.2004-1532>
PMID:[15845619](#)
25. McGowan BM, Stanley SA, Smith KL, Minnion JS, Donovan J, Thompson EL, Patterson M, Connolly MM, Abbott CR, Small CJ, Gardiner JV, Ghatei MA, Bloom SR. Effects of acute and chronic relaxin-3 on food intake and energy expenditure in rats. *Regul Pept*. 2006; 136:72–77.
<https://doi.org/10.1016/j.regpep.2006.04.009>
PMID:[16764952](#)
26. Smith CM, Ryan PJ, Hosken IT, Ma S, Gundlach AL. Relaxin-3 systems in the brain—the first 10 years. *J Chem Neuroanat*. 2011; 42:262–75.
<https://doi.org/10.1016/j.jchemneu.2011.05.013>
PMID:[21693186](#)
27. Smith CM, Shen PJ, Banerjee A, Bonaventure P, Ma S, Bathgate RA, Sutton SW, Gundlach AL. Distribution of relaxin-3 and RXFP3 within arousal, stress, affective, and cognitive circuits of mouse brain. *J Comp Neurol*. 2010; 518:4016–45.
<https://doi.org/10.1002/cne.22442> PMID:[20737598](#)
28. Ryan PJ, Kastman HE, Krstew EV, Rosengren KJ, Hossain MA, Churilov L, Wade JD, Gundlach AL, Lawrence AJ. Relaxin-3/RXFP3 system regulates alcohol-seeking. *Proc Natl Acad Sci USA*. 2013; 110:20789–94.
<https://doi.org/10.1073/pnas.1317807110>
PMID:[24297931](#)
29. Liu C, Chen J, Kuei C, Sutton S, Nepomuceno D, Bonaventure P, Lovenberg TW. Relaxin-3/insulin-like peptide 5 chimeric peptide, a selective ligand for G protein-coupled receptor (GPCR)135 and GPCR142 over leucine-rich repeat-containing G protein-coupled receptor 7. *Mol Pharmacol*. 2005; 67:231–40.
<https://doi.org/10.1124/mol.104.006700>
PMID:[15465925](#)
30. Ma S, Gundlach AL. Relaxin-family peptide and receptor systems in brain: insights from recent anatomical and functional studies. *Adv Exp Med Biol*. 2007; 612:119–37.
https://doi.org/10.1007/978-0-387-74672-2_9
PMID:[18161485](#)
31. Sutton SW, Bonaventure P, Kuei C, Roland B, Chen J, Nepomuceno D, Lovenberg TW, Liu C. Distribution of G-protein-coupled receptor (GPCR)135 binding sites and receptor mRNA in the rat brain suggests a role for relaxin-3 in neuroendocrine and sensory processing. *Neuroendocrinology*. 2004; 80:298–307.
<https://doi.org/10.1159/000083656> PMID:[15677880](#)
32. Miyamoto Y, Watanabe Y, Tanaka M. Developmental expression and serotonergic regulation of relaxin 3/INSL7 in the nucleus incertus of rat brain. *Regul Pept*. 2008; 145:54–59.
<https://doi.org/10.1016/j.regpep.2007.08.010>
PMID:[17870193](#)
33. Anckaerts C, van Gastel J, Leysen V, Hinz R, Azmi A, Simoens P, Shah D, Kara F, Langbeen A, Bols P, Laloux C, Prevot V, Verhoye M, et al. Image-guided phenotyping of ovariectomized mice: altered functional connectivity, cognition, myelination, and dopaminergic functionality. *Neurobiol Aging*. 2019; 74:77–89.
<https://doi.org/10.1016/j.neurobiolaging.2018.10.012>
PMID:[30439596](#)
34. van Gastel J, Cai H, Cong WN, Chadwick W, Daimon C, Leysen H, Hendrickx JO, De Schepper R, Vangenechten L, Van Turnhout J, Verswyvel J, Becker KG, Zhang Y, et al. Multidimensional informatic deconvolution defines gender-specific roles of hypothalamic GIT2 in aging trajectories. *Mech Ageing Dev*. 2019; 184:111150.
<https://doi.org/10.1016/j.mad.2019.111150>
PMID:[31574270](#)
35. Roux BT, Cottrell GS. G protein-coupled receptors: what a difference a 'partner' makes. *Int J Mol Sci*. 2014; 15:1112–42.
<https://doi.org/10.3390/ijms15011112>
PMID:[24441568](#)
36. Römpler H, Yu HT, Arnold A, Orth A, Schöneberg T. Functional consequences of naturally occurring DRY motif variants in the mammalian chemoattractant receptor GPR33. *Genomics*. 2006; 87:724–32.
<https://doi.org/10.1016/j.ygeno.2006.02.009>
PMID:[16595170](#)
37. Maudsley S, Martin B, Luttrell LM. The origins of diversity and specificity in g protein-coupled receptor

- signaling. *J Pharmacol Exp Ther.* 2005; 314:485–94.
<https://doi.org/10.1124/jpet.105.083121>
PMID:15805429
38. Chadwick W, Maudsley S. The Devil is in the Dose: Complexity of Receptor Systems and Responses. In: Mattson M., Calabrese E. (eds) *Hormesis*, pp 95–108. Humana Press. 2010. https://doi.org/10.1007/978-1-60761-495-1_5
39. Vaidehi N, Kenakin T. The role of conformational ensembles of seven transmembrane receptors in functional selectivity. *Curr Opin Pharmacol.* 2010; 10:775–81.
<https://doi.org/10.1016/j.coph.2010.09.004>
PMID:20933468
40. Ottosson-Laakso E, Krus U, Storm P, Prasad RB, Oskolkov N, Ahlqvist E, Fadista J, Hansson O, Groop L, Vikman P. Glucose-Induced Changes in Gene Expression in Human Pancreatic Islets: Causes or Consequences of Chronic Hyperglycemia. *Diabetes.* 2017; 66:3013–28. <https://doi.org/10.2337/db17-0311>
PMID:28882899
41. Tan R, Nakajima S, Wang Q, Sun H, Xue J, Wu J, Hellwig S, Zeng X, Yates NA, Smithgall TE, Lei M, Jiang Y, Levine AS, Su B, Lan L. Nek7 Protects Telomeres from Oxidative DNA Damage by Phosphorylation and Stabilization of TRF1. *Mol Cell.* 2017; 65:818–831.e5.
<https://doi.org/10.1016/j.molcel.2017.01.015>
PMID:28216227
42. Jabir MS, Hopkins L, Ritchie ND, Ullah I, Bayes HK, Li D, Tourlomousis P, Lupton A, Puleston D, Simon AK, Bryant C, Evans TJ. Mitochondrial damage contributes to *Pseudomonas aeruginosa* activation of the inflammasome and is downregulated by autophagy. *Autophagy.* 2015; 11:166–82.
<https://doi.org/10.4161/15548627.2014.981915>
PMID:25700738
43. Wang Y, Chen X, Chen X, Chen Q, Huo K. Transcriptional profiling and dynamical regulation analysis identify potential kernel target genes of SCYL1-BP1 in HEK293T cells. *Mol Cells.* 2014; 37:691–98.
<https://doi.org/10.14348/molcells.2014.0184>
PMID:25234469
44. Lu CC, Lee CC, Tseng CT, Tarn WY. Y14 governs p53 expression and modulates DNA damage sensitivity. *Sci Rep.* 2017; 7:45558.
<https://doi.org/10.1038/srep45558>
PMID:28361991
45. Izumi Y, Fujii K, Yamamoto S, Matsuo K, Namatame H, Taniguchi M, Yokoya A. DNA damage response induces structural alterations in histone H3-H4. *J Radiat Res.* 2017; 58:59–65.
<https://doi.org/10.1093/jrr/rrw086> PMID:27672100
46. Lefebvre V, Du Q, Baird S, Ng AC, Nascimento M, Campanella M, McBride HM, Sreaton RA. Genome-wide RNAi screen identifies ATPase inhibitory factor 1 (ATPIF1) as essential for PARK2 recruitment and mitophagy. *Autophagy.* 2013; 9:1770–79.
<https://doi.org/10.4161/auto.25413> PMID:24005319
47. Takada M, Nagai S, Haruta M, Sugino RP, Tozuka K, Takei H, Ohkubo F, Inoue K, Kurosumi M, Miyazaki M, Sato-Otsubo A, Sato Y, Ogawa S, Kaneko Y. BRCA1 alterations with additional defects in DNA damage response genes may confer chemoresistance to BRCA-like breast cancers treated with neoadjuvant chemotherapy. *Genes Chromosomes Cancer.* 2017; 56:405–20.
<https://doi.org/10.1002/gcc.22445>
PMID:28124401
48. Lian H, Wei J, Zang R, Ye W, Yang Q, Zhang XN, Chen YD, Fu YZ, Hu MM, Lei CQ, Luo WW, Li S, Shu HB. ZCCHC3 is a co-sensor of cGAS for dsDNA recognition in innate immune response. *Nat Commun.* 2018; 9:3349. <https://doi.org/10.1038/s41467-018-05559-w>
PMID:30135424
49. Napolitano M, Comegna M, Succio M, Leggiero E, Pastore L, Faraonio R, Cimino F, Passaro F. Comparative analysis of gene expression data reveals novel targets of senescence-associated microRNAs. *PLoS One.* 2014; 9:e98669.
<https://doi.org/10.1371/journal.pone.0098669>
PMID:24905922
50. Kuleshov MV, Jones MR, Rouillard AD, Fernandez NF, Duan Q, Wang Z, Koplev S, Jenkins SL, Jagodnik KM, Lachmann A, McDermott MG, Monteiro CD, Gundersen GW, Ma'ayan A. Enrichr: a comprehensive gene set enrichment analysis web server 2016 update. *Nucleic Acids Res.* 2016; 44:W90-7.
<https://doi.org/10.1093/nar/gkw377>
PMID:27141961
51. Hoefen RJ, Berk BC. The multifunctional GIT family of proteins. *J Cell Sci.* 2006; 119:1469–75.
<https://doi.org/10.1242/jcs.02925> PMID:16598076
52. van Gastel J, Boddaert J, Jushaj A, Premont RT, Luttrell LM, Janssens J, Martin B, Maudsley S. GIT2-A keystone in ageing and age-related disease. *Ageing Res Rev.* 2018; 43:46–63.
<https://doi.org/10.1016/j.arr.2018.02.002>
PMID:29452267
53. Phee H, Dzhagalov I, Mollenauer M, Wang Y, Irvine DJ, Robey E, Weiss A. Regulation of thymocyte positive selection and motility by GIT2. *Nat Immunol.* 2010; 11:503–11.
<https://doi.org/10.1038/ni.1868>
PMID:20431621
54. Chen H, Martin B, Daimon CM, Siddiqui S, Luttrell LM, Maudsley S. Textrou!: extracting semantic textual

- meaning from gene sets. *PLoS One*. 2013; 8:e62665. <https://doi.org/10.1371/journal.pone.0062665> PMID:[23646135](https://pubmed.ncbi.nlm.nih.gov/23646135/)
55. Martin B, Brenneman R, Golden E, Walent T, Becker KG, Prabhu VV, Wood W 3rd, Ladenheim B, Cadet JL, Maudsley S. Growth factor signals in neural cells: coherent patterns of interaction control multiple levels of molecular and phenotypic responses. *J Biol Chem*. 2009; 284:2493–511. <https://doi.org/10.1074/jbc.M804545200> PMID:[19038969](https://pubmed.ncbi.nlm.nih.gov/19038969/)
56. Maudsley S, Patel SA, Park SS, Luttrell LM, Martin B. Functional signaling biases in G protein-coupled receptors: game Theory and receptor dynamics. *Mini Rev Med Chem*. 2012; 12:831–40. <https://doi.org/10.2174/138955712800959071> PMID:[22681251](https://pubmed.ncbi.nlm.nih.gov/22681251/)
57. Zhou XE, Melcher K, Xu HE. Understanding the GPCR biased signaling through G protein and arrestin complex structures. *Curr Opin Struct Biol*. 2017; 45:150–59. <https://doi.org/10.1016/j.sbi.2017.05.004> PMID:[28558341](https://pubmed.ncbi.nlm.nih.gov/28558341/)
58. Rothkamm K, Barnard S, Moquet J, Ellender M, Rana Z, Burdak-Rothkamm S. DNA damage foci: meaning and significance. *Environ Mol Mutagen*. 2015; 56:491–504. <https://doi.org/10.1002/em.21944> PMID:[25773265](https://pubmed.ncbi.nlm.nih.gov/25773265/)
59. Siddiqui MS, François M, Fenech MF, Leifert WR. Persistent γ H2AX: A promising molecular marker of DNA damage and aging. *Mutat Res Rev Mutat Res*. 2015; 766:1–19. <https://doi.org/10.1016/j.mrrev.2015.07.001> PMID:[26596544](https://pubmed.ncbi.nlm.nih.gov/26596544/)
60. Liang S, Ju X, Zhou Y, Chen Y, Ke G, Wen H, Wu X. Downregulation of eukaryotic initiation factor 4A1 improves radiosensitivity by delaying DNA double strand break repair in cervical cancer. *Oncol Lett*. 2017; 14:6976–82. <https://doi.org/10.3892/ol.2017.7040> PMID:[29163714](https://pubmed.ncbi.nlm.nih.gov/29163714/)
61. Nosrati N, Kapoor NR, Kumar V. DNA damage stress induces the expression of ribosomal protein S27a gene in a p53-dependent manner. *Gene*. 2015; 559:44–51. <https://doi.org/10.1016/j.gene.2015.01.014> PMID:[25592822](https://pubmed.ncbi.nlm.nih.gov/25592822/)
62. Zhang CC, Yang JM, Bash-Babula J, White E, Murphy M, Levine AJ, Hait WN. DNA damage increases sensitivity to vinca alkaloids and decreases sensitivity to taxanes through p53-dependent repression of microtubule-associated protein 4. *Cancer Res*. 1999; 59:3663–70. PMID:[10446979](https://pubmed.ncbi.nlm.nih.gov/10446979/)
63. Francisco G, Gonçalves FT, Luiz OC, Saito RF, Toledo RA, Sekiya T, Tortelli TC Jr, Violla ED, Furuya Mazzotti TK, Cirilo PD, Festa-Neto C, Sanches JA, Gattás GJ, et al. Polymorphisms in the p27kip-1 and prohibitin genes denote novel genes associated with melanoma risk in Brazil, a high ultraviolet index region. *Melanoma Res*. 2013; 23:231–36. <https://doi.org/10.1097/CMR.0b013e3283612483> PMID:[23624368](https://pubmed.ncbi.nlm.nih.gov/23624368/)
64. Haliloglu T, Bahar I. Adaptability of protein structures to enable functional interactions and evolutionary implications. *Curr Opin Struct Biol*. 2015; 35:17–23. <https://doi.org/10.1016/j.sbi.2015.07.007> PMID:[26254902](https://pubmed.ncbi.nlm.nih.gov/26254902/)
65. Chhunchha B, Singh P, Stamer WD, Singh DP. Prdx6 retards senescence and restores trabecular meshwork cell health by regulating reactive oxygen species. *Cell Death Discov*. 2017; 3:17060. <https://doi.org/10.1038/cddiscovery.2017.60> PMID:[28904819](https://pubmed.ncbi.nlm.nih.gov/28904819/)
66. Ozkosem B, Feinstein SI, Fisher AB, O’Flaherty C. Advancing age increases sperm chromatin damage and impairs fertility in peroxiredoxin 6 null mice. *Redox Biol*. 2015; 5:15–23. <https://doi.org/10.1016/j.redox.2015.02.004> PMID:[25796034](https://pubmed.ncbi.nlm.nih.gov/25796034/)
67. Hampp S, Kiessling T, Buechle K, Mansilla SF, Thomale J, Rall M, Ahn J, Pospiech H, Gottifredi V, Wiesmüller L. DNA damage tolerance pathway involving DNA polymerase ι and the tumor suppressor p53 regulates DNA replication fork progression. *Proc Natl Acad Sci USA*. 2016; 113:E4311–19. <https://doi.org/10.1073/pnas.1605828113> PMID:[27407148](https://pubmed.ncbi.nlm.nih.gov/27407148/)
68. Cobb AM, Murray TV, Warren DT, Liu Y, Shanahan CM. Disruption of PCNA-lamins A/C interactions by prelamin A induces DNA replication fork stalling. *Nucleus*. 2016; 7:498–511. <https://doi.org/10.1080/19491034.2016.1239685> PMID:[27676213](https://pubmed.ncbi.nlm.nih.gov/27676213/)
69. Wang H, Guo W, Mitra J, Hegde PM, Vandoorne T, Eckelmann BJ, Mitra S, Tomkinson AE, Van Den Bosch L, Hegde ML. Mutant FUS causes DNA ligation defects to inhibit oxidative damage repair in Amyotrophic Lateral Sclerosis. *Nat Commun*. 2018; 9:3683. <https://doi.org/10.1038/s41467-018-06111-6> PMID:[30206235](https://pubmed.ncbi.nlm.nih.gov/30206235/)
70. Munschauer M, Nguyen CT, Sirokman K, Hartigan CR, Hogstrom L, Engreitz JM, Ulirsch JC, Fulco CP, Subramanian V, Chen J, Schenone M, Guttman M, Carr SA, Lander ES. The NORAD lncRNA assembles a topoisomerase complex critical for genome stability. *Nature*. 2018; 561:132–36. <https://doi.org/10.1038/s41586-018-0453-z> PMID:[30150775](https://pubmed.ncbi.nlm.nih.gov/30150775/)

71. Boesten DM, de Vos-Houben JM, Timmermans L, den Hartog GJ, Bast A, Hageman GJ. Accelerated aging during chronic oxidative stress: a role for PARP-1. *Oxid Med Cell Longev*. 2013; 2013:680414. <https://doi.org/10.1155/2013/680414> PMID:[24319532](https://pubmed.ncbi.nlm.nih.gov/24319532/)
72. Smith S. Telomerase can't handle the stress. *Genes Dev*. 2018; 32:597–99. <https://doi.org/10.1101/gad.316042.118> PMID:[29802121](https://pubmed.ncbi.nlm.nih.gov/29802121/)
73. Ahmed W, Lingner J. PRDX1 and MTH1 cooperate to prevent ROS-mediated inhibition of telomerase. *Genes Dev*. 2018; 32:658–69. <https://doi.org/10.1101/gad.313460.118> PMID:[29773556](https://pubmed.ncbi.nlm.nih.gov/29773556/)
74. Khatiwala RV, Zhang S, Li X, Devejian N, Bennett E, Cai C. Inhibition of p16^{INK4A} to Rejuvenate Aging Human Cardiac Progenitor Cells via the Upregulation of Anti-oxidant and NFκB Signal Pathways. *Stem Cell Rev Rep*. 2018; 14:612–25. <https://doi.org/10.1007/s12015-018-9815-z> PMID:[29675777](https://pubmed.ncbi.nlm.nih.gov/29675777/)
75. Zhang Y, Unnikrishnan A, Deepa SS, Liu Y, Li Y, Ikeno Y, Sosnowska D, Van Remmen H, Richardson A. A new role for oxidative stress in aging: the accelerated aging phenotype in *Sod1*^{-/-} mice is correlated to increased cellular senescence. *Redox Biol*. 2017; 11:30–37. <https://doi.org/10.1016/j.redox.2016.10.014> PMID:[27846439](https://pubmed.ncbi.nlm.nih.gov/27846439/)
76. Yang M, Peng Y, Liu W, Zhou M, Meng Q, Yuan C. Sirtuin 2 expression suppresses oxidative stress and senescence of nucleus pulposus cells through inhibition of the p53/p21 pathway. *Biochem Biophys Res Commun*. 2019; 513:616–22. <https://doi.org/10.1016/j.bbrc.2019.03.200> PMID:[30981502](https://pubmed.ncbi.nlm.nih.gov/30981502/)
77. Massey AJ. Modification of tumour cell metabolism modulates sensitivity to Chk1 inhibitor-induced DNA damage. *Sci Rep*. 2017; 7:40778. <https://doi.org/10.1038/srep40778> PMID:[28106079](https://pubmed.ncbi.nlm.nih.gov/28106079/)
78. de Souza-Pinto NC, Mason PA, Hashiguchi K, Weissman L, Tian J, Guay D, Lebel M, Stevnsner TV, Rasmussen LJ, Bohr VA. Novel DNA mismatch-repair activity involving YB-1 in human mitochondria. *DNA Repair (Amst)*. 2009; 8:704–19. <https://doi.org/10.1016/j.dnarep.2009.01.021> PMID:[19272840](https://pubmed.ncbi.nlm.nih.gov/19272840/)
79. Supale S, Thorel F, Merkwirth C, Gjinovci A, Herrera PL, Scorrano L, Meda P, Langer T, Maechler P. Loss of prohibitin induces mitochondrial damages altering β-cell function and survival and is responsible for gradual diabetes development. *Diabetes*. 2013; 62:3488–99. <https://doi.org/10.2337/db13-0152> PMID:[23863811](https://pubmed.ncbi.nlm.nih.gov/23863811/)
80. Jazwinski SM. Yeast replicative life span—the mitochondrial connection. *FEMS Yeast Res*. 2004; 5:119–25. <https://doi.org/10.1016/j.femsyr.2004.04.005> PMID:[15489194](https://pubmed.ncbi.nlm.nih.gov/15489194/)
81. Piper PW, Jones GW, Bringloe D, Harris N, MacLean M, Mollapour M. The shortened replicative life span of prohibitin mutants of yeast appears to be due to defective mitochondrial segregation in old mother cells. *Aging Cell*. 2002; 1:149–57. <https://doi.org/10.1046/j.1474-9728.2002.00018.x> PMID:[12882345](https://pubmed.ncbi.nlm.nih.gov/12882345/)
82. Merkwirth C, Martinelli P, Korwitz A, Morbin M, Brönneke HS, Jordan SD, Rugarli EI, Langer T. Loss of prohibitin membrane scaffolds impairs mitochondrial architecture and leads to tau hyperphosphorylation and neurodegeneration. *PLoS Genet*. 2012; 8:e1003021. <https://doi.org/10.1371/journal.pgen.1003021> PMID:[23144624](https://pubmed.ncbi.nlm.nih.gov/23144624/)
83. Baqri RM, Pietron AV, Gokhale RH, Turner BA, Kaguni LS, Shingleton AW, Kunes S, Miller KE. Mitochondrial chaperone TRAP1 activates the mitochondrial UPR and extends healthspan in *Drosophila*. *Mech Ageing Dev*. 2014; 141-142:35–45. <https://doi.org/10.1016/j.mad.2014.09.002> PMID:[25265088](https://pubmed.ncbi.nlm.nih.gov/25265088/)
84. Mancini A, Vitucci D, Randers MB, Schmidt JF, Hagman M, Andersen TR, Imperlini E, Mandola A, Orrù S, Krustup P, Buono P. Lifelong Football Training: Effects on Autophagy and Healthy Longevity Promotion. *Front Physiol*. 2019; 10:132. <https://doi.org/10.3389/fphys.2019.00132> PMID:[30837897](https://pubmed.ncbi.nlm.nih.gov/30837897/)
85. Kim J, Kang S, Kwon H, Moon H, Park MC. Dual functional bioactive-peptide, AIMP1-derived peptide (AdP), for anti-aging. *J Cosmet Dermatol*. 2019; 18:251–57. <https://doi.org/10.1111/jocd.12671> PMID:[29921010](https://pubmed.ncbi.nlm.nih.gov/29921010/)
86. Jang S, Lee JH, Sohn BK, Kim E, Park SG, Yoon KJ, Park M, Kim EW, Jeong J, Lee JY, Kim CH, Namkoong K. Suppression of AIMP1 protects cognition in Alzheimer's disease model mice 3xTg-AD. *Neuroreport*. 2017; 28:82–86. <https://doi.org/10.1097/WNR.0000000000000710> PMID:[27906773](https://pubmed.ncbi.nlm.nih.gov/27906773/)
87. Okano S, Yasui A, Kanno SI, Satoh K, Igarashi M, Nakajima O. Karyopherin Alpha 2-Expressing Pancreatic Duct Glands and Intra-Islet Ducts in Aged Diabetic C414A-Mutant-CRY1 Transgenic Mice. *J Diabetes Res*. 2019; 2019:7234549. <https://doi.org/10.1155/2019/7234549> PMID:[31179341](https://pubmed.ncbi.nlm.nih.gov/31179341/)

88. Wang R, Fan Q, Zhang J, Zhang X, Kang Y, Wang Z. Hydrogen Sulfide Demonstrates Promising Antitumor Efficacy in Gastric Carcinoma by Targeting MGAT5. *Transl Oncol.* 2018; 11:900–10. <https://doi.org/10.1016/j.tranon.2018.04.008> PMID:29800930
89. Liu J, Fang H, Chi Z, Wu Z, Wei D, Mo D, Niu K, Balajee AS, Hei TK, Nie L, Zhao Y. XPD localizes in mitochondria and protects the mitochondrial genome from oxidative DNA damage. *Nucleic Acids Res.* 2015; 43:5476–88. <https://doi.org/10.1093/nar/gkv472> PMID:25969448
90. Lattanzi G, Marmiroli S, Facchini A, Maraldi NM. Nuclear damages and oxidative stress: new perspectives for laminopathies. *Eur J Histochem.* 2012; 56:e45. <https://doi.org/10.4081/ejh.2012.e45> PMID:23361241
91. Nishii M, Nakano S, Nakamura S, Wate R, Shinde A, Kaneko S, Kusaka H. Myonuclear breakdown in sporadic inclusion body myositis is accompanied by DNA double strand breaks. *Neuromuscul Disord.* 2011; 21:345–52. <https://doi.org/10.1016/j.nmd.2011.02.004> PMID:21353553
92. Eid A, Bihagi SW, Renehan WE, Zawia NH. Developmental lead exposure and lifespan alterations in epigenetic regulators and their correspondence to biomarkers of Alzheimer's disease. *Alzheimers Dement (Amst).* 2016; 2:123–31. <https://doi.org/10.1016/j.dadm.2016.02.002> PMID:27239543
93. Luciano M, Lopez LM, de Moor MH, Harris SE, Davies G, Nutile T, Krueger RF, Esko T, Schlessinger D, Toshiko T, Derringer JL, Realo A, Hansell NK, et al. Longevity candidate genes and their association with personality traits in the elderly. *Am J Med Genet B Neuropsychiatr Genet.* 2012; 159B:192–200. <https://doi.org/10.1002/ajmg.b.32013> PMID:22213687
94. Huang CJ, Das U, Xie W, Ducasse M, Tucker HO. Altered stoichiometry and nuclear delocalization of NonO and PSF promote cellular senescence. *Aging (Albany NY).* 2016; 8:3356–74. <https://doi.org/10.18632/aging.101125> PMID:27992859
95. Fonseca Costa SS, Wegmann D, Ripperger JA. Normalisation against Circadian and Age-Related Disturbances Enables Robust Detection of Gene Expression Changes in Liver of Aged Mice. *PLoS One.* 2017; 12:e0169615. <https://doi.org/10.1371/journal.pone.0169615> PMID:28068403
96. de Silva HC, Lin MZ, Phillips L, Martin JL, Baxter RC. IGFBP-3 interacts with NONO and SFPQ in PARP-dependent DNA damage repair in triple-negative breast cancer. *Cell Mol Life Sci.* 2019; 76:2015–30. <https://doi.org/10.1007/s00018-019-03033-4> PMID:30725116
97. Krietsch J, Caron MC, Gagné JP, Ethier C, Vignard J, Vincent M, Rouleau M, Hendzel MJ, Poirier GG, Masson JY. PARP activation regulates the RNA-binding protein NONO in the DNA damage response to DNA double-strand breaks. *Nucleic Acids Res.* 2012; 40:10287–301. <https://doi.org/10.1093/nar/gks798> PMID:22941645
98. Salton M, Lerenthal Y, Wang SY, Chen DJ, Shiloh Y. Involvement of Matrin 3 and SFPQ/NONO in the DNA damage response. *Cell Cycle.* 2010; 9:1568–76. <https://doi.org/10.4161/cc.9.8.11298> PMID:20421735
99. Li S, Shu FJ, Li Z, Jaafar L, Zhao S, Dynan WS. Cell-type specific role of the RNA-binding protein, NONO, in the DNA double-strand break response in the mouse testes. *DNA Repair (Amst).* 2017; 51:70–78. <https://doi.org/10.1016/j.dnarep.2017.02.002> PMID:28209515
100. Kowalska E, Ripperger JA, Hoegger DC, Bruegger P, Buch T, Birchler T, Mueller A, Albrecht U, Contaldo C, Brown SA. NONO couples the circadian clock to the cell cycle. *Proc Natl Acad Sci USA.* 2013; 110:1592–99. <https://doi.org/10.1073/pnas.1213317110> PMID:23267082
101. Becher OJ, Peterson KM, Khatua S, Santi MR, MacDonald TJ. IGFBP2 is overexpressed by pediatric malignant astrocytomas and induces the repair enzyme DNA-PK. *J Child Neurol.* 2008; 23:1205–13. <https://doi.org/10.1177/0883073808321766> PMID:18952587
102. Zhou Z, Lu H, Zhu S, Gomaa A, Chen Z, Yan J, Washington K, El-Rifai W, Dang C, Peng D. Activation of EGFR-DNA-PKcs pathway by IGFBP2 protects esophageal adenocarcinoma cells from acidic bile salts-induced DNA damage. *J Exp Clin Cancer Res.* 2019; 38:13. <https://doi.org/10.1186/s13046-018-1021-y> PMID:30626422
103. Kirschner K, Singh R, Prost S, Melton DW. Characterisation of Ercc1 deficiency in the liver and in conditional Ercc1-deficient primary hepatocytes in vitro. *DNA Repair (Amst).* 2007; 6:304–16. <https://doi.org/10.1016/j.dnarep.2006.10.020> PMID:17126084
104. Tanikawa M, Sanjiv K, Helleday T, Herr P, Mortusewicz O. The spliceosome U2 snRNP factors promote genome stability through distinct mechanisms; transcription of repair factors and R-loop processing. *Oncogenesis.* 2016; 5:e280.

- <https://doi.org/10.1038/oncsis.2016.70>
PMID:27991914
105. Lee JH, Cheng R, Honig LS, Feitosa M, Kammerer CM, Kang MS, Schupf N, Lin SJ, Sanders JL, Bae H, Druley T, Perls T, Christensen K, et al. Genome wide association and linkage analyses identified three loci-4q25, 17q23.2, and 10q11.21-associated with variation in leukocyte telomere length: the Long Life Family Study. *Front Genet.* 2014; 4:310.
<https://doi.org/10.3389/fgene.2013.00310>
PMID:24478790
106. Ozeki K, Sugiyama M, Akter KA, Nishiwaki K, Asano-Inami E, Senga T. FAM98A is localized to stress granules and associates with multiple stress granule-localized proteins. *Mol Cell Biochem.* 2019; 451:107–15.
<https://doi.org/10.1007/s11010-018-3397-6>
PMID:29992460
107. Mehta M, Basalingappa K, Griffith JN, Andrade D, Babu A, Amreddy N, Muralidharan R, Gorospe M, Herman T, Ding WQ, Ramesh R, Munshi A. HuR silencing elicits oxidative stress and DNA damage and sensitizes human triple-negative breast cancer cells to radiotherapy. *Oncotarget.* 2016; 7:64820–35.
<https://doi.org/10.18632/oncotarget.11706>
PMID:27588488
108. Alfano L, Costa C, Caporaso A, Antonini D, Giordano A, Pentimalli F. HUR protects NONO from degradation by mir320, which is induced by p53 upon UV irradiation. *Oncotarget.* 2016; 7:78127–39.
<https://doi.org/10.18632/oncotarget.13002>
PMID:27816966
109. Al-Mohanna MA, Al-Khalaf HH, Al-Yousef N, Aboussekhra A. The p16INK4a tumor suppressor controls p21WAF1 induction in response to ultraviolet light. *Nucleic Acids Res.* 2007; 35:223–33.
<https://doi.org/10.1093/nar/gkl1075> PMID:17158160
110. Tang H, Wang H, Cheng X, Fan X, Yang F, Zhang M, Chen Y, Tian Y, Liu C, Shao D, Jiang B, Dou Y, Cong Y, et al. HuR regulates telomerase activity through TERC methylation. *Nat Commun.* 2018; 9:2213.
<https://doi.org/10.1038/s41467-018-04617-7>
PMID:29880812
111. Mark RJ, Hensley K, Butterfield DA, Mattson MP. Amyloid beta-peptide impairs ion-motive ATPase activities: evidence for a role in loss of neuronal Ca²⁺ homeostasis and cell death. *J Neurosci.* 1995; 15:6239–49.
<https://doi.org/10.1523/JNEUROSCI.15-09-06239.1995>
PMID:7666206
112. Niccoli T, Partridge L, Isaacs AM. Ageing as a risk factor for ALS/FTD. *Hum Mol Genet.* 2017; 26:R105–13.
<https://doi.org/10.1093/hmg/ddx247> PMID:28977441
113. Mihalas BP, Redgrove KA, McLaughlin EA, Nixon B. Molecular Mechanisms Responsible for Increased Vulnerability of the Ageing Oocyte to Oxidative Damage. *Oxid Med Cell Longev.* 2017; 2017:4015874.
<https://doi.org/10.1155/2017/4015874>
PMID:29312475
114. Andriani GA, Almeida VP, Faggioli F, Mauro M, Tsai WL, Santambrogio L, Maslov A, Gadina M, Campisi J, Vijg J, Montagna C. Whole Chromosome Instability induces senescence and promotes SASP. *Sci Rep.* 2016; 6:35218.
<https://doi.org/10.1038/srep35218> PMID:27731420
115. Zhou G, Soufan O, Ewald J, Hancock RE, Basu N, Xia J. NetworkAnalyst 3.0: a visual analytics platform for comprehensive gene expression profiling and meta-analysis. *Nucleic Acids Res.* 2019; 47:W234–41.
<https://doi.org/10.1093/nar/gkz240> PMID:30931480
116. Xu R, Yuan Z, Yang L, Li L, Li D, Lv C. Inhibition of NAMPT decreases cell growth and enhances susceptibility to oxidative stress. *Oncol Rep.* 2017; 38:1767–73. <https://doi.org/10.3892/or.2017.5793>
PMID:28714034
117. Yu J, Shi J, Zhang Y, Zhang Y, Huang Y, Chen Z, Yang J. The replicative senescent mesenchymal stem / stromal cells defect in DNA damage response and anti-oxidative capacity. *Int J Med Sci.* 2018; 15:771–81.
<https://doi.org/10.7150/ijms.24635> PMID:30008586
118. Liu JY, Souroullas GP, Diekman BO, Krishnamurthy J, Hall BM, Sorrentino JA, Parker JS, Sessions GA, Gudkov AV, Sharpless NE. Cells exhibiting strong p16^{INK4a} promoter activation in vivo display features of senescence. *Proc Natl Acad Sci USA.* 2019; 116:2603–11.
<https://doi.org/10.1073/pnas.1818313116>
PMID:30683717
119. Sharpless NE, Sherr CJ. Forging a signature of in vivo senescence. *Nat Rev Cancer.* 2015; 15:397–408.
<https://doi.org/10.1038/nrc3960> PMID:26105537
120. Gundersen GW, Jagodnik KM, Woodland H, Fernandez NF, Sani K, Dohlman AB, Ung PM, Monteiro CD, Schlessinger A, Ma'ayan A. GEN3VA: aggregation and analysis of gene expression signatures from related studies. *BMC Bioinformatics.* 2016; 17:461.
<https://doi.org/10.1186/s12859-016-1321-1>
PMID:27846806
121. van Gestel J, Hendrickx JO, Leysen H, Martin B, Veenker L, Beuning S, Coppens V, Morrens M, Maudsley S. Enhanced Molecular Appreciation of Psychiatric Disorders Through High-Dimensionality Data Acquisition and Analytics. *Methods Mol Biol.* 2019; 2011:671–723. https://doi.org/10.1007/978-1-4939-9554-7_39 PMID:31273728
122. Cashion A, Stanfill A, Thomas F, Xu L, Sutter T, Eason J, Ensell M, Homayouni R. Expression levels of obesity-

- related genes are associated with weight change in kidney transplant recipients. *PLoS One*. 2013; 8:e59962. <https://doi.org/10.1371/journal.pone.0059962> PMID:[23544116](https://pubmed.ncbi.nlm.nih.gov/23544116/)
123. Goldstein M, Kastan MB. Repair versus Checkpoint Functions of BRCA1 Are Differentially Regulated by Site of Chromatin Binding. *Cancer Res*. 2015; 75:2699–707. <https://doi.org/10.1158/0008-5472.CAN-15-0400> PMID:[25939603](https://pubmed.ncbi.nlm.nih.gov/25939603/)
124. Parameswaran B, Chiang HC, Lu Y, Coates J, Deng CX, Baer R, Lin HK, Li R, Paull TT, Hu Y. Damage-induced BRCA1 phosphorylation by Chk2 contributes to the timing of end resection. *Cell Cycle*. 2015; 14:437–48. <https://doi.org/10.4161/15384101.2014.972901> PMID:[25659039](https://pubmed.ncbi.nlm.nih.gov/25659039/)
125. Cortez D, Wang Y, Qin J, Elledge SJ. Requirement of ATM-dependent phosphorylation of brca1 in the DNA damage response to double-strand breaks. *Science*. 1999; 286:1162–66. <https://doi.org/10.1126/science.286.5442.1162> PMID:[10550055](https://pubmed.ncbi.nlm.nih.gov/10550055/)
126. Chadwick W, Brenneman R, Martin B, Maudsley S. Complex and multidimensional lipid raft alterations in a murine model of Alzheimer's disease. *Int J Alzheimers Dis*. 2010; 2010:604792. <https://doi.org/10.4061/2010/604792> PMID:[21151659](https://pubmed.ncbi.nlm.nih.gov/21151659/)
127. Wang X, Liao S, Nelson ER, Schmalzigaug R, Spurney RF, Guilak F, Premont RT, Gesty-Palmer D. The cytoskeletal regulatory scaffold protein GIT2 modulates mesenchymal stem cell differentiation and osteoblastogenesis. *Biochem Biophys Res Commun*. 2012; 425:407–12. <https://doi.org/10.1016/j.bbrc.2012.07.111> PMID:[22846567](https://pubmed.ncbi.nlm.nih.gov/22846567/)
128. Singh MK, Gao H, Sun W, Song Z, Schmalzigaug R, Premont RT, Zhang Q. Structure-activity relationship studies of QS11, a small molecule Wnt synergistic agonist. *Bioorg Med Chem Lett*. 2015; 25:4838–42. <https://doi.org/10.1016/j.bmcl.2015.06.062> PMID:[26152429](https://pubmed.ncbi.nlm.nih.gov/26152429/)
129. Luttrell LM, Maudsley S, Gesty-Palmer D. Translating in vitro ligand bias into in vivo efficacy. *Cell Signal*. 2018; 41:46–55. <https://doi.org/10.1016/j.cellsig.2017.05.002> PMID:[28495495](https://pubmed.ncbi.nlm.nih.gov/28495495/)
130. Maudsley S, Martin B, Gesty-Palmer D, Cheung H, Johnson C, Patel S, Becker KG, Wood WH 3rd, Zhang Y, Lehrmann E, Luttrell LM. Delineation of a conserved arrestin-biased signaling repertoire in vivo. *Mol Pharmacol*. 2015; 87:706–17. <https://doi.org/10.1124/mol.114.095224> PMID:[25637603](https://pubmed.ncbi.nlm.nih.gov/25637603/)
131. Tréfier A, Musnier A, Landomiel F, Bourquard T, Boulo T, Ayoub MA, León K, Bruneau G, Chevalier M, Durand G, Blache MC, Inoue A, Fontaine J, et al. G protein-dependent signaling triggers a β -arrestin-scaffolded p70S6K/ rpS6 module that controls 5'TOP mRNA translation. *FASEB J*. 2018; 32:1154–69. <https://doi.org/10.1096/fj.201700763R> PMID:[29084767](https://pubmed.ncbi.nlm.nih.gov/29084767/)
132. Liu C, Eriste E, Sutton S, Chen J, Roland B, Kuei C, Farmer N, Jörnvall H, Sillard R, Lovenberg TW. Identification of relaxin-3/INSL7 as an endogenous ligand for the orphan G-protein-coupled receptor GPCR135. *J Biol Chem*. 2003; 278:50754–64. <https://doi.org/10.1074/jbc.M308995200> PMID:[14522968](https://pubmed.ncbi.nlm.nih.gov/14522968/)
133. Jensen AS, Sparre-Ulrich AH, Davis-Poynter N, Rosenkilde MM. Structural Diversity in Conserved Regions Like the DRY-Motif among Viral 7TM Receptors-A Consequence of Evolutionary Pressure? *Adv Virol*. 2012; 2012:231813. <https://doi.org/10.1155/2012/231813> PMID:[22899926](https://pubmed.ncbi.nlm.nih.gov/22899926/)
134. Schneider EH, Schnell D, Strasser A, Dove S, Seifert R. Impact of the DRY motif and the missing “ionic lock” on constitutive activity and G-protein coupling of the human histamine H4 receptor. *J Pharmacol Exp Ther*. 2010; 333:382–92. <https://doi.org/10.1124/jpet.109.163220> PMID:[20106995](https://pubmed.ncbi.nlm.nih.gov/20106995/)
135. Luttrell LM, Ferguson SS, Daaka Y, Miller WE, Maudsley S, Della Rocca GJ, Lin F, Kawakatsu H, Owada K, Luttrell DK, Caron MG, Lefkowitz RJ. Beta-arrestin-dependent formation of beta2 adrenergic receptor-Src protein kinase complexes. *Science*. 1999; 283:655–61. <https://doi.org/10.1126/science.283.5402.655> PMID:[9924018](https://pubmed.ncbi.nlm.nih.gov/9924018/)
136. Stallaert W, Dorn JF, van der Westhuizen E, Audet M, Bouvier M. Impedance responses reveal β_2 -adrenergic receptor signaling pluridimensionality and allow classification of ligands with distinct signaling profiles. *PLoS One*. 2012; 7:e29420. <https://doi.org/10.1371/journal.pone.0029420> PMID:[22242170](https://pubmed.ncbi.nlm.nih.gov/22242170/)
137. Kenakin T. Biased Receptor Signaling in Drug Discovery. *Pharmacol Rev*. 2019; 71:267–315. <https://doi.org/10.1124/pr.118.016790> PMID:[30914442](https://pubmed.ncbi.nlm.nih.gov/30914442/)
138. Stäubert C, Schöneberg T. GPCR Signaling From Intracellular Membranes - A Novel Concept. *BioEssays*. 2017; 39:39. <https://doi.org/10.1002/bies.201700200> PMID:[29136291](https://pubmed.ncbi.nlm.nih.gov/29136291/)
139. Estelles A, Sperinde J, Roulon T, Aguilar B, Bonner C, LePecq JB, Delcayre A. Exosome nanovesicles

- displaying G protein-coupled receptors for drug discovery. *Int J Nanomedicine*. 2007; 2:751–60. PMID:[18203441](https://pubmed.ncbi.nlm.nih.gov/18203441/)
140. Pérez VI, Lew CM, Cortez LA, Webb CR, Rodriguez M, Liu Y, Qi W, Li Y, Chaudhuri A, Van Remmen H, Richardson A, Ikeno Y. Thioredoxin 2 haploinsufficiency in mice results in impaired mitochondrial function and increased oxidative stress. *Free Radic Biol Med*. 2008; 44:882–92. <https://doi.org/10.1016/j.freeradbiomed.2007.11.018> PMID:[18164269](https://pubmed.ncbi.nlm.nih.gov/18164269/)
141. Tsunoda S, Sierralta J, Sun Y, Bodner R, Suzuki E, Becker A, Socolich M, Zuker CS. A multivalent PDZ-domain protein assembles signalling complexes in a G-protein-coupled cascade. *Nature*. 1997; 388:243–49. <https://doi.org/10.1038/40805> PMID:[9230432](https://pubmed.ncbi.nlm.nih.gov/9230432/)
142. Martin B, Pearson M, Brenneman R, Golden E, Wood W, Prabhu V, Becker KG, Mattson MP, Maudsley S. Gonadal transcriptome alterations in response to dietary energy intake: sensing the reproductive environment. *PLoS One*. 2009; 4:e4146. <https://doi.org/10.1371/journal.pone.0004146> PMID:[19127293](https://pubmed.ncbi.nlm.nih.gov/19127293/)
143. Uversky VN. The multifaceted roles of intrinsic disorder in protein complexes. *FEBS Lett*. 2015; 589:2498–506. <https://doi.org/10.1016/j.febslet.2015.06.004> PMID:[26073257](https://pubmed.ncbi.nlm.nih.gov/26073257/)
144. Mikulecky DC. Complexity, communication between cells, and identifying the functional components of living systems: some observations. *Acta Biotheor*. 1996; 44:179–208. <https://doi.org/10.1007/BF00046527> PMID:[8953209](https://pubmed.ncbi.nlm.nih.gov/8953209/)
145. Van Regenmortel MH. Reductionism and complexity in molecular biology. Scientists now have the tools to unravel biological and overcome the limitations of reductionism. *EMBO Rep*. 2004; 5:1016–20. <https://doi.org/10.3410/f.1024612.298776> PMID:[15520799](https://pubmed.ncbi.nlm.nih.gov/15520799/)
146. Mazzocchi F. Complexity in biology. Exceeding the limits of reductionism and determinism using complexity theory. *EMBO Rep*. 2008; 9:10–14. <https://doi.org/10.1038/sj.embor.7401147> PMID:[18174892](https://pubmed.ncbi.nlm.nih.gov/18174892/)
147. von Kriegsheim A, Preisinger C, Kolch W. Mapping of signaling pathways by functional interaction proteomics. *Methods Mol Biol*. 2008; 484:177–92. https://doi.org/10.1007/978-1-59745-398-1_12 PMID:[18592180](https://pubmed.ncbi.nlm.nih.gov/18592180/)
148. Morris JH, Knudsen GM, Verschueren E, Johnson JR, Cimermanic P, Greninger AL, Pico AR. Affinity purification-mass spectrometry and network analysis to understand protein-protein interactions. *Nat Protoc*. 2014; 9:2539–54. <https://doi.org/10.1038/nprot.2014.164> PMID:[25275790](https://pubmed.ncbi.nlm.nih.gov/25275790/)
149. Cutler JA, Udainiya S, Madugundu AK, Renuse S, Xu Y, Jung J, Kim KP, Wu X, Pandey A. Integrative phosphoproteome and interactome analysis of the role of Ubash3b in BCR-ABL signaling. *Leukemia*. 2019. [Epub ahead of print] <https://doi.org/10.1038/s41375-019-0535-4> PMID:[31399640](https://pubmed.ncbi.nlm.nih.gov/31399640/)
150. Munk R, Panda AC, Grammatikakis I, Gorospe M, Abdelmohsen K. Senescence-Associated MicroRNAs. *Int Rev Cell Mol Biol*. 2017; 334:177–205. <https://doi.org/10.1016/bs.ircmb.2017.03.008> PMID:[28838538](https://pubmed.ncbi.nlm.nih.gov/28838538/)
151. Wang R, Yu Z, Sunchu B, Shoaf J, Dang I, Zhao S, Caples K, Bradley L, Beaver LM, Ho E, Löhr CV, Perez VI. Rapamycin inhibits the secretory phenotype of senescent cells by a Nrf2-independent mechanism. *Aging Cell*. 2017; 16:564–74. <https://doi.org/10.1111/acer.12587> PMID:[28371119](https://pubmed.ncbi.nlm.nih.gov/28371119/)
152. Wheaton K, Campuzano D, Ma W, Sheinis M, Ho B, Brown GW, Benchimol S. Progerin-Induced Replication Stress Facilitates Premature Senescence in Hutchinson-Gilford Progeria Syndrome. *Mol Cell Biol*. 2017; 37:37. <https://doi.org/10.1128/MCB.00659-16> PMID:[28483909](https://pubmed.ncbi.nlm.nih.gov/28483909/)
153. Hekmatimoghaddam S, Dehghani Firoozabadi A, Zare-Khormizi MR, Pourrajab F. Sirt1 and Parp1 as epigenome safeguards and microRNAs as SASP-associated signals, in cellular senescence and aging. *Ageing Res Rev*. 2017; 40:120–41. <https://doi.org/10.1016/j.arr.2017.10.001> PMID:[28993289](https://pubmed.ncbi.nlm.nih.gov/28993289/)
154. Iannetti A, Ledoux AC, Tudhope SJ, Sellier H, Zhao B, Mowla S, Moore A, Hummerich H, Gewurz BE, Cockell SJ, Jat PS, Willmore E, Perkins ND. Regulation of p53 and Rb links the alternative NF-κB pathway to EZH2 expression and cell senescence. *PLoS Genet*. 2014; 10:e1004642. <https://doi.org/10.1371/journal.pgen.1004642> PMID:[25255445](https://pubmed.ncbi.nlm.nih.gov/25255445/)
155. Zhou TB, Qin YH. Signaling pathways of prohibitin and its role in diseases. *J Recept Signal Transduct Res*. 2013; 33:28–36. <https://doi.org/10.3109/10799893.2012.752006> PMID:[23327602](https://pubmed.ncbi.nlm.nih.gov/23327602/)
156. Huen MS, Chen J. Assembly of checkpoint and repair machineries at DNA damage sites. *Trends Biochem Sci*. 2010; 35:101–08. <https://doi.org/10.1016/j.tibs.2009.09.001>

PMID:[19875294](#)

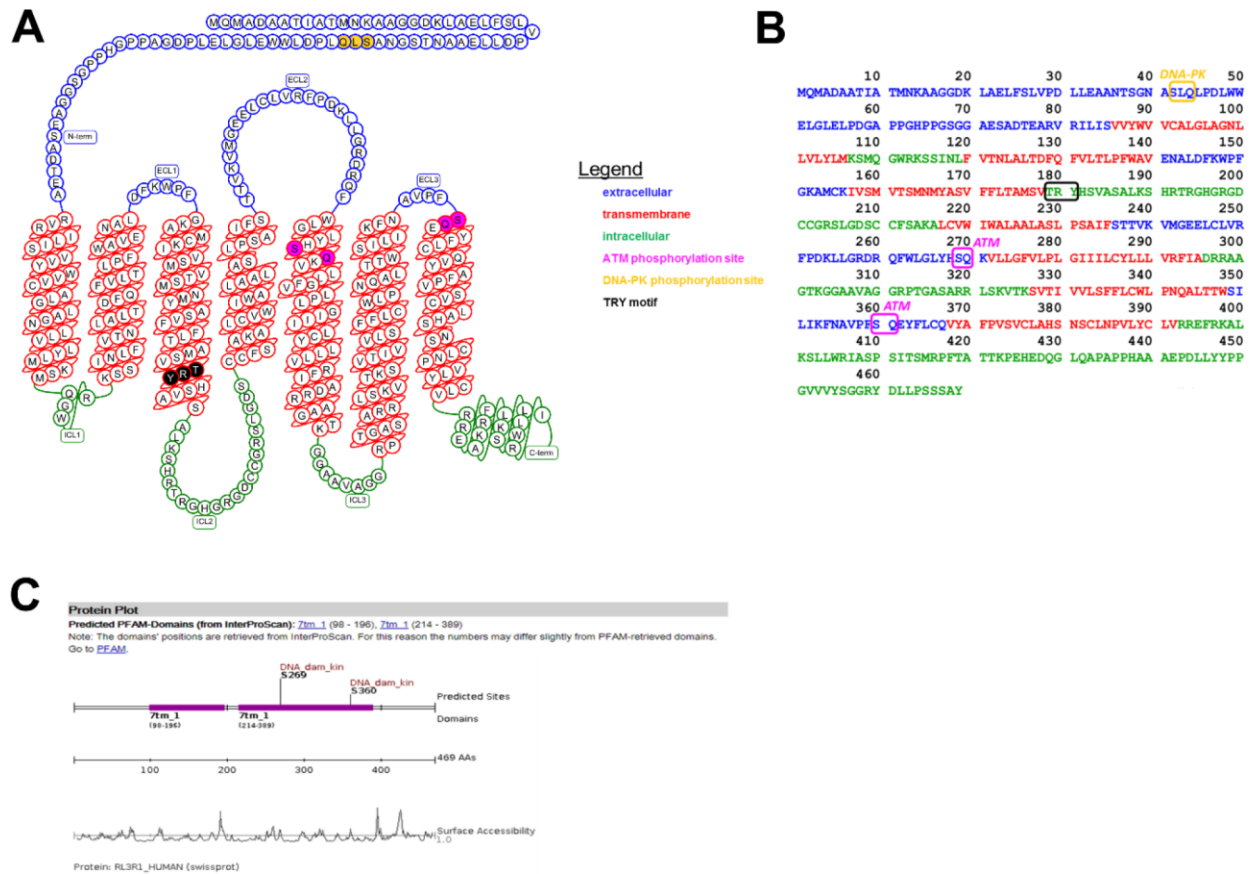
157. Ciccia A, Elledge SJ. The DNA damage response: making it safe to play with knives. *Mol Cell*. 2010; 40:179–204. <https://doi.org/10.1016/j.molcel.2010.09.019> PMID:[20965415](#)
158. Lukas J, Lukas C, Bartek J. More than just a focus: the chromatin response to DNA damage and its role in genome integrity maintenance. *Nat Cell Biol*. 2011; 13:1161–69. <https://doi.org/10.1038/ncb2344> PMID:[21968989](#)
159. Scully R, Chen J, Ochs RL, Keegan K, Hoekstra M, Feunteun J, Livingston DM. Dynamic changes of BRCA1 subnuclear location and phosphorylation state are initiated by DNA damage. *Cell*. 1997; 90:425–35. [https://doi.org/10.1016/S0092-8674\(00\)80503-6](https://doi.org/10.1016/S0092-8674(00)80503-6) PMID:[9267023](#)
160. Carr MI, Jones SN. Regulation of the Mdm2-p53 signaling axis in the DNA damage response and tumorigenesis. *Transl Cancer Res*. 2016; 5:707–24. <https://doi.org/10.21037/tcr.2016.11.75> PMID:[28690977](#)
161. Jette N, Lees-Miller SP. The DNA-dependent protein kinase: A multifunctional protein kinase with roles in DNA double strand break repair and mitosis. *Prog Biophys Mol Biol*. 2015; 117:194–205. <https://doi.org/10.1016/j.pbiomolbio.2014.12.003> PMID:[25550082](#)
162. Gurley KE, Ashley AK, Moser RD, Kemp CJ. Synergy between Prkdc and Trp53 regulates stem cell proliferation and GI-ARS after irradiation. *Cell Death Differ*. 2017; 24:1853–60. <https://doi.org/10.1038/cdd.2017.107> PMID:[28686579](#)
163. Fridovich I. Superoxide radical and superoxide dismutases. *Annu Rev Biochem*. 1995; 64:97–112. <https://doi.org/10.1146/annurev.bi.64.070195.000525> PMID:[7574505](#)
164. Zhang W, Huang Q, Zeng Z, Wu J, Zhang Y, Chen Z. Sirt1 Inhibits Oxidative Stress in Vascular Endothelial Cells. *Oxid Med Cell Longev*. 2017; 2017:7543973. <https://doi.org/10.1155/2017/7543973> PMID:[28546854](#)
165. Singh P, Hanson PS, Morris CM. SIRT1 ameliorates oxidative stress induced neural cell death and is down-regulated in Parkinson's disease. *BMC Neurosci*. 2017; 18:46. <https://doi.org/10.1186/s12868-017-0364-1> PMID:[28578695](#)
166. Moujaber O, Mahboubi H, Kodiha M, Bouttier M, Bednarz K, Bakshi R, White J, Larose L, Colmegna I, Stochaj U. Dissecting the molecular mechanisms that impair stress granule formation in aging cells. *Biochim Biophys Acta Mol Cell Res*. 2017; 1864:475–86. <https://doi.org/10.1016/j.bbamcr.2016.12.008> PMID:[27965113](#)
167. Lee JH, Park SJ, Hariharasudhan G, Kim MJ, Jung SM, Jeong SY, Chang IY, Kim C, Kim E, Yu J, Bae S, You HJ. ID3 regulates the MDC1-mediated DNA damage response in order to maintain genome stability. *Nat Commun*. 2017; 8:903. <https://doi.org/10.1038/s41467-017-01051-z> PMID:[29026069](#)
168. Enriquez-Rios V, Dumitrache LC, Downing SM, Li Y, Brown EJ, Russell HR, McKinnon PJ. DNA-PKcs, ATM, and ATR Interplay Maintains Genome Integrity during Neurogenesis. *J Neurosci*. 2017; 37:893–905. <https://doi.org/10.1523/JNEUROSCI.4213-15.2016> PMID:[28123024](#)
169. Busuttill RA, Garcia AM, Cabrera C, Rodriguez A, Suh Y, Kim WH, Huang TT, Vijg J. Organ-specific increase in mutation accumulation and apoptosis rate in CuZn-superoxide dismutase-deficient mice. *Cancer Res*. 2005; 65:11271–75. <https://doi.org/10.1158/0008-5472.CAN-05-2980> PMID:[16357131](#)
170. Elchuri S, Oberley TD, Qi W, Eisenstein RS, Jackson Roberts L, Van Remmen H, Epstein CJ, Huang TT. CuZnSOD deficiency leads to persistent and widespread oxidative damage and hepatocarcinogenesis later in life. *Oncogene*. 2005; 24:367–80. <https://doi.org/10.1038/sj.onc.1208207> PMID:[15531919](#)
171. Elchuri S, Naeemuddin M, Sharpe O, Robinson WH, Huang TT. Identification of biomarkers associated with the development of hepatocellular carcinoma in CuZn superoxide dismutase deficient mice. *Proteomics*. 2007; 7:2121–29. <https://doi.org/10.1002/pmic.200601011> PMID:[17514684](#)
172. Hou M, Zuo X, Li C, Zhang Y, Teng Y. Mir-29b Regulates Oxidative Stress by Targeting SIRT1 in Ovarian Cancer Cells. *Cell Physiol Biochem*. 2017; 43:1767–76. <https://doi.org/10.1159/000484063> PMID:[29050034](#)
173. Takahashi M, Higuchi M, Matsuki H, Yoshita M, Ohsawa T, Oie M, Fujii M. Stress granules inhibit apoptosis by reducing reactive oxygen species production. *Mol Cell Biol*. 2013; 33:815–29. <https://doi.org/10.1128/MCB.00763-12> PMID:[23230274](#)
174. Buchan JR, Parker R. Eukaryotic stress granules: the ins and outs of translation. *Mol Cell*. 2009; 36:932–41. <https://doi.org/10.1016/j.molcel.2009.11.020> PMID:[20064460](#)
175. Arimoto K, Fukuda H, Imajoh-Ohmi S, Saito H, Takekawa M. Formation of stress granules inhibits

- apoptosis by suppressing stress-responsive MAPK pathways. *Nat Cell Biol.* 2008; 10:1324–32.
<https://doi.org/10.1038/ncb1791>
PMID:18836437
176. Solomon S, Xu Y, Wang B, David MD, Schubert P, Kennedy D, Schrader JW. Distinct structural features of caprin-1 mediate its interaction with G3BP-1 and its induction of phosphorylation of eukaryotic translation initiation factor 2alpha, entry to cytoplasmic stress granules, and selective interaction with a subset of mRNAs. *Mol Cell Biol.* 2007; 27:2324–42.
<https://doi.org/10.1128/MCB.02300-06>
PMID:17210633
177. Tourrière H, Chebli K, Zekri L, Courselaud B, Blanchard JM, Bertrand E, Tazi J. The RasGAP-associated endoribonuclease G3BP assembles stress granules. *J Cell Biol.* 2003; 160:823–31.
<https://doi.org/10.1083/jcb.200212128>
PMID:12642610
178. Wolozin B. Physiological protein aggregation run amuck: stress granules and the genesis of neurodegenerative disease. *Discov Med.* 2014; 17:47–52. PMID:24411700
179. Joyce EM, Roiser JP. Cognitive heterogeneity in schizophrenia. *Curr Opin Psychiatry.* 2007; 20:268–72.
<https://doi.org/10.1097/YCO.0b013e3280ba4975>
PMID:17415081
180. Owen MJ, Sawa A, Mortensen PB. Schizophrenia. *Lancet.* 2016; 388:86–97.
[https://doi.org/10.1016/S0140-6736\(15\)01121-6](https://doi.org/10.1016/S0140-6736(15)01121-6)
PMID:26777917
181. Smith CM, Walker AW, Hosken IT, Chua BE, Zhang C, Haidar M, Gundlach AL. Relaxin-3/RXFP3 networks: an emerging target for the treatment of depression and other neuropsychiatric diseases? *Front Pharmacol.* 2014; 5:46. <https://doi.org/10.3389/fphar.2014.00046>
PMID:24711793
182. Gatei M, Scott SP, Filippovitch I, Soronika N, Lavin MF, Weber B, Khanna KK. Role for ATM in DNA damage-induced phosphorylation of BRCA1. *Cancer Res.* 2000; 60:3299–304. PMID:10866324
183. Yoshida K, Miki Y. Role of BRCA1 and BRCA2 as regulators of DNA repair, transcription, and cell cycle in response to DNA damage. *Cancer Sci.* 2004; 95:866–71.
<https://doi.org/10.1111/j.1349-7006.2004.tb02195.x>
PMID:15546503
184. Scully R, Chen J, Plug A, Xiao Y, Weaver D, Feunteun J, Ashley T, Livingston DM. Association of BRCA1 with Rad51 in mitotic and meiotic cells. *Cell.* 1997; 88:265–75. [https://doi.org/10.1016/S0092-8674\(00\)81847-4](https://doi.org/10.1016/S0092-8674(00)81847-4)
PMID:9008167
185. Venkitaraman AR. Functions of BRCA1 and BRCA2 in the biological response to DNA damage. *J Cell Sci.* 2001; 114:3591–98. PMID:11707511
186. Wang Y, Cortez D, Yazdi P, Neff N, Elledge SJ, Qin J. BASC, a super complex of BRCA1-associated proteins involved in the recognition and repair of aberrant DNA structures. *Genes Dev.* 2000; 14:927–39.
PMID:10783165
187. Rogakou EP, Pilch DR, Orr AH, Ivanova VS, Bonner WM. DNA double-stranded breaks induce histone H2AX phosphorylation on serine 139. *J Biol Chem.* 1998; 273:5858–68. <https://doi.org/10.1074/jbc.273.10.5858>
PMID:9488723
188. Rogakou EP, Boon C, Redon C, Bonner WM. Megabase chromatin domains involved in DNA double-strand breaks in vivo. *J Cell Biol.* 1999; 146:905–16.
<https://doi.org/10.1083/jcb.146.5.905> PMID:10477747
189. Farmer H, McCabe N, Lord CJ, Tutt AN, Johnson DA, Richardson TB, Santarosa M, Dillon KJ, Hickson I, Knights C, Martin NM, Jackson SP, Smith GC, Ashworth A. Targeting the DNA repair defect in BRCA mutant cells as a therapeutic strategy. *Nature.* 2005; 434:917–21.
<https://doi.org/10.1038/nature03445> PMID:15829967
190. Suberbielle E, Djukic B, Evans M, Kim DH, Taneja P, Wang X, Finucane M, Knox J, Ho K, Devidze N, Maslah E, Mucke L. DNA repair factor BRCA1 depletion occurs in Alzheimer brains and impairs cognitive function in mice. *Nat Commun.* 2015; 6:8897.
<https://doi.org/10.1038/ncomms9897> PMID:26615780
191. Riabinska A, Daheim M, Herter-Sprie GS, Winkler J, Fritz C, Hallek M, Thomas RK, Kreuzer KA, Frenzel LP, Monfared P, Martins-Boucas J, Chen S, Reinhardt HC. Therapeutic targeting of a robust non-oncogene addiction to PRKDC in ATM-defective tumors. *Sci Transl Med.* 2013; 5:189ra78.
<https://doi.org/10.1126/scitranslmed.3005814>
PMID:23761041
192. Gurley KE, Kemp CJ. Synthetic lethality between mutation in *Atm* and DNA-PK(cs) during murine embryogenesis. *Curr Biol.* 2001; 11:191–94.
[https://doi.org/10.1016/S0960-9822\(01\)00048-3](https://doi.org/10.1016/S0960-9822(01)00048-3)
PMID:11231155
193. Gao Y, Chaudhuri J, Zhu C, Davidson L, Weaver DT, Alt FW. A targeted DNA-PKcs-null mutation reveals DNA-PK-independent functions for KU in V(D)J recombination. *Immunity.* 1998; 9:367–76.
[https://doi.org/10.1016/S1074-7613\(00\)80619-6](https://doi.org/10.1016/S1074-7613(00)80619-6)
PMID:9768756
194. Xu Y, Ashley T, Brainerd EE, Bronson RT, Meyn MS, Baltimore D. Targeted disruption of ATM leads to growth retardation, chromosomal fragmentation during meiosis, immune defects, and thymic lymphoma. *Genes Dev.* 1996; 10:2411–22.

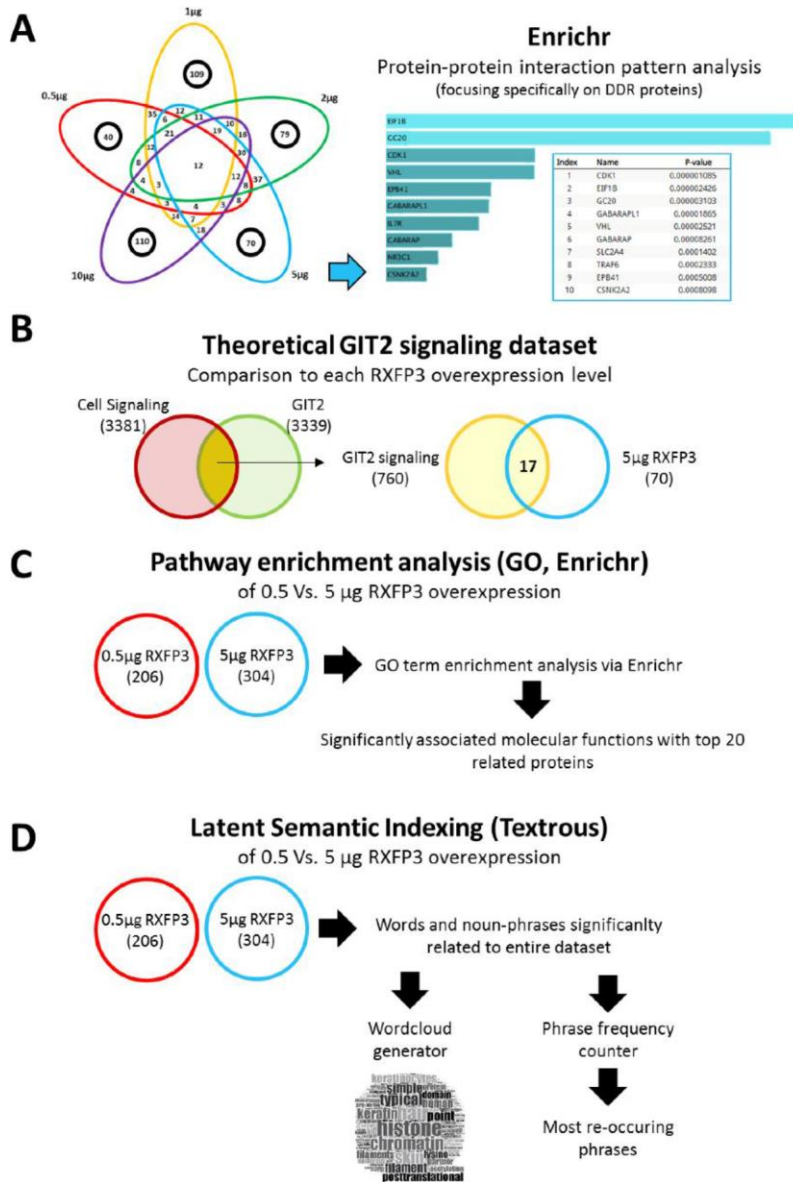
- <https://doi.org/10.1101/gad.10.19.2411>
PMID:[8843194](https://pubmed.ncbi.nlm.nih.gov/8843194/)
195. Leysen H, van Gastel J, Hendrickx JO, Santos-Otte P, Martin B, Maudsley S. G Protein-Coupled Receptor Systems as Crucial Regulators of DNA Damage Response Processes. *Int J Mol Sci*. 2018; 19:19.
<https://doi.org/10.3390/ijms19102919>
PMID:[30261591](https://pubmed.ncbi.nlm.nih.gov/30261591/)
196. Jiang T, Xue LJ, Yang Y, Wang QG, Xue X, Ou Z, Gao Q, Shi JQ, Wu L, Zhang YD. AVE0991, a nonpeptide analogue of Ang-(1-7), attenuates aging-related neuroinflammation. *Aging (Albany NY)*. 2018; 10:645–57.
<https://doi.org/10.18632/aging.101419>
PMID:[29667931](https://pubmed.ncbi.nlm.nih.gov/29667931/)
197. Tamma G, Goswami N, Reichmuth J, De Santo NG, Valenti G. Aquaporins, vasopressin, and aging: current perspectives. *Endocrinology*. 2015; 156:777–88.
<https://doi.org/10.1210/en.2014-1812>
PMID:[25514088](https://pubmed.ncbi.nlm.nih.gov/25514088/)
198. Sutton RE, Koob GF, Le Moal M, Rivier J, Vale W. Corticotropin releasing factor produces behavioural activation in rats. *Nature*. 1982; 297:331–33.
<https://doi.org/10.1038/297331a0> PMID:[6978997](https://pubmed.ncbi.nlm.nih.gov/6978997/)
199. Mellon PL, Windle JJ, Goldsmith PC, Padula CA, Roberts JL, Weiner RI. Immortalization of hypothalamic GnRH neurons by genetically targeted tumorigenesis. *Neuron*. 1990; 5:1–10.
[https://doi.org/10.1016/0896-6273\(90\)90028-E](https://doi.org/10.1016/0896-6273(90)90028-E)
PMID:[2196069](https://pubmed.ncbi.nlm.nih.gov/2196069/)
200. Mirshamsi S, Laidlaw HA, Ning K, Anderson E, Burgess LA, Gray A, Sutherland C, Ashford ML. Leptin and insulin stimulation of signalling pathways in arcuate nucleus neurones: PI3K dependent actin reorganization and KATP channel activation. *BMC Neurosci*. 2004; 5:54.
<https://doi.org/10.1186/1471-2202-5-54>
PMID:[15581426](https://pubmed.ncbi.nlm.nih.gov/15581426/)
201. Park SS, Wu WW, Zhou Y, Shen RF, Martin B, Maudsley S. Effective correction of experimental errors in quantitative proteomics using stable isotope labeling by amino acids in cell culture (SILAC). *J Proteomics*. 2012; 75:3720–32.
<https://doi.org/10.1016/j.jprot.2012.04.035>
PMID:[22575385](https://pubmed.ncbi.nlm.nih.gov/22575385/)
202. Cai H, Chen H, Yi T, Daimon CM, Boyle JP, Peers C, Maudsley S, Martin B. VennPlex—a novel Venn diagram program for comparing and visualizing datasets with differentially regulated datapoints. *PLoS One*. 2013; 8:e53388.
<https://doi.org/10.1371/journal.pone.0053388>
PMID:[23308210](https://pubmed.ncbi.nlm.nih.gov/23308210/)
203. Martin B, Chadwick W, Yi T, Park SS, Lu D, Ni B, Gadkaree S, Farhang K, Becker KG, Maudsley S. VENNTURE—a novel Venn diagram investigational tool for multiple pharmacological dataset analysis. *PLoS One*. 2012; 7:e36911.
<https://doi.org/10.1371/journal.pone.0036911>
PMID:[22606307](https://pubmed.ncbi.nlm.nih.gov/22606307/)
204. Rolland T, Taşan M, Charlotheaux B, Pevzner SJ, Zhong Q, Sahni N, Yi S, Lemmens I, Fontanillo C, Mosca R, Kamburov A, Ghiassian SD, Yang X, et al. A proteome-scale map of the human interactome network. *Cell*. 2014; 159:1212–26.
<https://doi.org/10.1016/j.cell.2014.10.050>
PMID:[25416956](https://pubmed.ncbi.nlm.nih.gov/25416956/)
205. Schmalzigaug R, Rodriguiz RM, Phillips LE, Davidson CE, Wetsel WC, Premont RT. Anxiety-like behaviors in mice lacking GIT2. *Neurosci Lett*. 2009; 451:156–61.
<https://doi.org/10.1016/j.neulet.2008.12.034>
PMID:[19114090](https://pubmed.ncbi.nlm.nih.gov/19114090/)

SUPPLEMENTARY MATERIALS

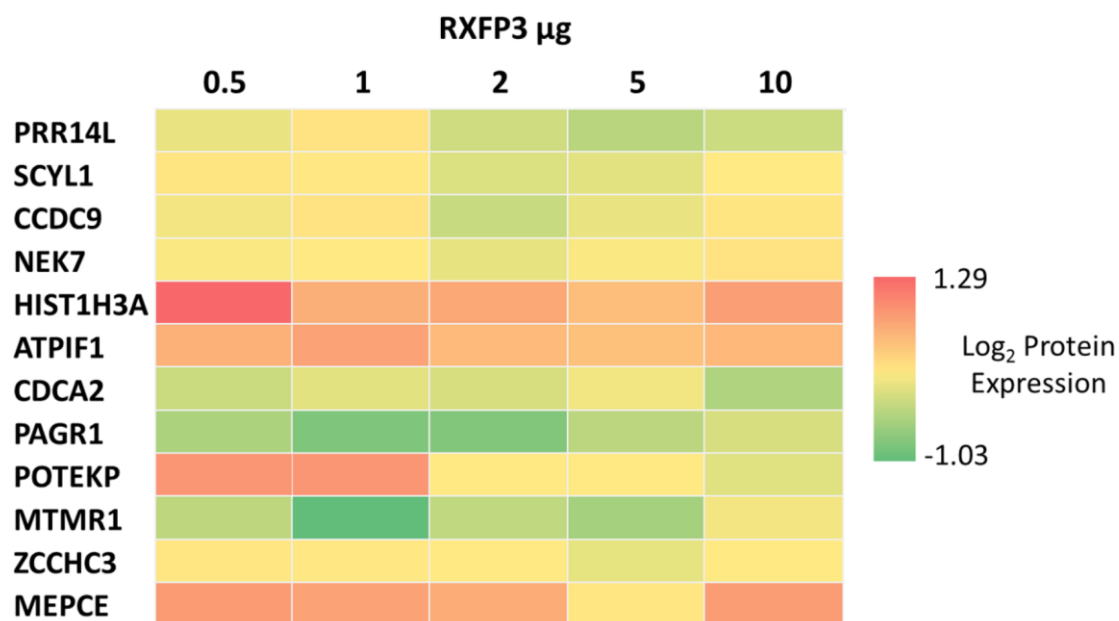
Supplementary Figures



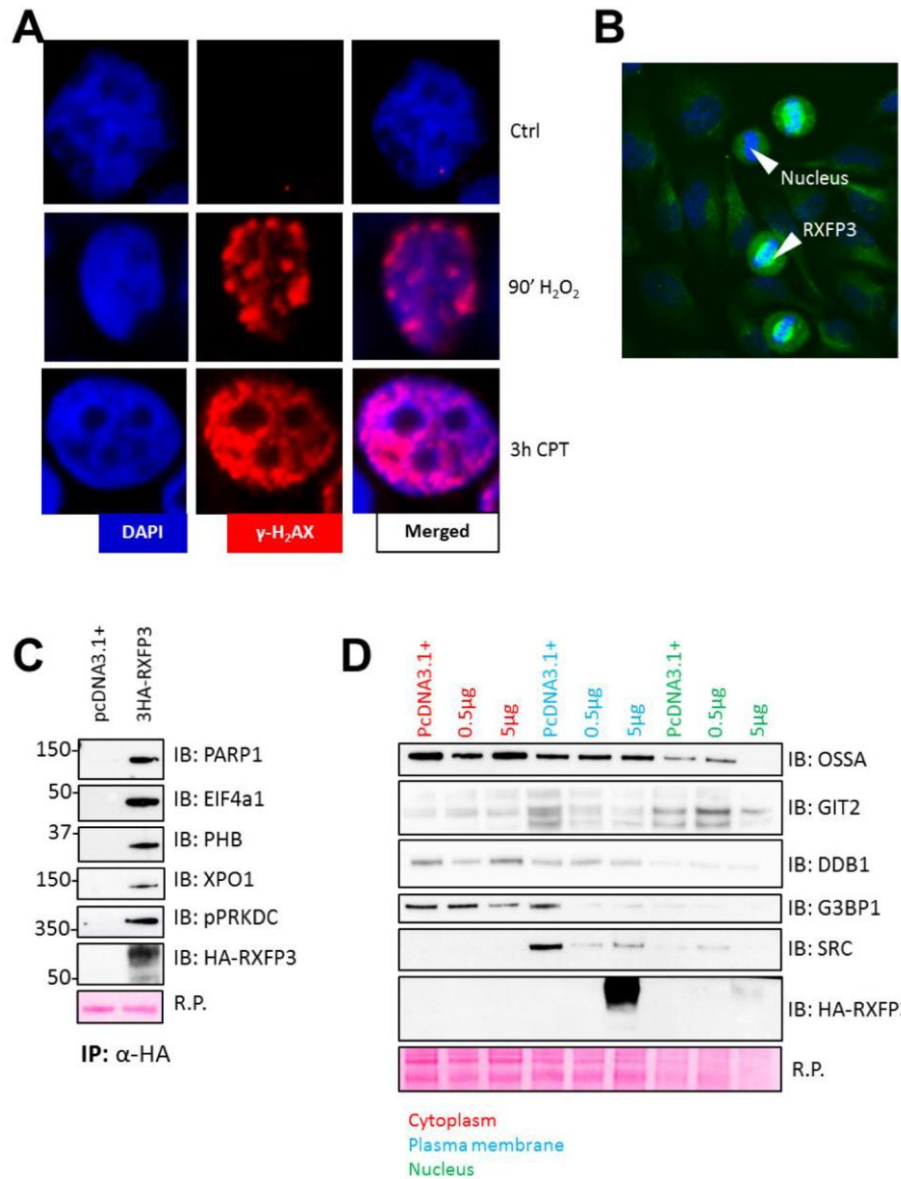
Supplementary Figure 1. Analysis of the RXFP3 amino acid structure indicates a potential role in the DNA damage response. (A, B) Amino acid structure of RXFP3. (A) RXFP3 represented as a heptahelical snake extracted from GPCRdb (www.GPCRdb.org), and (B) as an amino acid sequence. Visualized in both A and B are the predicted extracellular (blue), transmembrane (red), and intracellular (green) domains. Further investigation into the different motifs in the sequence indicates the absence of the typical “DRY” or Asp-Arg-Tyr motif responsible for receptor conformation change after ligand activation, instead a “TRY” or Thr-Arg-Tyr motif (Black) is present. In addition, we identified two phosphorylation sites for Ataxia Telangiectasia Mutated (ATM), with typical motif: Sx, in this case SQ or Ser-Gln (Pink), and one phosphorylation site for DNA protein kinase C (DNA-PK also known as PRKDC); with typical SxQ motif, in this case SLQ or Ser-Leu-Gln (Yellow). Potential phosphorylation sites were identified using Scansite (<https://scansite4.mit.edu>) and InterProScan (<http://www.ebi.ac.uk/interpro/interproscan.html>).



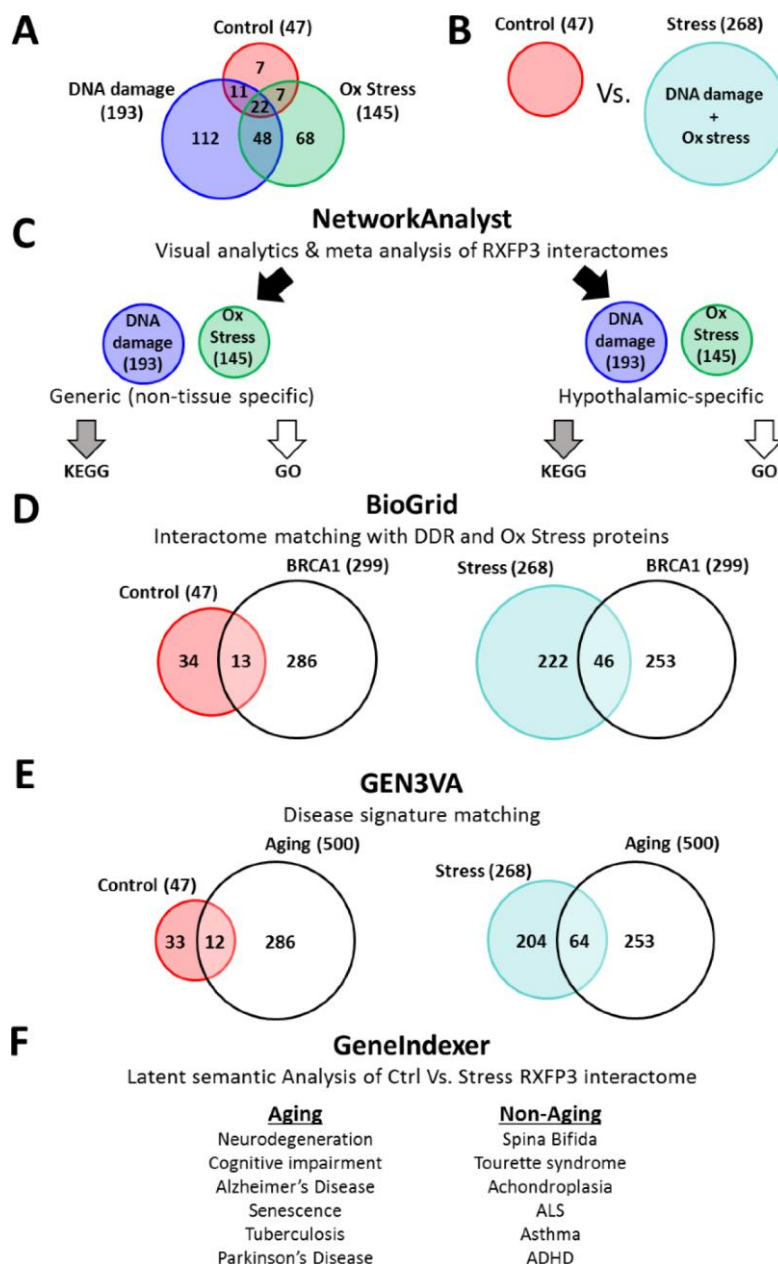
Supplementary Figure 2. Flowchart of the quantitative proteome Bioinformatic pipeline. For the bioinformatics analysis of our quantitative proteomics data of the different receptorsomes of RXFP3 obtained through our constellation experiment, we have used the following investigative techniques organized in a flowchart. **(A)** First we isolated the proteins unique to each overexpression level of RXFP3 (0.5 µg, Red; 1 µg, yellow; 2 µg, green; 5 µg, blue; 10 µg, purple), and analyzed each level individually using the PPI-hub function of Enrichr. As such we performed a protein-protein interaction pattern analysis of the constellation perturbagens, where we focused specifically on DNA damage response proteins in order to investigate which overexpression level shows the clearest relationship to DNA damage repair. **(B)** Next, we used latent semantic indexing to create a theoretical dataset for ‘GIT2 signaling’ (760 proteins, yellow), by overlapping the genes extracted from GeneIndexer significantly correlated to interrogator terms related to ‘Cell Signaling’ (3381 proteins, Red) and ‘GIT2’ (3339 proteins, green). This theoretical GIT2 signaling dataset was then compared to the different overexpression levels of RXFP3, where we found that the 5 µg dataset was the most reminiscent of GIT2 signaling. To further interrogate the role of this 5 µg dataset, we compared the full datasets of 5 µg and 0.5 µg overexpression with **(C)** Gene Ontology, which allowed us to extract the significantly associated molecular functions, associated with the dataset, and **(D)** latent semantic indexing tool Textroux! which allows us to extract the words and noun-phrases significantly associated to the entire gene list of each dataset. These words and noun-phrases were then organized in a word cloud which correlates word frequency with word size and writewords, which allows us to identify the most re-occurring phrases.



Supplementary Figure 3. Expression level-independent RXFP3 associated proteins. Through InteractiVenn (www.interactivenn.net), we were able to investigate the unique and overlapping proteins for the RXFP3 constellation experiment. 12 proteins were significantly altered across each of the RXFP3 overexpression levels, *i.e.* PRR14L, SCYL1, CCDC9, NEK7, HIST1H3A, ATPIF1, CDCA2, PAGR1, POTEKP, MTMR1, ZCCHC3, and MEPCE. These proteins show involvement in energy metabolism regulation, DNA damage associated with aging, and cell senescence. Using a heatmap we are able to show the protein expression of each protein, where green is downregulation and red is upregulation. Certain proteins were contra-regulated in the different overexpression levels and cellular fractions, and are therefore neither upregulated nor downregulated (yellow).



Supplementary Figure 4. Molecular Analyses of stress-associated damage and protein-protein interaction. (A) Validation of mass spectrometry data (RXFP3 0.5 and 5 μg overexpression) through immunoblotting, testing: SRC, G3BP1, OSSA, DDB1, and HA (RXFP3), with Red Ponceau as a loading control. (B) Validation of interactomics experiment using co-immunoprecipitation. (C) DNA damage validation after oxidative stress and camptothecin, using the DNA damage responder γ -H2AX as a marker, indicating the 90 minute exposure of 100 nM H_2O_2 can cause a possibly survivable amount of DNA damage, while 3 h of 1 μM camptothecin elicits a larger amount of DNA damage. (D) Confocal microscopy was used to investigate the expression of RXFP3 (green), where we see that RXFP3 expression can overlap with the mitotic spindle (blue) during mitosis, indicating a role in cell cycle control.



Supplementary Figure 5. Flowchart of the interactome Bioinformatic pipeline. To further elucidate the role of RXFP3 we have continued by investigating its interacting proteins in three different conditions, (A) *i*) Control (Red, 47 proteins), *ii*) Oxidative stress (Ox stress, Green; 145 proteins), and *iii*) DNA damage (Blue, 193 protein). Initially, we started the interactome analysis by isolating the unique proteins to each condition, and analyzing them with textous, word clouds and write words, similar to what we have described in Supplementary Figure 2D. (B) For further analysis we also created a ‘stress’ dataset (turquoise) where we have combined the oxidative stress and DNA damage interactomes. (C) The network analyst platform was used to assess the potential of these proteins to create a dynamic physical network. In order to do so, we employed both non-tissue specific (generic) and hypothalamic-specific datasets, to generate interaction networks for both KEGG pathway enrichment (grey arrow) and Gene Ontology (GO; white arrow). These datasets we then overlapped with our experimentally generated RXFP3 interactome after DNA damage and Oxidative stress. (D) We then performed a comparative interactome analysis, by investigating the overlap of the interacting proteins of several DNA damage-related (PRKDC, H2AFX, MDC1, TP53, BRCA1), and oxidative stress-related (G3BP1, SIRT1, SOD1) proteins, with our control and ‘stress’ interactome dataset (as described in B). As a control for the specificity of the overlap, we also extracted the interacting proteins of several proteins which are unrelated to DNA damage response and oxidative stress (other; CNTRL, CRP, LONP2). (E) to further elaborate a role for RXFP3 in aging, we compared our datasets (Control and Stress) to several aging related disease signatures extracted from GEN3VA, to establish the specificity of this overlap we also used several control signatures such as aortic aneurysm, which are not age-related. (F) Lastly, we used latent semantic indexing tool GeneIndexer to interrogate our control and stress dataset with age-related (Aging) and –unrelated terms (Non-Aging). GeneIndexer associates our dataset with these interrogation terms and expresses significance with a cosine similarity score.

Supplementary Tables

Please browse Full Text version to see the data of Supplementary Tables 1–26

Supplementary Table 1. Proteins selectively affected by the RXFP3 constellation. In an unbiased manner we discovered the proteomic ‘constellation’ perturbation response to ascending expression levels of RXFP3 expression (0.5, 1, 2, 5, 10 µg of cDNA expressed). Protein extracts were investigated as a multiplex using quantitative proteomics through iTRAQ labelling with each RXFP3 expression level compared ratiometrically to the proteomic response effects to empty vector ectopic expression. The ratios were then normalized using a Log₂ transformation, allowing us to identify the significantly up- and downregulated proteins.

Supplementary Table 2. Enrichr-based PPI Hub Protein enrichment analysis (0.5 µg RXFP3). Hub Protein-Protein Interaction enrichment analysis was performed using the Enrichr (<http://amp.pharm.mssm.edu/Enrichr/>) functional annotation suite with the 0.5 µg perturbation level of RXFP3 expression. For each enriched target PPI hub protein the overlap protein identity from the input dataset with the Enrichr-curated hub data (Overlap), the probability of PPI hub enrichment (P-value), cumulated Z-score (Z-score), Combined ranking score (Combined Score) and the protein identities from the input dataset that overlap with the Enrichr-curated PPI Hub dataset (Proteins) are detailed.

Supplementary Table 3. Enrichr-based PPI Hub Protein enrichment analysis (1.0 µg RXFP3). Hub Protein-Protein Interaction enrichment analysis was performed using the Enrichr (<http://amp.pharm.mssm.edu/Enrichr/>) functional annotation suite with the 1.0 µg perturbation level of RXFP3 expression. For each enriched target PPI hub protein the overlap protein identity from the input dataset with the Enrichr-curated hub data (Overlap), the probability of PPI hub enrichment (P-value), cumulated Z-score (Z-score), Combined ranking score (Combined Score) and the protein identities from the input dataset that overlap with the Enrichr-curated PPI Hub dataset (Proteins) are detailed.

Supplementary Table 4. Enrichr-based PPI Hub Protein enrichment analysis (2.0 µg RXFP3). Hub Protein-Protein Interaction enrichment analysis was performed using the Enrichr (<http://amp.pharm.mssm.edu/Enrichr/>) functional annotation suite with the 2.0 µg perturbation level of RXFP3 expression. For each enriched target PPI hub protein the overlap protein identity from the input dataset with the Enrichr-curated hub data (Overlap), the probability of PPI hub enrichment (P-value), cumulated Z-score (Z-score), Combined ranking score (Combined Score) and the protein identities from the input dataset that overlap with the Enrichr-curated PPI Hub dataset (Proteins) are detailed.

Supplementary Table 5. Enrichr-based PPI Hub Protein enrichment analysis (5.0 µg RXFP3). Hub Protein-Protein Interaction enrichment analysis was performed using the Enrichr (<http://amp.pharm.mssm.edu/Enrichr/>) functional annotation suite with the 5.0 µg perturbation level of RXFP3 expression. For each enriched target PPI hub protein the overlap protein identity from the input dataset with the Enrichr-curated hub data (Overlap), the probability of PPI hub enrichment (P-value), cumulated Z-score (Z-score), Combined ranking score (Combined Score) and the protein identities from the input dataset that overlap with the Enrichr-curated PPI Hub dataset (Proteins) are detailed.

Supplementary Table 6. Enrichr-based PPI Hub Protein enrichment analysis (10 µg RXFP3). Hub Protein-Protein Interaction enrichment analysis was performed using the Enrichr (<http://amp.pharm.mssm.edu/Enrichr/>) functional annotation suite with the 10.0 µg perturbation level of RXFP3 expression. For each enriched target PPI hub protein the overlap protein identity from the input dataset with the Enrichr-curated hub data (Overlap), the probability of PPI hub enrichment (P-value), cumulated Z-score (Z-score), Combined ranking score (Combined Score) and the protein identities from the input dataset that overlap with the Enrichr-curated PPI Hub dataset (Proteins) are detailed.

Supplementary Table 7. Cellular Signaling theoretical data set. Biomedical text word items, *i.e.* Gene Symbols, associated with generic 'Cellular Signaling' extraction terms are represented. All proteins identified possess a Cosine Similarity score of association with the interrogator term of >0.1.

Supplementary Table 8. GIT2 theoretical data set. Biomedical text word items, *i.e.* Gene Symbols, associated with generic 'GIT2' linked extraction terms are represented. All proteins identified possess a Cosine Similarity score of association with the interrogator term of >0.1.

Supplementary Table 9. Concatenated GIT2 signaling theoretical data set. Biomedical text word items, *i.e.* Gene Symbols, associated with both GIT2 and Cellular Signaling extraction terms are represented. Hence the concatenation of GIT2 with Cell Signaling protein sets results in the theoretical 'GIT2-Signaling' dataset. All proteins identified possess a Cosine Similarity score of association with the interrogator term of >0.1.

Supplementary Table 10. Canonical Signaling Pathway Analysis of theoretical GIT2-Signaling dataset. Ingenuity Pathway Analysis was employed to generate a Canonical Signaling Pathway appreciation of the molecular nature of the theoretical GIT2-Signaling dataset created using latent semantic association analysis.

Supplementary Table 11. RXFP3 interacting proteins. Interacting proteins of RXFP3 in control conditions, after oxidative stress (H₂O₂) and DNA damage (CPT). The list termed 'stress' are all the proteins of oxidative stress and DNA damage combined, without duplicates.

Supplementary Table 12. NetworkAnalyst-based Gene Ontology analysis of the RXFP3 interactome stabilized in the presence of peroxide cellular perturbation (hypothalamic database). The proteins consistently associated with the RXFP3 receptor following exposure to hydrogen peroxide were analyzed using a human hypothalamic tissue database derived from DIFFERENTIALNET (<http://netbio.bgu.ac.il/diffnet/>). For the most stringent analysis process we employed a Zero Order Network approach. Gene Ontology (Biological Process) annotation was performed on all identified nodes using the built-in Gene Ontology analysis module of NetworkAnalyst (<https://www.networkanalyst.ca>). For each significantly-populated Gene Ontology term group ($p < 0.05$) the total number of proteins associated with that group (Total), the expected (Expected) number of identified proteins from a random data sample (Hypergeometric test based), the actual number of GO term-populating proteins from the experimental dataset (Hits), the enrichment P value (P.Value) as well as the enrichment FDR are given (FDR).

Supplementary Table 13. NetworkAnalyst-based Gene Ontology analysis of the RXFP3 interactome stabilized in the presence of CPT cellular perturbation (hypothalamic database). The proteins consistently associated with the RXFP3 receptor following exposure to CPT were analyzed using a human hypothalamic tissue database derived from DIFFERENTIALNET (<http://netbio.bgu.ac.il/diffnet/>). For the most stringent analysis process we employed a Zero Order Network approach. Gene Ontology (Biological Process) annotation was performed on all identified nodes using the built-in Gene Ontology analysis module of NetworkAnalyst (<https://www.networkanalyst.ca>). For each significantly-populated Gene Ontology term group ($p < 0.05$) the total number of proteins associated with that group (Total), the expected (Expected) number of identified proteins from a random data sample (Hypergeometric test based), the actual number of GO term-populating proteins from the experimental dataset (Hits), the enrichment P value (P.Value) as well as the enrichment FDR are given (FDR).

Supplementary Table 14. NetworkAnalyst-based Gene Ontology analysis of the RXFP3 interactome stabilized in the presence of peroxide cellular perturbation (generic database). The proteins consistently associated with the RXFP3 receptor following exposure to hydrogen peroxide were analyzed using a generic human tissue database derived from IMEx (<https://www.imexconsortium.org/>). For the most stringent analysis process we employed a Zero Order Network approach. Gene

Ontology (Biological Process) annotation was performed on all identified nodes using the built-in Gene Ontology analysis module of NetworkAnalyst (<https://www.networkanalyst.ca>). For each significantly-populated Gene Ontology term group ($p < 0.05$) the total number of proteins associated with that group (Total), the expected (Expected) number of identified proteins from a random data sample (Hypergeometric test based), the actual number of GO term-populating proteins from the experimental dataset (Hits), the enrichment P value (P.Value) as well as the enrichment FDR are given (FDR).

Supplementary Table 15. NetworkAnalyst-based Gene Ontology analysis of the RXFP3 interactome stabilized in the presence of CPT cellular perturbation (generic database). The proteins consistently associated with the RXFP3 receptor following exposure to CPT were analyzed using a generic human tissue database derived from IMEx (<https://www.imexconsortium.org/>). For the most stringent analysis process we employed a Zero Order Network approach. Gene Ontology (Biological Process) annotation was performed on all identified nodes using the built-in Gene Ontology analysis module of NetworkAnalyst (<http://www.networkanalyst.ca>). For each significantly-populated Gene Ontology term group ($p < 0.05$) the total number of proteins associated with that group (Total), the expected (Expected) number of identified proteins from a random data sample (Hypergeometric test based), the actual number of GO term-populating proteins from the experimental dataset (Hits), the enrichment P value (P.Value) as well as the enrichment FDR are given (FDR).

Supplementary Table 16. NetworkAnalyst-based KEGG pathway analysis of the RXFP3 interactome stabilized in the presence of peroxide cellular perturbation (generic database). The proteins consistently associated with the RXFP3 receptor following exposure to hydrogen peroxide were analyzed using a generic human tissue database derived from IMEx (<https://www.imexconsortium.org/>). For the most stringent analysis process we employed a Zero Order Network approach. KEGG signaling pathway annotation was performed on all identified nodes using the built-in KEGG Pathway analysis module of NetworkAnalyst (<http://www.networkanalyst.ca>). For each significantly-populated KEGG Pathway ($p < 0.05$) the total number of proteins associated with that group (Total), the expected (Expected) number of identified proteins from a random data sample (Hypergeometric test based), the actual number of GO term-populating proteins from the experimental dataset (Hits), the enrichment P value (P.Value) as well as the enrichment FDR are given (FDR).

Supplementary Table 17. NetworkAnalyst-based KEGG pathway analysis of the RXFP3 interactome stabilized in the presence of peroxide cellular perturbation (hypothalamic database). The proteins consistently associated with the RXFP3 receptor following exposure to hydrogen peroxide were analyzed using a human hypothalamic tissue database derived from DIFFERENTIALNET (<http://netbio.bgu.ac.il/diffnet/>). For the most stringent analysis process we employed a Zero Order Network approach. KEGG signaling pathway annotation was performed on all identified nodes using the built-in KEGG Pathway analysis module of NetworkAnalyst (<http://www.networkanalyst.ca>). For each significantly-populated KEGG Pathway ($p < 0.05$) the total number of proteins associated with that group (Total), the expected (Expected) number of identified proteins from a random data sample (Hypergeometric test based), the actual number of GO term-populating proteins from the experimental dataset (Hits), the enrichment P value (P.Value) as well as the enrichment FDR are given (FDR).

Supplementary Table 18. NetworkAnalyst-based KEGG pathway analysis of the RXFP3 interactome stabilized in the presence of CPT cellular perturbation (generic database). The proteins consistently associated with the RXFP3 receptor following exposure to CPT were analyzed using a generic human tissue database derived from IMEx (<http://www.imexconsortium.org/>). For the most stringent analysis process we employed a Zero Order Network approach. KEGG signaling pathway annotation was performed on all identified nodes using the built-in KEGG Pathway analysis module of NetworkAnalyst (<http://www.networkanalyst.ca>). For each significantly-populated KEGG Pathway ($p < 0.05$) the total number of proteins associated with that group (Total), the expected (Expected) number of identified proteins from a random data sample (Hypergeometric test based), the actual number of GO term-populating proteins from the experimental dataset (Hits), the enrichment P value (P.Value) as well as the enrichment FDR are given (FDR).

Supplementary Table 19. NetworkAnalyst-based KEGG pathway analysis of the RXFP3 interactome stabilized in the presence of CPT cellular perturbation (hypothalamic database). The proteins consistently associated with the RXFP3

receptor following exposure to CPT were analyzed using a human hypothalamic tissue database derived from DIFFERENTIALNET (<http://netbio.bgu.ac.il/diffnet/>). For the most stringent analysis process we employed a Zero Order Network approach. KEGG signaling pathway annotation was performed on all identified nodes using the built-in KEGG Pathway analysis module of NetworkAnalyst (<http://www.networkanalyst.ca>). For each significantly-populated KEGG Pathway ($p < 0.05$) the total number of proteins associated with that group (Total), the expected (Expected) number of identified proteins from a random data sample (Hypergeometric test based), the actual number of GO term-populating proteins from the experimental dataset (Hits), the enrichment P value (P.Value) as well as the enrichment FDR are given (FDR).

Supplementary Table 20. BioGRID interactomes for DNA damage response, and oxidative stress. To investigate the role for RXFP3 in oxidative stress and DNA damage response, we compared its interacting proteins in different conditions to the interacting proteins of several well-known DNA damage response and oxidative stress-related proteins, which we extracted from the freely available BioGRID database (<https://thebiogrid.org/>). As a control we used proteins which are so far known not to play a role in these processes. DNA damage response/repair: BRCA1, MDM2, PRKDC, TP53, MDC1, H2AFX; Oxidative stress: G3BP1, SOD1, SIRT1; Control/Non-stress: CNTRL, CRP, LONP2.

Supplementary Table 21. GEN3VA disease signature lists. To investigate the potential role for RXFP3 in aging, we extracted three disease signatures from GEN3VA (GENE Expression and Enrichment Vector Analyzer; <http://amp.pharm.mssm.edu/gen3va/>): 'Aging' (found in GEN3VA under the name "Model of cerebral aging and Alzheimer's disease: temporal cortex"), 'Schizophrenia' (in GEN3VA "Schizophrenia: postmortem superior temporal cortex") and 'Aortic aneurysm' (in GEN3VA "Abdominal aortic aneurysm") the latter of which is used as a control, to assure the protein overlap between the GEN3VA signatures and our own RXFP3 interactome dataset is specific. GEN3VA is a web-based system enabling the integrative analysis of a collective of gene expression signatures identified and extracted from GEO. Allowing us to extract specific disease signatures, which we can compare to our own data.

Supplementary Table 22. GeneIndexer interrogation of RXFP3 'control' interactome.

Supplementary Table 23. GeneIndexer interrogation of RXFP3 'control' interactome. Latent Semantic Indexing (LSI)-based informatic platform GeneIndexer (<https://geneindexer.com/>) is able to measure the degree of association of biomedical gene symbol identifiers of proteins with input interrogator concept terms through unbiased Cosine Similarity Score analysis. We cross-interrogated the obtained RXFP3 interactome dataset, with the following age-related syntactic concepts (Aging): *Neurodegeneration (ND)*, *Cognitive impairment (CI)*, *Senescence (S)*, *Parkinson's Disease (PD)*, *Amyotrophic lateral sclerosis (ALS)*, *Alzheimer's Disease (AD)*; and non-age-related terms (non-Aging): *Tuberculosis (TB)*, *Spina Bifida (SB)*, *Asthma (A)*, *Tourette syndrome (TS)*, *ADHD*, *Achondroplasia (AP)*. GeneIndexer extracts all gene-to-word relationships from the literature using LSI, which we then averaged per interrogator term and per interrogator group, *i.e.* 'Aging' vs. 'non-Aging'. Here a cosine similarity score larger than 0.2 typically specifies an explicit association, while a score lower than 0.2 indicates an implied relationship, a cutoff score was set at 0.1.

Supplementary Table 24. RXFP3 constellation TOP 15 and contra-regulated proteins. TOP15 up (red) and down (green) regulated proteins, after 0.5 μ g and 5 μ g of RXFP3 overexpression. In addition, we have noted the contra-regulated proteins, which were upregulated in on cellular fraction, while being downregulated in another. Molecular function and Biological processes were identified using Uniprot (<https://www.uniprot.org>).

Supplementary Table 25. Disease continuum. To assess the potential role of RXFP3 in controlling aging-associated diseases, we employed an entirely unbiased analysis. We created a database of proteins, extracted from the entire human genome, explicitly and implicitly associated (via PubMed Central text mining using GeneIndexer (<https://geneindexer.com/>)) with input interrogator terms covering the majority of age-associated disease conditions. We termed this dataset of disease-associated proteins the 'Disease Continuum'. Abbreviations are as follows: Alzheimer's disease (AD); Amyotrophic Lateral Sclerosis (ALS); Liver disease (LD);

Diabetes mellitus (DM); Dementia (D); Chronic obstructive pulmonary disease (COPD); Stroke (S); Chronic Kidney Disease (CKD); Frontotemporal dementia (FTD); Frontotemporal lobar degeneration (FTLD); Huntington's disease (HD); Chronic Heart Failure (CHF); Mild cognitive impairment (MCI); Neurodegeneration (N); Parkinson's disease (PD); Cancer (C).

Supplementary Table 26. Therapeutic continuum. To identify potential therapeutic targets that could interact and potentially control the 'Disease Continuum' listed in Supplementary Table 25 in a multidimensional manner we investigated the proteins within this continuum with interrogators most strongly associated with battery of terms linked to central nervous system function, energy metabolism and GPCR-focused signaling (via PubMed Central text mining using GeneIndexer (<https://geneindexer.com/>): 1) GPCR, 2)gpcr, 3) G protein-coupled receptor, 4) G protein coupled receptor, 5) heptahelical, 6) G protein, 7) receptor, 8) target, 9) therapeutic, 10) serpentine, 11) seven transmembrane, 12) brain, 13) cortex, 14) hippocampus, 15) central nervous system, 16) CNS, 17) diabetes, 18) energy, 19) metabolism, 20) glucose, and 21) mitochondria). Ranking the Cosine Similarity scores of the resultant factors that were prominent in the disease continuum and the 'Therapeutic Interrogators' we found that, based on a correlation ranking probability score ($p < 0.001$, ***) there were 37 specific protein targets demonstrating a number of correlations within the therapeutic interrogators that was greater than the 99% percentile (representing only 0.67% of the input 'Disease Continuum' dataset). The top three proteins that could represent effective targets against age-related diseases were, AVPR1B (arginine vasopressin receptor 1B), MAS1 (MAS1 proto-oncogene, G protein-coupled receptor) and RLN3, the cognate ligand for the RXFP3.